Sap flow and sugar transport in plants

K. H. Jensen, K. Berg-Sørensen, H. Bruus, N. M. Holbrook, J. Liesche, A. Schulz, M. A. Zwieniecki, and T. Bohr

Sap flow and sugar transport in plants

K. H. Jensen[1][*] and K. Berg-Sørensen[1], H. Bruus[1], N. M. Holbrook[2], J. Liesche[3], A. Schulz[4], M. A. Zwieniecki[5] and T. Bohr[1]

[1] *Department of Physics,*
Technical University of Denmark,
DK-2800 Kongens Lyngby, Denmark
[2] *Department of Organismic and Evolutionary Biology,*
Harvard University,
Cambridge, MA 02138, USA
[3] *College of Life Sciences,*
Northwest A&F University,
712100 Yangling, China
[4] *Department of Plant and Environmental Sciences,*
University of Copenhagen,
DK-1871 Frederiksberg C, Denmark
[5] *Department of Plant Sciences,*
University of California,
Davis, CA 95616,
USA

(Dated: Wednesday 27th April, 2016, at 08:55)

Green plants are Earth's primary solar energy collectors. They harvest the energy of the sun by converting light energy into chemical energy stored in the bonds of sugar molecules. A multitude of carefully orchestrated transport processes are needed to move water and minerals from the soil to sites of photosynthesis, and to distribute energy-rich sugars throughout the plant body to support metabolism and growth. The long-distance transport happens in the plants' vascular system, where water and solutes are moved along the entire length of the plant. In this review, we discuss the current understanding of the mechanism and the quantitative description of these flows, connecting theory and experiments as far as possible.

We begin begin with an overview of low-Reynolds-number transport processes, followed by an introduction to the anatomy and physiology of vascular transport in the phloem and xylem. Next, sugar transport in the phloem is explored with attention given to experimental results as well as the fluid mechanics of osmotically driven flows. Then water transport in the xylem is discussed with focus on embolism dynamics, conduit optimization, and couplings between water and sugar transport. Finally, remarks are given on some of the open questions of this research field.

CONTENTS

* khjensen@fysik.dtu.dk

I. INTRODUCTION

From the point of view of a physicist, plants are full of mysteries. They are among the most successful organisms on earth both in terms of total biomass and individual size range, and yet they lack the central organs which we associate with life, such as heart or brain, and on which animals rely for control and function. Indeed, plants are masters of decentralized management, since they thrive and maintain coherence even in very large organisms without these central units. This requires an efficient and robust vascular system, which sustains growth and communication throughout the entire organism, from root to leaf of even the tallest tree, without, that is, a central heart to drive the sap. The basic mechanisms, or driving forces, for the flows in these vascular systems have proven difficult to elucidate because the conduits are sensitive to manipulation, ceasing transport when exposed to only slight disturbances. Considering the importance of plants, as crops in the fields or trees in the forests, to the existence of other life forms on this planet, this is amazing. These basic mechanisms are the focus of the present review, and we shall in particular discuss the fluid dynamics emerging from the basic hypotheses and the ensuing consequences for structure and function, testable by field measurements. By thus investigating the mechanisms for the functioning of the entire organisms, we hope to expose the reader to interesting and challenging physics deserving to be better known to active researchers in many fields of physics.

The two main parts of the vascular system, the *xylem* and the *phloem* play a very different role in the life of plants (Fig. 1). Their remarkable names were coined by German botanists from the Greek words *xylon*: wood and *phloos*: tree bark. The xylem is the "water highway" which brings large amounts of water from the roots to the leaves. Xylem tubes come in two varieties: *tracheids* and *vessels*. The latter are the largest and they can reach hundreds of μm in diameter and meters in length. They are made up of cellular segments, *vessel elements* of up to around 1 mm, separated by porous *perforation plates*.

In a large tree, the xylem is well-protected inside the trunk and can daily carry several hundred liters of water to the leaves, most of which is evaporated into the surrounding air. The reason for this wasteful handling of the – often scarce – water resources, lies in the plants' approach to the acquisition of carbon dioxide. Plants acquire CO_2 simply by opening their "mouths", i. e., the *stomata* (pores) on the surface of their leaves. Opening the stomata does let CO_2 diffuse in, but much more water is lost: since living plant cells need to be soaked in water, the humidity inside a leaf is near 100%, typically much higher than outside, and thus several hundreds of water molecules will be lost for every CO_2 molecule gained. Together with sunlight, and a bit of the water, CO_2 is the basic ingredient for photosynthesis, primarily taking place in the leaves, leading to the creation of sugars; sugars which, through the phloem, provide the building material for practically all growth in the plant – from root to leaf, including, in a tree, the annual radial growth of the trunk. We find the concentration of CO_2 of 0.04 % vol in the atmosphere threateningly high due to global warming, but, presumably, trees find it threateningly low.

The theoretical understanding of the upward flows of water came around 1900 in the form of the *Cohesion-Tension theory* (Dixon and Joly, 1895): that the driving force for the flow in the xylem comes from suction generated in the leaves by evaporation of water vapor into the atmosphere (Fig. 1(a,c)). The surprise was that the pressures in the xylem is even lower than vacuum: they are *negative*. Negative pressures are somewhat counterintuitive, in particular if our intuition comes from equilibrium thermodynamics and gases. Negative pressures only occur in non-equilibrium or *metastable* states and only in substances with strong cohesion, e.g., liquids. The magnitude of these negative pressures (typically −2 MPa) does remain surprising, as does the fact that water inside living trees is transported in a metastable state. Thus a lot of recent effort went into understanding how trees avoid or cope with the local return to equilibrium in the form of cavitation, or *embolisms* in biological terminology, which would seem to be fatal for efficient water transport.

Compared to the water highway of the xylem, the phloem is more like the small country roads passing through the villages. Everything is an order of magnitude smaller – the size of the tubing and the maximum flow velocities. The pressure differs not only in strength, but also in sign: the phloem runs under positive pressure of the order of 1 MPa. The phloem is no less important, however, since it carries the valuable sugars from the mature leaves where they are produced to e.g., new leaves, roots, shoots or fruits where they are needed. In contrast to the xylem, the phloem tubes (*sieve elements*) are living cells, but still the main transport mechanism, the so-called *Münch mechanism* (Münch, 1930), is believed to be the purely passive osmotic pressure differences caused
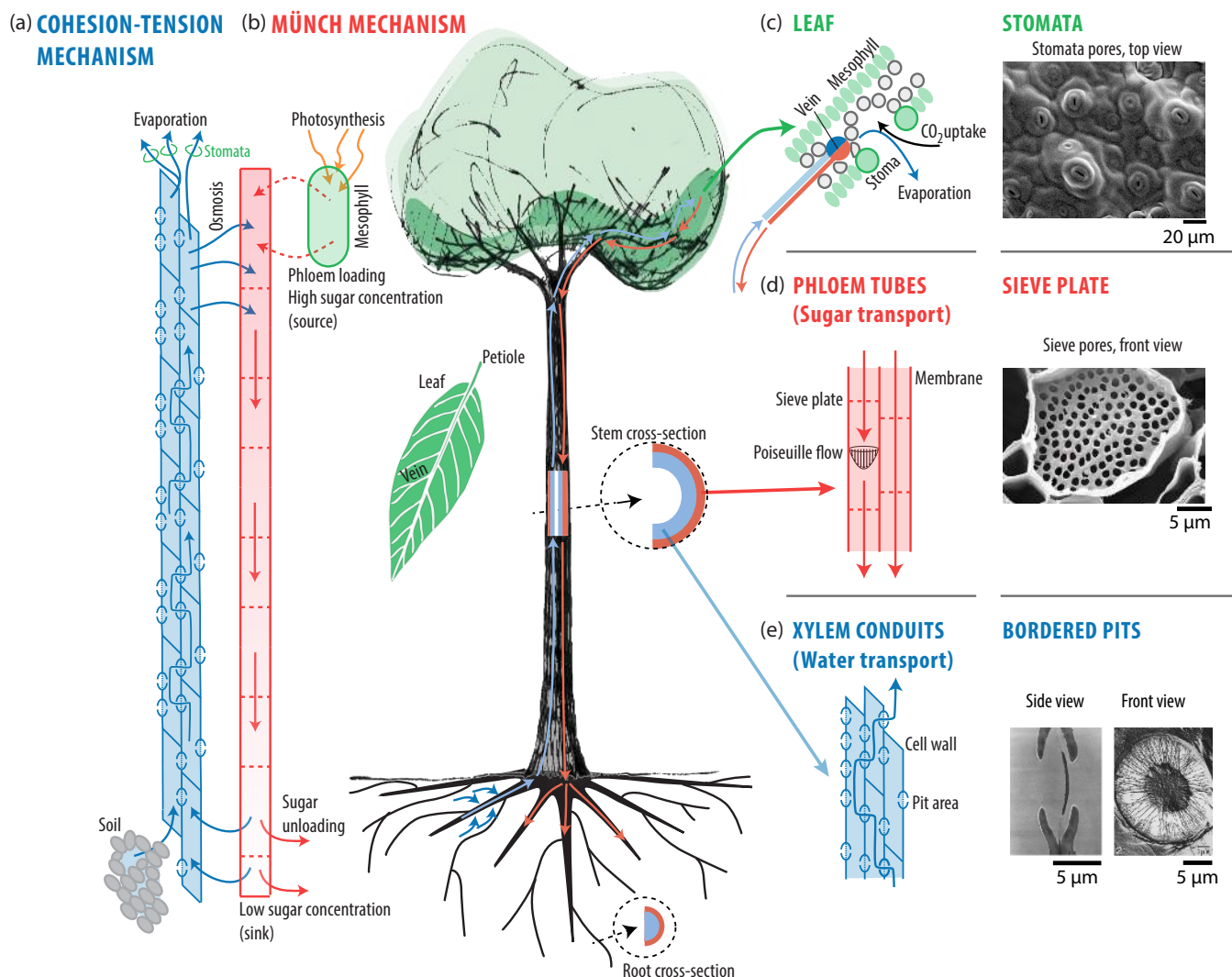
Figure 1 Schematic representation of vascular transport processes in plants. (a) Xylem water transport from soil to shoot is driven by evaporation from leaves via the cohesion-tension mechanism. (b) Phloem sugar transport from leaves to regions of growth is driven by differences in osmotic pressure according to the Münch mechanism. Details of transport processes in (c) leaves, (d) phloem tubes, and (e) xylem conduits are also shown. For clarity xylem and phloem tubes are drawn as same size. See further details in text. (d) As originally published in Jensen et al., Front. Plant Sci. 3, 151 (2012) (Jensen *et al.*, 2012c). (e) Adapted from (Bauch *et al.*, 1972). The background drawing of a tree courtesy of Camille Lucas and Alexandre Ponomarenko.

by the gradients in sugar concentration between *sources* and *sinks* of sugar (Fig. 1(b)). A large part of this review will be devoted to the consequences of this hypothesis, applied to the long distance sugar translocation from one end of the organism to the other. The basis is formed by the equations for the dynamics of osmotically driven flows, which seem quite unique to plants and fungi. Of course, osmosis plays a large role in animals, e.g., for the filtration in the kidneys, but the flow past the kidney is generated by the heart, not by osmosis.

In a tree, the phloem resides on the inside of the bark and is therefore easily destroyed if the bark is removed. On the other hand, the phloem is well-protected by the construction and constituents of the tubes. Phloem tubes consist of cylindrical sieve elements (perhaps around 10 µm in radius and 1 mm in length) separated by perforated sieve plates. Disturbance of the sieve element (e.g. mechanically or by cooling) can cause local stopping of the flow, for instance by occlusion of the sieve tube by *forisomes* (a class of contractile proteins) or by clogging of the sieve plates (Fig. 1(d)) (Knoblauch *et al.*, 2014; Lang and Minchin, 1986). Suspension of translocation is widespread throughout the plant kingdom and may be an important control mechanism. The hydrodynamic mechanisms involved in these processes, however, remain poorly understood. The sensitivity of the phloem makes

its contents inaccessible to most. The remarkable exceptions from this rule are a group of small insects, *aphids*, who are actually able to penetrate into the sieve elements and tap the valuable sweet sap, without stopping the phloem. Aphids remain important for investigations of the phloem, but despite of their life-sacrificing effort (letting biologists sever their body from the stylet inserted into the plant) our knowledge about local pressures and concentrations in the phloem are limited. Again, this makes it paramount to extract measurable consequences from this special type of fluid dynamics.

The phloem and the xylem interact and exchange water along the entire length of the plant. This interaction is particularly strong in the leaves, where the outlet from the xylem (the *tracheary elements*) and the inlet to the phloem (the sieve elements) are only separated by a few microns, with a pressure in the former, say, around -2 MPa and $+1$ MPa in the latter. Part of the water coming out from the tracheary element should end up in the nearby sieve element, pushing the sugar solution back into the tree. But only a small part of it. Most of the water leaving the xylem moves into the leaf mesophyll and evaporates through the stomata. On the way out, a small part, perhaps a percent, of the water enters into the *mesophyll* cells where the photosynthesis takes place – partly to contribute to the photosynthesis and partly to assist the sugars on their way back to the phloem. This coupled water-sugar transport – *sugar loading* – is currently an active field of research, and we shall discuss some recent developments.

One point of view to which we shall return frequently, is that of *optimality*. We know that plants – as other living organisms – have been carefully selected by evolution, and thus function rather efficiently. This paper primarily deals with the physical factors that characterize vascular transport processes. However, numerous other effects play equally important roles. For instance, mechanical effects impose important constraints on leaf morphology and venation patterns. Moreover, environmental factors and ecological interactions between plants and animals influence the distribution of species. In general, however, one can ask whether the choice of a particular strategy can be motivated by some criterion of optimality by which one can gauge the performance of plants in using a particular strategy. Scientists have pondered this question for centuries. In particular, the energy budget of living organisms have been the focus of much attention, where energy broadly defined denotes resources necessary for metabolism, growth, and reproduction (e.g. nutrients, light, water, CO_2 etc.). One perspective due to Lotka (1922) (p. 150) that links fitness and energy consumption strategies is: *Where the supply of available energy is limited, the advantage will go to that organism which is most efficient, most economical, in applying to preservative uses such energy as it captures. Where the energy supply is capable of expansion, efficiency or economy, though still an advantage, is only one way of meeting the situation, and, so long as there remains an unutilized margin of available energy, sooner or later the battle, presumably, will be between two groups or species equally efficient, equally economical, but the one more apt than the other in tapping previously unutilized sources of available energy.*

To test optimality hypotheses against biological data, two different approaches are feasible (Brenner, 2014): Either one must sample the characteristics of many species in the phylogeny, and compare results over a wide class of organisms or one can use engineering principles to hypothesize adaptations by the organisms to achieve optimality. The advantage of the first approach is that it allows us to broadly determine if the systems are optimized for a certain function and evaluate potential performance metrics to elucidate sources of variability. As an example, we show in Section IV.C that the Münch mechanism implies an optimal choice of the diameter of the sieve tubes connecting the leaves of a plant to its root. Specifically, we find that the competition between efficient osmotic pumping (in the leaves) and efficient long-distance transfer (through the stem) leads to the simple result that the optimal diameter of the sieve tubes (leading to the largest flow velocity) should scale as the cubic root of the product of the length of the leaves and that of the stem. We find broad agreement between this prediction and data, but outliers also help identify drivers of variability. The second approach can be used if the number of species is limited or not enough is known about the physiology to make concrete statements about optimality. If the engineering challenge, however, is clear we can make hypotheses about what the individual organism can do to enhance transport. From this, one can propose concrete experiments to test specific cases that may reveal new aspects of physiology. In Sec. VI.B, we give examples of how this strategy has been applied to understand vascular structure of leaves. As we focus on the basic physics of fluid transport, the principles discussed are relevant for all vascular plants. Aspects of conduit structure, however, vary among different groups of plants. Here we emphasize transport in two groups: *gymnosperms*, which are cone-forming plants that include conifers and thus common trees such as pines, spruce and yew, and *angiosperms*, which include all of the plants that produce flowers (e.g., oak trees, grasses, and grape vines).

Another recurring topic will be that of biomimetics. With the dual purpose of understanding plants and learning from plants, many researchers (including ourselves) have designed fluidic devices based on certain features of the fluid dynamics of plants. They have shown to be very helpful in highlighting basic features, mostly of the vascular system. We shall review the current state of the art and problems in this field, which we find very promising.

The layout of the review is as follows. We shall start with a short review of transport in low-Reynolds-number

Table I Comparison of parameters for flow in a phloem tube, xylem vessel, and the human aorta. The diffusivity for sucrose in water $D = 5 \times 10^{-10}$ m²/s is used in the calculation of the Péclet number Pe. Adapted from Rand (1983)

	Phloem	Xylem	Human aorta
Velocity u [m/s]	10^{-4}	10^{-3}	4×10^{-1}
Radius a [m]	10^{-5}	10^{-4}	1.5×10^{-2}
Viscosity η [Pa s]	2×10^{-3}	10^{-3}	3×10^{-3}
Density ρ [kg/m³]	$\sim 10^3$	$\sim 10^3$	$\sim 10^3$
Reynolds number ($\text{Re} = \rho u a/\eta$)	5×10^{-4}	10^{-1}	2×10^3
Péclet number ($\text{Pe} = ua/D$)	2	2×10^2	1.2×10^7
Schmidt number ($\text{Sc} = \eta/(\rho D)$)	4×10^3	2×10^3	6×10^3

flows of relevance for plants' vascular systems and similar micro-fluidic systems. This section should provide the physicist reader, inexperienced in fluid dynamics, with a useful introduction necessary for several later sections, as well as provide some terminology to be used in the rest of the review. Similarly, we do not assume the reader to have prior knowledge on plant physiology, and Sec. III gives a review of the relevant aspects of plant anatomy and physiology, in particular the vascular system. Thus, the phloem, the xylem and the leaves are described without going into too much detail, but providing the reader with the necessary terminology as well as theoretical and experimental background for the rest of the review.

In Section IV on sugar transport in plants, we shall first discuss the available data on phloem flow translocation. After that we discuss various biomimetic models for osmotically driven sugar transport akin to the phloem. We then give a simplistic "hydraulic resistor" theory for the phloem flow, leading to the optimality criterion for the diameter of the sieve tubes, limits to leaf sizes and optimal sugar concentrations.

Then, in Section V, we shall embark on the more detailed hydrodynamical theory of the flow in the phloem, the so-called Münch-Horwitz equations, including some analytical solutions for both transient and stationary flow, allowing us to return to the optimality question in a more consistent way. After this we shall briefly discuss the so-called *unstirred layers*, beyond the Münch-Horwitz equations, occurring due to inhomogeneities in osmotic flows and reducing the osmotic efficiency.

In Section VI, we take up the water transport in the xylem. After an experimental subsection, we shall discuss the details of the Cohesion-Tension theory and the role of the *bordered pits* controlling the water -and air flow between neighbouring xylem tubes. We shall conclude the section by reviewing recent results on conduit optimization and on the combined water/sugar translocation in the leaves, specifically in connection with the "polymer-trap" loading mechanism.

A large body of literature has been devoted to plant vascular biology, and for each topic discussed we have attempted to give references to the relevant literature. For textbook introductions to plant biology, the reader may wish to consult Evert (2006); Morris *et al.* (2013); Nobel (2009); Raven *et al.* (2005); Taiz and Zeiger (2010) and Canny (1973); Crafts and Crisp (1971); Holbrook and Zwieniecki (2005); Kramer and Boyer (1995); Niklas (1994); Tyree and Zimmermann (2002); Vogel (2013) for more comprehensive discussions of vascular physiology and plant biomechanics. There are also several review type papers related to the topics we cover which the reader may wish do consult. The following is a partial list: Boyer (1985); De Schepper *et al.* (2013); Dumais and Forterre (2012); Gibson (2012); MacRobbie (1971); Pickard (1981); Rand (1983); Stroock *et al.* (2014). In some ways one can think of the present review as a follow-up of the impressive earlier reviews by Pickard (1981), Rand (1983), and Stroock *et al.* (2014) which also stressed the physical mechanisms involved in sap translocation, but with the emphasis primarily on the xylem. In the present paper, the physical modeling has more focus on the phloem (Secs. IV–V) since the fascinating fluid mechanics of osmotically driven flows has, in our opinion, not quite received the attention it deserves.

II. TRANSPORT AT LOW REYNOLDS NUMBERS

A. Microscale Hydrodynamics

We begin with a short review of transport in low-Reynolds-number flows of relevance to plants. This section should provide the reader with a useful introduction necessary for several later sections, as well as provide some terminology to be used in the rest of the review.

The flow of sap (aqueous solutions of nutrients) in the sub-millimeter-diameter conduits inside plants, Fig. 1(d) and (e), is described using classical continuum theory in the microfluidic regime as treated in textbooks by Berthier and Silberzan (2010); Bruus (2008); Kirby (2010); Tabeling (2005). Theoretically, the basic entity in microfluidics, and hydrodynamics in general, is the so-called liquid particle. In the Eulerian picture, this particle is a small region $\Omega(\boldsymbol{r})$ of volume ΔV centered around the fixed position $\boldsymbol{r}$. The detailed molecular properties of the liquid are replaced by averages over molecules i with mass m_i and momentum $m_i \boldsymbol{v}_i$ present in this volume at time t, and thus the classical continuum description is used involving the density field $\rho(\boldsymbol{r}, t)$ (mass per volume), the velocity field $\boldsymbol{v}(\boldsymbol{r}, t)$ (momentum per mass in the volume), and the pressure field $p(\boldsymbol{r}, t)$ (normal force per area). This averaging typically requires ΔV to be $(10 \text{ nm})^3$ or larger.

For brevity we often suppress the arguments $\boldsymbol{r}$ and t in the following.

The sap in plants is well described as incompressible, Newtonian liquids with viscosity η. The viscosity combined with the narrow conduits in plants results in such low flow speeds $\boldsymbol{v}$ that non-linear velocity terms can be neglected. This approximation is valid when the dimensionless Reynolds number Re is small,

$$\text{Re} = \frac{UL}{\nu} \ll 1, \quad \text{with} \quad \nu = \frac{\eta}{\rho}. \quad (1)$$

Here L is the characteristic width of the conduit, U is a characteristic flow speed, and ν is the kinematic viscosity. For sap in the phloem $\nu \approx 2 \times 10^{-6}$ m^2/s, and with a maximum flow speed of $U \approx 0.1$ mm/s in a 10-μm-radius plant cell we obtain Re $\approx 5 \times 10^{-4}$. This number and other characteristic numbers for microfluidic flows in plants is given in table I.

Further simplifications can be obtained by noting that the body force density $\boldsymbol{g} = -g\boldsymbol{e}_z$ due to gravity is balanced by the hydrostatic pressure p_{hs},

$$p_{\text{hs}} = -\rho g z, \quad (2)$$

so henceforth gravity is left out of the flow equations for the sap and p is without p_{hs}. With these simplifications, we arrive at the governing equations for plant microfluidics, the Stokes and continuity equations expressing the conservation of momentum and mass in the sap,

$$\rho \frac{\partial \boldsymbol{v}}{\partial t} = -\boldsymbol{\nabla} p + \eta \nabla^2 \boldsymbol{v}, \quad \text{with } \boldsymbol{\nabla} \cdot \boldsymbol{v} = 0. \quad (3a)$$

The most common boundary condition on the sidewalls of a liquid-carrying channel is the no-slip condition,

$$\boldsymbol{v}(\text{at wall}) = \boldsymbol{v}_{\text{wall}}, \quad (= \boldsymbol{0} \text{ for stationary walls}). \quad (3b)$$

By taking the divergence of Eq. (3a) and then using the incompressibility condition $\boldsymbol{\nabla} \cdot \boldsymbol{v} = 0$, it is seen that the pressure must be a solution to the Laplace equation,

$$\nabla^2 p = 0. \quad (3c)$$

As a first example, we study the classical steady ($\partial \boldsymbol{v}/\partial t = \boldsymbol{0}$) Poiseuille flow in an infinitely long cylindrical pipe of radius a centered on the x-axis driven by a pressure difference which drops from $p = \Delta p$ to $p = 0$ over the finite section of the pipe between $x = 0$ and $x = L$, Fig. 1(d). The symmetry of the problem favors the use of cylindrical coordinates (r, x) for which $\nabla^2 = \frac{\partial^2}{\partial r^2} + \frac{1}{r}\frac{\partial}{\partial r} + \frac{\partial^2}{\partial x^2}$, and it leads to an axisymmetric solution, where the pressure only depends on z as $p = p(x)$, while the velocity field is parallel to the z-axis, but depends only on the radial coordinate $r = \sqrt{y^2 + z^2}$, $\boldsymbol{v}(r, x) = v_x(r)\,\boldsymbol{e}_x$. Since $\nabla^2 p(x) = 0$ leads to a linear pressure drop, we obtain

$$p = \left(1 - \frac{x}{L}\right)\Delta p, \quad (4a)$$

$$\frac{\partial^2 v_x(r)}{\partial r^2} + \frac{1}{r}\frac{\partial^2 v_x(r)}{\partial r^2} = \frac{1}{\eta}\frac{\partial p}{\partial x} = -\frac{\Delta p}{\eta L}, \quad (4b)$$

yielding the well-known paraboloid velocity profile $v_x(r)$,

$$v_x(r, x) = \frac{\Delta p}{4\eta L}\left(a^2 - r^2\right), \quad \text{fulfilling } v_x(a, x) = 0. \quad (4c)$$

By integration of the velocity profile across a circular cross section, we obtain the volumetric flow rate Q and the hydraulic resistance $R_{\text{hyd}}^{\text{poi}}$ defined by the Hagen–Poiseuille relation $\Delta p = R_{\text{hyd}}^{\text{poi}} Q$,

$$Q = \int_0^a 2\pi r v_x(r)\,\mathrm{d}r = \frac{\pi a^4}{8\eta L}\,\Delta p, \quad (4d)$$

$$R_{\text{hyd}}^{\text{poi}} = \frac{8\eta L}{\pi a^4}. \quad (4e)$$

Using that $\Delta p/L = -\partial p/\partial x$, we get the Darcy equation

$$\frac{\partial p}{\partial x} = -\frac{8\eta}{\pi a^4}\,Q = -\frac{\eta}{k}\,\bar{v}, \quad \text{with} \quad \bar{v} = \frac{Q}{\pi a^2}, \quad (5)$$

where $\bar{v}$ is the flow speed averaged over the cross section, and k is a coefficient of dimension length squared. Allowing k to be weakly dependent on the axial position ($\partial k/\partial x \ll k/a$), Eq. (5) describes what is known as Darcy flow. The same equation can also describe the situation, where $\bar{v}$ changes weakly with axial position, e.g. due to influx of liquid through weakly permeable side walls, see Sec. II.D.

The Poiseuille flow is a first illustration of the fact that for steady low-Reynolds-number flow, the length scale over which the velocity field is changing is entirely set by the geometry of the confining channel, here the radius a of the cylindrical pipe. A second, and less trivial example of this, is the entrance length, the distance ℓ into the pipe over which a non-paraboloid velocity profile $v_z(0, r)$ at the inlet $z = 0$ relaxes to the paraboloid Poiseuille profile Eq. (4c) with its linear pressure drop Eq. (4a), in the following denoted $v_x^{\text{poi}}(r)$ and $p^{\text{poi}}(x)$, respectively. Splitting off the Poiseuille solution in a sum of two solutions, we write the fields as

$$v_x(r, x) = \hat{v}_x(r, x) + v_x^{\text{poi}}(r), \quad (6a)$$

$$p(r, x) = \hat{p}(r, x) + p^{\text{poi}}(r), \quad (6b)$$

and seek to determine $\hat{v}_x$ and $\hat{p}$. The starting point is $\nabla^2 \hat{p} = \nabla^2 p - \nabla^2 p^{\text{poi}} = 0$, and the fact that far from the entrance $\hat{p}(r, \infty) = 0$ since $p(r, \infty) = p^{\text{poi}}(r)$. The pressure $\hat{p}(r, x)$ can therefore be written as a Fourier-Bessel series decaying in the axial direction $x \to \infty$, known to solve the Laplace equation,

$$\hat{p}(r, x) = p_0 \sum_{n=0}^{\infty} c_n\, J_0(k_n r)\, e^{-k_n x}, n = 1, 2, 3, \ldots \quad (6c)$$

where J_0 is the Bessel function of the first kind of order zero with roots $k_n a$, $J_0(k_n a) = 0$, and with expansion coefficients c_n to be determined below. It is verified by
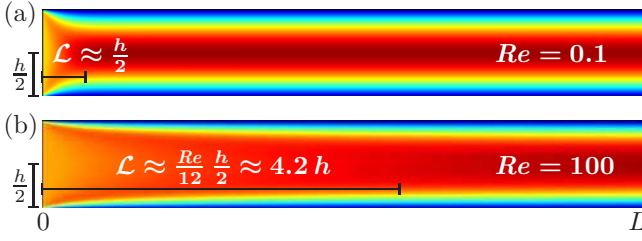
Figure 2   Color plots of the axial velocity from zero (dark blue) to $v_x^{\max}$ (dark red) in a cylindrical channel (side view) of length L and radius a. The velocity field on the inlet to the left is set to be a constant. (a) In the low Reynolds number limit (Re = 0.1) the entrance length over which a full Poiseuille flow profile is established is given by $\ell \approx a$. (b) In the medium Reynolds number limit (Re = 100) the entrance length is given by Re $\approx \frac{\text{Re}}{24} a$. From Bruus (2011).
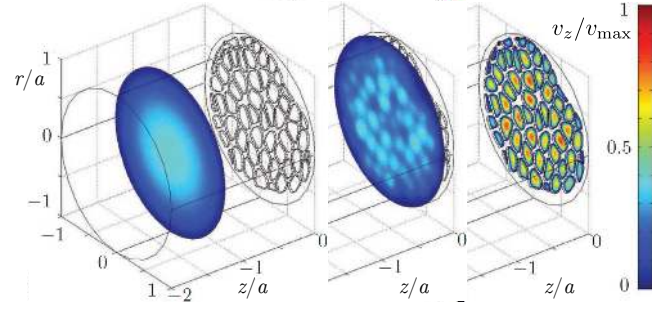

Figure 3   Numerical simulation of the flow moving from left to right close to a *Curcubita maxima* sieve plate with multiple irregularly shaped pores in a cylindrical pipe. Pore structures were extracted from scanning electron microscopy images (Mullendore *et al.*, 2010). Three color plots of the normalized magnitude $v(r,x)/v_{\max}$ of the flow velocity (from blue zero to red unity) at distances $z = 2.5a$, $0.25a$, and $0.05a$ from the sieve plate. The flow profile is seen to adapt from the Poiseuille paraboloid to each of the many pores within a distance of a few times a from the sieve plate. As originally published in Jensen et al., Front. Plant Sci. 3, 151 (2012) (Jensen *et al.*, 2012c).

direct substitution that the solution to the Stokes and continuity equations is

$$\hat{v}_r(r,x) = \sum_{n=0}^{\infty} \frac{p_0}{2\eta} \frac{c_n}{k_n} \left(-k_n x\right) J_0'(k_n r)\, e^{-k_n x}, \qquad (6\text{d})$$

$$\hat{v}_x(r,x) = \sum_{n=0}^{\infty} \frac{p_0}{2\eta} \frac{c_n}{k_n} \left(k_n x + 1\right) J_0(k_n r)\, e^{-k_n x}. \qquad (6\text{e})$$

The expansion coefficients are determined from the velocity profile $v_x(r,0)$ at the entrance, which in terms of $\hat{v}_x$ becomes $\hat{v}_x(r,0) = v_x(r,0) - v_x^{\text{poi}}(r)$

$$c_n = \int_0^a \frac{\eta k_n r \left[v_x(r,0) - v_x^{\text{poi}}(r)\right]}{p_0 \left[a J_0'(k_n a)\right]^2} J_0(k_n r)\, \mathrm{d}r \qquad (6\text{f})$$

The important implication of this analysis is as follows: the distance ℓ along the axial direction over which the velocity profile relaxes to the Poiseuille paraboloid is given by using the smallest Bessel-function root in the argument of the exponential decaying term, $k_1 \ell = 1$ or $\ell = 1/k_1 \approx a/2.4048$. This result is illustrated in Fig. 2(a), which is a numerical simulation of the velocity field, given a constant inlet velocity profile $v_x(r,0) = v_0$ at $x = 0$ for the low Reynolds number Re = 0.1. In Fig. 2(b) is shown how this result is modified for the larger Reynolds number Re = 100, for which the advective term $\rho(\boldsymbol{v}\cdot\boldsymbol{\nabla})\boldsymbol{v}$ present in the full Navier–Stokes equation, but not in the approximate Stokes equation (3a), leads to an enhanced entrance length $\ell \approx \frac{1}{12}\text{Re}\, a \approx 8.4a$. A similar effect is shown in Fig. 3. Here, modeling a sieve plate with multiple pores in a plant cell, Fig. 1(d), a low-Reynolds-number pressure-driven flow is moving towards a sieve plate in a cylindrical tube (mathematically equivalent to the flow away from a sieve plate). The flow profile at the sieve plate adopts to the individual pores with local maxima at the centers of the pores, while the Poiseuille paraboloid is established in the main tube a few times the tube radius a away from the sieve plate.

Next, we consider the flow rate q through a single pore in a sieve plate based on Eq. (3a) in steady-state, $\partial \boldsymbol{v}/\partial t = \boldsymbol{0}$. For a circular pore of radius a in an infinitely thin plate with a pressure drop Δp_{smp} applied across the pore as shown in Fig. 4(a), the hydraulic resistance $R_{\text{hyd}}^{\text{smp}}$ and circular flow profile $v_x(r)$ inside the pore was obtained by Sampson (1891) and later improved by Roscoe (1949),

$$R_{\text{hyd}}^{\text{smp}} = \frac{\Delta p_{\text{smp}}}{q} = \frac{3\eta}{a^3}, \qquad (7\text{a})$$

$$v_x(r) = \frac{\Delta p_{\text{smp}}}{2\pi\eta}\sqrt{a^2 - r^2}, \qquad (7\text{b})$$

where r is the distance in the pore to the center of the pore. A simple scaling argument explains the form of Eq. (7a): Hydraulic resistance has the unit $\text{Pa}\,\text{s}/\text{m}^3$, viscosity has the unit $\text{Pa}\,\text{s}$, while the infinite plane with a circular hole has the radius a as the only length scale, consequently $R_{\text{hyd}}^{\text{smp}} \propto \eta/a^3$, only missing the factor 3. A real pore plate has a finite thickness d, so inside the pore a Poiseuille flow develops, Fig. 4(b), adding to the total hydraulic resistance $R_{\text{hyd}}^{\text{pore}}$ of a single pore. Thus, for a pore flow with Re $\ll 1$, $R_{\text{hyd}}^{\text{pore}}$ is well approximated by the sum of the Sampson and Poiseuille flow resistances (Dagan *et al.*, 1982; Weissberg, 1962),

$$R_{\text{hyd}}^{\text{pore}} \approx R_{\text{hyd}}^{\text{smp}} + R_{\text{hyd}}^{\text{poi}} = \frac{3\eta}{a^3} + \frac{8\eta d}{\pi a^4} = \frac{3\eta}{a^3}\left[1 + \frac{8d}{3\pi a}\right]. \quad (8)$$

The error turns out to be greatest when $d = 2a$, but it is less than 1% for all values of d/a. Recently, Jensen
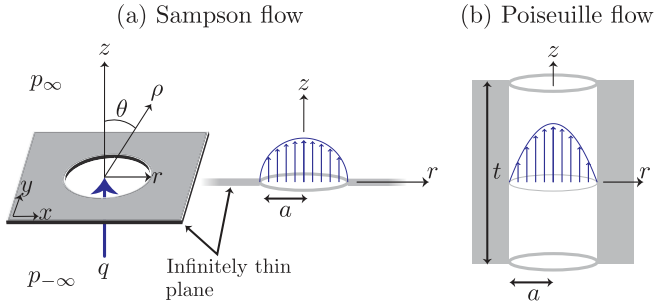
(a) Sampson flow   (b) Poiseuille flow

Figure 4 (a) Sampson flow defined as a pressure-driven flow through a circular pore of radius a in an infinitely thin plate. The pressure drop is $\Delta p_{\mathrm{smp}} = p_{-\infty} - p_{\infty}$, and the flow rate is q. (b) Poiseuille flow along a pore of length t equal to the the thickness d of the plate. At low Reynolds numbers, the flow resistance is well approximated by adding the flow resistance from the Sampson and Poiseuille flow, see Eq. (8). Adapted from Jensen et al. (2014).

et al. (2014) analyzed various corrections to the expression for the single-pore hydraulic resistance $R_{\mathrm{hyd}}^{\mathrm{pore}}$. For liquids flowing through a plate of thickness d with a regular array of identical circular pores of radius a with a characteristic distance ℓ_{p} between neighboring pores, the flow pattern from one pore is influenced by that of the neighboring pores (hydrodynamic interaction), and inertial effects enter through the Reynolds number Re, resulting in corrections characterized by a term $G(a/\ell_{\mathrm{p}})^3$ and $f(\mathrm{Re})$, respectively,

$$R_{\mathrm{hyd}}^{\mathrm{array}} = \frac{3\eta}{a^3}\left[1 + \frac{8d}{3\pi a} - G\frac{a^3}{\ell_{\mathrm{p}}^3} + f(\mathrm{Re})\right]. \qquad (9a)$$

where G is a factor which depends on the geometry of the array, but is typically around 2 (Jensen et al., 2014). Similarly, for an ensemble of pores with a statistical distribution $P(a)$ of pore radii a with mean value $\bar{a}$ and dimensionless statistical moments $M_n = \int \xi^n \bar{a} P(\bar{a}\xi)\,\mathrm{d}\xi$ with $\xi = a/\bar{a}$, they found the average hydraulic resistance per pore $\langle R_{\mathrm{hyd}}^{\mathrm{pore}}\rangle$ to be given by

$$\left\langle R_{\mathrm{hyd}}^{\mathrm{pore}}\right\rangle = \frac{3\eta}{\bar{a}^3}\left[\frac{1}{M_3} + \frac{1}{M_4}\frac{8d}{3\pi\bar{a}}\right], \qquad (9b)$$

where hydrodynamic interactions and inertial effects have been neglected. The relative magnitude of the former is estimated as $G\frac{a^3}{\ell_{\mathrm{p}}^3} \approx 2\times\left(\frac{1}{3}\right)^2 \approx 0.1$ and of the latter by $\mathrm{Re} \approx 5\times 10^{-4}$ (see Table I). It is interesting in this context to mention that recent theoretical estimates show relative changes of 20 % in the sap flow through bordered pit membranes when electroviscous effects are included from ions in and just outside the membrane (Santiago et al., 2013).

B. Advection-diffusion Phenomena

To study the transport of suspended particles or molecules in microfluidics, we introduce for the solute species α in a given solvent, the concentration field $c_\alpha(\boldsymbol{r}, t)$ defined as the number of molecules per volume of species α in a small neighborhood of the point $\boldsymbol{r}$ and thus having the SI unit m^{-3}. The governing equation of the field c_α is the so-called advection-diffusion equation,

$$\frac{\partial c_\alpha}{\partial t} + \boldsymbol{\nabla}\cdot(\boldsymbol{v}c_\alpha) = D_\alpha\nabla^2 c_\alpha + \Upsilon, \qquad (10)$$

where Υ is a bulk source term (SI unit m^{-3}s^{-1}) and D_α is the diffusivity (SI unit m^2/s) of solute α in the given solvent. Using the incompressibility condition $\boldsymbol{\nabla}\cdot\boldsymbol{v} = 0$ we can rewrite it as

$$\frac{\partial c_\alpha}{\partial t} + (\boldsymbol{v}\cdot\boldsymbol{\nabla})c_\alpha = D_\alpha\nabla^2 c_\alpha + \Upsilon, \qquad (11)$$

Typical values of the diffusivity in water at room temperature are $D_{\mathrm{ion}} \approx 2\times 10^{-9}$ m^2/s (elementary ions), $D_{\mathrm{sug}} \approx 5\times 10^{-10}$ m^2/s (sucrose), and $D_{\mathrm{GFP}} \approx 9\times 10^{-11}$ m^2/s (green fluorescent protein).

Without advection, $\boldsymbol{v} = \boldsymbol{0}$, we retrieve the usual diffusion equation for $c_\alpha(\boldsymbol{r}, t)$. A standard example is to place N_0 molecules of species α in a point-like volume at the center of the coordinate system in an infinite volume. This results in the well-known Gaussian solution,

$$\frac{\partial c_\alpha}{\partial t} = D_\alpha\nabla^2 c_\alpha, \quad c_\alpha(\boldsymbol{r}, t) = \frac{N_0}{(4\pi D_\alpha t)^{\frac{3}{2}}}\,\mathrm{e}^{-\frac{r^2}{4D_\alpha t}}. \quad (12)$$

From this and the variance $\langle r^2(t)\rangle = \int r^2 c(\boldsymbol{r}, t)\mathrm{d}V = 6D_\alpha t$, we are lead to introduce the diffusion length ℓ_{diff} for a given diffusion time t_{diff} through the root-mean-square value of the variance of distance r,

$$\ell_{\mathrm{diff}}(t_{\mathrm{diff}}) = \sqrt{\langle r^2(t_{\mathrm{diff}})\rangle} = \sqrt{2dD_\alpha t_{\mathrm{diff}}}, \qquad (13)$$

for diffusion in d spatial dimensions.

Characteristic times $t_{\mathrm{diff}} = \ell_{\mathrm{diff}}^2/(2D_\alpha)$ for diffusion along a tube of length $\ell_{\mathrm{diff}} = 1$ mm are $t_{\mathrm{diff}}^{\mathrm{ion}} = 250$ s, $t_{\mathrm{diff}}^{\mathrm{sug}} = 1000$ s, and $t_{\mathrm{diff}}^{\mathrm{GFP}} = 5556$ s.

With advection, $\boldsymbol{v} \neq \boldsymbol{0}$, based on Eq. (11) and in analogy with the Reynolds number Eq. (1), we introduce for the typical concentration $c_\alpha = c_0$, velocity $|\boldsymbol{v}| = U$, and length scale L of concentration variations, the Péclet number Pe, the ratio between transport by advection and by diffusion,

$$\frac{|(\boldsymbol{v}\cdot\boldsymbol{\nabla})c_\alpha|}{|D_\alpha\nabla^2 c_\alpha|} \approx \frac{U\dfrac{1}{L}c_0}{D_\alpha\dfrac{1}{L^2}U} = \frac{UL}{D_\alpha}, \quad \text{so} \quad \mathrm{Pe} = \frac{UL}{D_\alpha}. \quad (14)$$

Advection is dominating for Pe $\gg 1$ (say large U, large L and/or small D_α), while diffusion is dominating for

Pe $\ll 1$ (say small U, small L and/or large D_α). The Péclet number can also be introduced by considering the time scale for diffusion, $t_{\mathrm{diff}} = L^2/D_\alpha$, which follows from $\partial c_\alpha/\partial t = D_\alpha \nabla^2 c_\alpha$, and for advection, $t_{\mathrm{adv}} = L/U$, which follows from $\partial c_\alpha/\partial t = -(\boldsymbol{v} \cdot \boldsymbol{\nabla})c_\alpha$, as $\mathrm{Pe} = t_{\mathrm{diff}}/t_{\mathrm{adv}} = UL/D_\alpha$.

Another aspect of advection-diffusion phenomena is the different time scales associated with the relaxation of velocity gradients and of concentration gradients. The former is given by the diffusivity ν of momentum, Eq. (1), derived from the Stokes equation (3a) setting $\boldsymbol{\nabla}p$ to zero, $\partial\boldsymbol{v}/\partial t = \nu\nabla^2 v$ and the latter by the mass diffusivity D_α of the solute. The ratio of these time scales is the Schmidt number Sc,

$$\mathrm{Sc} = \frac{t_{\mathrm{diff}}^{\mathrm{mass}}}{t_{\mathrm{diff}}^{\mathrm{mom}}} = \frac{\nu}{D_\alpha}. \qquad (15)$$

A typical value for aqueous solutions is $\mathrm{Sc} = 10^3$, which implies that the velocity field in a given advection-diffusion problem adjusts to changes much faster than the solute concentration profile. Consequently, it is often a good approximation to treat the velocity field as being in a steady state, while the solute concentration is time dependent.

As an example of this faster relaxation of the flow than of the solute concentration profile, we can use Fig. 2(a). Here $\mathrm{Re} = 0.1$, and now consider a solute entering at the inlet with a concentration c_0 in the lower half and zero in the upper half having $\mathrm{Sc} = 4 \times 10^3$, see Table I. The ratio $t_{\mathrm{diff}}/t_{\mathrm{adv}}$ of the times it takes the solute to diffuse the same distance across as it advects along is given by $t_{\mathrm{diff}}/t_{\mathrm{adv}} \approx \frac{1}{8}\,\mathrm{Sc}\,\mathrm{Re} \approx 50$. In the given situation, it thus requires a length L being 50 times the half-height $\frac{1}{2}h$ for the solute to have relaxed completely by diffusion, while the flow is already relaxed on the length h.

C. Osmosis and the Water Potential

In plants, due to the presence of ion-selective membranes at the cell walls (see Sec. III), liquid can be moved by a difference in the osmotic pressure Π caused by a difference in concentration c of some solute (nutrient) on either side of the membrane, Fig. 1(a) and (b). For dilute concentrations, Π is given in terms of the gas constant R, the absolute temperature T and the concentration c by the classical van 't Hoff relation (Nobel, 2009),

$$\Pi = RT\,c. \qquad (16)$$

With this given, we can introduce the potential Ψ (SI-value $\mathrm{J/m^3} = \mathrm{Pa}$) referred to as the "water potential" by plant biologists (Nobel, 2009). The water potential is responsible for moving water through a plant, and when osmosis across an ideal membrane is involved, it is given as

$$\Psi = (p - \Pi - p_{\mathrm{hs}}) - p_0 \approx p - p_0 - RTc + \rho g z, \quad (17)$$

where p is the pressure of water at height z with solute concentration c, and p_0 is the reference atmospheric pressure at reference height zero (typically ground level). The osmotic pressure Π of Eq. (16) and the hydrostatic p_{hs} of Eq. (2) represent the effects of changes in solute concentration and gravitational energy, respectively, going from the reference point to the probing point. For this case of an ideal membrane completely impermeable to the solute, the osmotic velocity v_0 of water at the membrane is given in terms of the difference $\Delta\Psi$ in the water potential Ψ, and the membrane conductance L_p or water permeability [SI-unit $\mathrm{m/(Pa\,s)}$] as,

$$v_0(z) = -L_p\Delta\Psi = L_p(RT\Delta c - \Delta p). \qquad (18)$$

Plant cells are elastic, and will swell and shrink in response to changes in the osmotic pressure. If, following Dumais and Forterre (2012), we consider a cell with initial volume V_0, bulk modulus $\epsilon = V(\partial P/\partial V)$ and area A, suddenly exposed to a change π in osmotic pressure, we get from Eq. (18)

$$\frac{dV}{dt} \approx AL_p\left(\pi - \frac{\epsilon}{V_0}(V - V_0)\right) \qquad (19)$$

which shows that V will approach its new value $V_f = V_0(1 + \pi/\epsilon)$ exponentially on the time scale

$$t_\epsilon = \frac{V_0}{AL_p\epsilon} \approx \frac{R}{L_p\epsilon} \qquad (20)$$

where R is a characteristic length scale of the cell. With typical values for sieve tubes: $\epsilon \approx 30$ MPa, $L_p \approx 5\times10^{-14}$ m s^{-1} Pa^{-1} and $R \approx 10$ μm, we get $t_\epsilon \approx 7$ s. Only well above this time scale will our "rigid" approach to the water flow be valid. However, since it is relatively short compared to diurnal variations in plant vascular transport patterns, we shall neglect it in the following.

For non-ideal membranes, partly permeable to the solute, the flux density J_w of water (flow rate per area having the SI unit m/s) and that of the solute J_s (number flow rate per area having the SI unit $\mathrm{m^{-4}s^{-1}}$) are coupled since the solvent is partially dragged by the water and the osmosis is weakened by solute leaking. The appropriate equations were given by Kedem and Katchalsky (1958). They are derived on the basis of linearized non-equilibrium thermodynamics, assuming the system to be nearly in equilibrium. Expressing the "fluxes" J_w and J_s in terms of the two "driving forces", Δp and Δc across the membrane, one can utilize the symmetry of the kinetic coefficients to reduce the number of coefficients from four to three and write

$$J_w = L_p\big[\Delta p - (1-W)\Delta\Pi\big] = L_p\big[\Delta\Psi + W\Delta\Pi\big], \quad (21a)$$

$$J_s = W J_w\bar{c} + \frac{1}{d}D\Delta c, \qquad (21b)$$

here expressed in terms of the advective *hindrance factor* W of Dechadilok and Deen (2006) instead of the reflection coefficient $\sigma = 1 - W$ used by Kedem and Katchalsky

(1958). An ideal membrane has $W = 0$. D is the diffusivity of the solute, d is the thickness of the membrane, and $\bar{c}$ entering the advective term is the average concentration across the membrane. This framework is appropriate for small Péclet numbers, where the concentration will vary approximately linearly across the membrane. For more details, see the textbooks by Schultz (1980) and Nobel (2009). Recent reviews include Kargol and Kargol (2003) and Wang *et al.* (2014). Note that, for flow through such a leaky membrane, the water potential does not necessarily have to decrease. As can be seen from Eq. (21a) the water flow can be positive, i.e., go from 1 to 2, even for negative $\Delta\Psi$, as long as $\Delta\Psi > -W\Delta\Pi$ since the diffusing sugar will drag along water. We shall have the opportunity to use this formalism in Sec. VI.C.

D. Flow in Tubes with Membrane Walls

An example of relevance for plant microfluidics including osmosis, Fig. 1(b), is the Aldis flow (Aldis, 1988b). This flow is defined as a pressure-driven flow through a cylindrical tube radius a and having a section of the wall of length L consisting of a permeable membrane through which a radial osmotically-driven flow v_0 enters, see Fig. 5. This model forms the basis for the analysis of osmotically-driven flow in the phloem of plants. In the following we consider an axisymmetric system and use cylindrical coordinates (r, x). We employ the notation that the solvent velocity field is $\boldsymbol{v} = v_r(r, x)\boldsymbol{e}_r + v_x(r, x)\boldsymbol{e}_x$, the azimuthal velocity component is $v_\phi = 0$, the in-tube pressure is $p(r, x)$, the radial component of the osmotically-driven flow through the membrane is $v_0(x)$, while the difference in solute concentration across the membrane is $c(x)$. In steady state, Eq. (3a) for this problem becomes,

$$\frac{1}{r}\frac{\partial}{\partial r}\left(r\frac{\partial v_r}{\partial r}\right) - \frac{1}{r^2}v_r + \frac{\partial^2 v_r}{\partial x^2} = \frac{1}{\eta}\frac{\partial p}{\partial r}, \qquad (22a)$$

$$\frac{1}{r}\frac{\partial}{\partial r}\left(r\frac{\partial v_x}{\partial r}\right) + \frac{\partial^2 v_x}{\partial x^2} = \frac{1}{\eta}\frac{\partial p}{\partial x}, \qquad (22b)$$

$$\frac{1}{r}\frac{\partial(rv_r)}{\partial r} + \frac{\partial v_x}{\partial x} = 0. \qquad (22c)$$

The boundary conditions along the center axis $r = 0$ is the usual $v_r = 0$, whereas at the wall $r = a$, the tangential velocity vanishes while the inward radial velocity is $-v_0$,

$$v_r(0, x) = 0, \qquad v_r(a, x) = -v_0(x), \qquad (23a)$$

$$\frac{\partial}{\partial r}v_x(0, x) = 0, \qquad v_x(a, x) = 0. \qquad (23b)$$

In the limit of a long narrow tube, $a \ll L$, the so-called lubrication limit, we expect $\frac{\partial}{\partial r} \simeq 1/a$ and $\frac{\partial}{\partial x} \simeq 1/L$. This together with the continuity equation (22c) implies that $v_r \simeq (a/L)v_x \ll v_x$, and thus from Eqs. (22a)
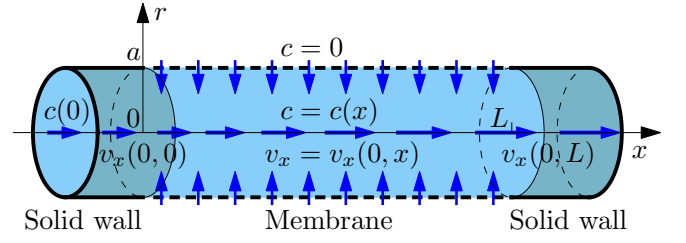

Figure 5 Aldis flow through a cylinder of radius a, of which a section of length L of the wall (dashed) consists of a semipermeable membrane through which a radial flow (small vertical arrows) enters, driven by an osmotic difference in solute concentration c between the internal and external liquids. The axial Poiseuille flow increases (horizontal arrows) for $0 < x < L$ due to the radial inflow.

and (22b) that $\partial p/\partial r \simeq (a/L)\partial p/\partial x \ll \partial p/\partial x$. To leading order in (a/L) we can therefore disregard the r-component of the Stokes equation (22a). Turning to the x-component Eq. (22b), we need to find an expression for the x-dependent pressure gradient $\partial p/\partial x$. This is provided by the Darcy law Eq. (5) using the form involving Q. At the position x, the flow rate is the surface integral of all fluid influx through the side wall between 0 and x, and consequently

$$\frac{1}{\eta}\frac{\partial p}{\partial x} = -\frac{8}{\pi a^4}Q = -\frac{16}{a^3}\int_0^x v_0(x')\,\mathrm{d}x'. \qquad (24a)$$

Inserting this result into Eq. (23b) together with the ansatz $v_x(r, x) = R(r)\int_0^x v_0(x')\,\mathrm{d}x'$, and neglecting the term $\partial^2 v_x/\partial x^2 \simeq v_x/L^2$ relative to $\partial^2 v_x/\partial r^2 \simeq v_x/a^2$ leads to an ordinary differential equation for $R(r)$, $\frac{1}{r}\frac{\partial}{\partial r}(r\frac{\partial}{\partial r}R) = -16/a^3$. The solution fulfilling the boundary conditions Eq. (23b) is $R(r) = (4/a)(1 - r^2/a^2)$, which determines v_x, which upon insertion into Eq. (22c) leads to an equation for v_r. The resulting Aldis velocity field is

$$v_r(r, x) = \left[\frac{r^3}{a^3} - 2\frac{r}{a}\right]v_0(x), \qquad (24b)$$

$$v_x(r, x) = \left[1 - \frac{r^2}{a^2}\right]\frac{4}{a}\int_0^x v_0(x')\,\mathrm{d}x'. \qquad (24c)$$

To relate pressure and velocity, we use Eq. (18) for the osmotic velocity together with the cross-sectional average $\langle v_x \rangle = Q/(\pi a^2)$ and Eq. (24a) to obtain

$$\left\langle\frac{\partial v_x}{\partial x}\right\rangle = \frac{1}{\pi a^2}\frac{\partial Q}{\partial x} = \frac{2}{a}v_0(x) = \frac{2L_p}{a}(RTc - p). \qquad (25)$$

This expression is the starting point for analysis of the Münch model for sugar transport in the phloem, see Sec. V.

E. Free Surfaces

A free interface between a liquid and a gas contains a certain free energy per area, denoted the surface tension γ (SI-unit J/m^2). This energy arises because a molecule of the liquid at the surface has fewer neighboring liquid molecules than one in the bulk of the liquid. The surface molecules have a higher free energy, since each neighboring liquid molecule contributes with a certain (negative) temperature-dependent cohesion energy, which ultimately is responsible for the existence of the liquid phase. For a given volume, the liquid tends to minimize its surface to lower the costly surface free energy. A curved surface therefore represents a higher free energy than a straight surface. In equilibrium, thermodynamic arguments (Bruus, 2008) leads to the so-called Young–Laplace law, which states that a non-zero mean radius of curvature R can only be maintained by a pressure difference Δp_{surf} across the interface,

$$\Delta p_{\mathrm{surf}} = \frac{1}{R}\,\gamma. \qquad (26)$$

For the surface between water and water-saturated air, the surface tension is $\gamma = 0.072$ J/m^2.

A liquid-gas interface touching the wall of a confining tube is furthermore characterized by the contact angle, defined as the angle between the tangents of the wall. For angles less than 90° (hydrophilic), the liquid is attracted by the wall surface stronger than the gas, while for angles larger than 90° (hydrophobic) the reverse is the case. If a liquid with a free surface is inside a hydrophilic capillary tube, a capillary rise results, where the liquid is sucked into the tube. The most hydrophilic case corresponds to $\theta = 0°$. For plant tissue, a range of contact angles have been measured, such as values from 42° to 55° for bordered pit chambers in various species (Zwieniecki and Holbrook, 2000), and in some cases this distributions has been accompanied by a second distribution of values clustering near 0° (Kohonen, 2006). For a tube with circular cross-section of radius a, the mean curvature of the liquid-gas surface is determined by a and the contact angle θ, and ΔP_{surf} becomes

$$\Delta p_{\mathrm{surf}} = \frac{2\cos\theta}{a}\,\gamma. \qquad (27)$$

For such a tube placed vertically, the liquid rises to height h, where the Young–Laplace pressure balances the hydrostatic pressure p_{hs}, Eq. (2), of the liquid column,

$$\rho g h = \frac{2\cos\theta}{a}\,\gamma. \qquad (28)$$

For a tube of radius $a = 1$ μm containing a water column interfacing with air, the resulting capillary rise height becomes $h = 14$ m for $\theta = 0°$ and $h = 9.6$ m for $\theta = 49°$. Capillary rise thus has the potential to play an important role in the transport of water in plants, and the details

of geometry and contact angles are crucial e.g., in the dynamics of the bordered pits connecting vessels in the xylem (Section VI) and protecting the plant against cavitation (Zwieniecki and Holbrook, 2000). Whether they are the primary source of the negative pressures in xylem is at present not fully understood, since gels in the cell walls of the mesophyll cells also have a strong potential for water absorption (Stroock et al., 2014).

F. Final remarks

In this section we have presented some basic and important concepts from continuum microscale hydrodynamics governing the flow of plant sap. In these flows viscosity dominates over inertia, and they are thus characterized by low Reynolds numbers, Re $\ll$ 1. In the framework of continuum fields, we briefly described the transport of solutes (nutrients) in various microchannels (phloem cells) adding to the complexity by including advection-diffusion processes, cellular sieve plates, osmosis and water potentials, semi-permeable membrane walls, and free surfaces. In the later sections of the paper we discuss the possible extension of these basic flow models to take into account the water transport across plasma membranes mediated by aquaporins, and water movement between cells mediated by the plasmodesmata.

In the theoretical description of microscale hydrodynamics in plants, a number of unresolved questions remain. One of these relates to a more complete understanding of the actual geometrical shape of the channels through which the biofluids are flowing. While the shape of the phloem cells themselves may be relatively well modeled, it is far more complex to describe and model the channel shapes in the inter-cellular space, as will be evident in the following section on the anatomy of the vascular tissues. Also, the extension of continuum hydrodynamics down to the nanometer scale of these structures must be done with care (Hansen et al., 2015).

Another unresolved question relates to the rheology of the biofluids. The high and variable content of sugars and other nutrients and of biomolecules in the sap, implies that the viscosity is not a constant and perhaps to other important non-Newtonian effects. Some of these can be handled within the framework of "generalized Newtonian" fluid dynamics (Bird et al., 1987), where the starting point is the stress tensor $\boldsymbol{\sigma}$ with components σ_{jk}, where $j,k = x,y,z$. It involves a shear viscosity $\eta(\partial\boldsymbol{v})$ and a dilatational viscosity $\zeta(\partial\boldsymbol{v})$, none of which are constant but depend on model-specific functions of the scalar invariants of the spatial derivatives of the velocity field $\boldsymbol{v}$, symbolically written as $\partial\boldsymbol{v}$,

$$\sigma_{jk} = -p\delta_{jk} + \eta\left[\frac{\partial v_j}{\partial x_k} + \frac{\partial v_k}{\partial x_j}\right] + \left[\frac{2}{3}\eta - \zeta\right]\frac{\partial v_k}{\partial x_k}\,\delta_{jk}.$$

Here δ_{jk} is the Kronecker delta, and we use the Einstein

summation convention of summing over repeated indices. With this general tensor formulation, the governing equation for the mass and momentum densities, ρ and $\rho\boldsymbol{v}$, for time-dependent, compressible flows become

$$\frac{\partial \rho}{\partial t} = -\frac{\partial \rho v_k}{\partial x_k},$$

$$\frac{\partial (\rho v_j)}{\partial t} = \frac{\partial \sigma_{jk}}{\partial x_k} - \frac{\partial (\rho v_j v_k)}{\partial x_k}, \text{ with } j, k = x, y, z.$$

where, ass one can see, the Newtonian governing equation (3a) is recovered for an incompressible flow with constant viscosity in the Low Reynolds number limit. A better description of the sap flow and sugar transport in plants can thus be obtained by employing an improved rheological model $\eta(\partial\boldsymbol{v})$ of the sap going beyond the simple Newtonian description presented in Sec. II.A. Such an improved rheological description must also contain the electroviscous effects briefly mentioned at the end of Sec. II.A. Indeed the role of this and other electrokinetic effects due to the ions in the sap needs to be clarified to understand the sap flow in plants better.

III. ANATOMY AND PHYSIOLOGY OF THE VASCULAR TISSUES

This section provides a broad overview of plant anatomy and physiology related to vascular transport. We focus on flow physics in subsequent sections, but note that it is necessary to know the basics of phloem anatomy (Sec. III.A) and xylem anatomy (Sec. III.C) to follow the later discussions.

The pathway of vascular transport in plants is fundamentally different from that of cardiovascular transport in animals. In plants, nutrients and assimilates move through the lumen of the conducting cells, and the cell wall of these cells forms the border of the transport pathway. In contrast, nutrients, electrolytes, oxygen and carbon dioxide as well as blood cells move through the lumen of blood vessels, the borders of which are formed by epithelial cells. Accordingly, long-distance vascular transport in plants takes intracellular pathways, while that in animals occurs extracellularly.

The vascular tissues in plants consist of assimilate-conducting phloem elements and xylem elements conducting water and mineral nutrients (Fig. 1). Vascular tissues link the organs specialized for water and nutrient uptake (roots) with the organs specialized for photosynthesis (mature leaves) where the assimilates (sugars and amino acids) are formed. The architecture of the vascular tissue in the different organs is quite diverse in different vascular plant *taxa*. However, a unifying feature of vascular tissues across nearly all taxa is that phloem and xylem run parallel to each other and that the conducting elements in each of the two tissues form an unbroken continuum between the uptake or loading sites and the
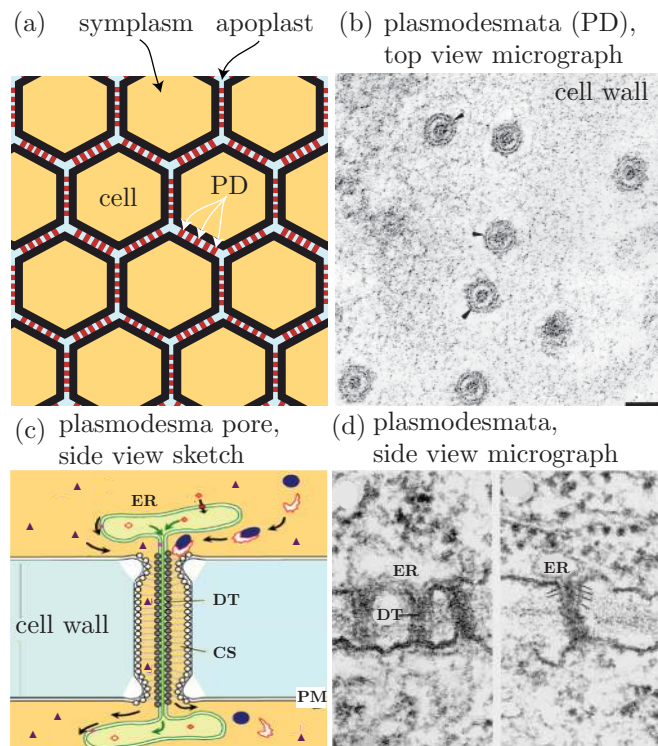

Figure 6 Sketch of plant tissue composed of the living supra-cellular symplasm and the external apoplast. (a) Plant cells (beige) bordered by the plasma membrane (black lines) and connected by narrow plasmodesmata channels (red lines) form the internal living symplasm. They are surrounded by the apoplast (blue) which is the water-filled cell wall matrix. (b) Eight plasmodesmata in the cell wall between two root cells (electron micrograph). (c) Schematic drawing of a plasmodesma pore connecting two cells by forming a channel through the cell wall lined by the plasma membrane (PM). The desmotubule (DT) - enclosed by the endoplasmic reticulum (ER) - fills the center of the pore. The annular space between the plasma membrane and the desmotubule (the cytoplasmic sleeve (CS) marked by arrowheads) allows passage of solutes (Δ) and viral nucleic acids (dark blue ellipsoids). Solutes inside the endoplasmic reticulum might be able to travel from cell to cell through the desmotubule. (d) electron micrographs showing longitudinal views of plasmodesmata. Scale bar = 50 nm. Adapted from (Schulz, 1995):(b,d) and (Schulz, 1999): (c).

delivery or unloading sites. For an in depth overview of the anatomy of vascular tissues in plants, see Evert (2006).

The parallel course of xylem and phloem and the continuity between uptake and delivery are determined quite early in development of a plant seedling, where three basic tissues are founded: the future epidermis, covering and protecting the plant body, the future cortex and pith, involved in photosynthesis, energy storage and internal air distribution, and the procambium, delineating the future vascular bundles in shoot and root. Even earlier in plant development, already with the first divisions of

the embryo, two complementary entities can be discriminated in the young plant body: the porous, water-filled external *apoplast* (i.e., the space outside of the cell membrane comprised of the cell walls) and the living internal *symplasm* (Fig. 6). The apoplast and symplasm are separated from each other by a thin, but physiologically significant bilayer of phospholipids, the plasma membrane, which has a thickness of about 10 nm. The symplasm of neighboring cells are connected by *plasmodesmata* (Fig. 6 (a)), narrow cylindrical conduits that traverse the cell wall. Most are formed during division between daughter cells, but can also develop later (Fig. 6 (b) and (d)); for a review see Roberts (2005). Each plasmodesma contains a tubule related to the *endoplasmic reticulum*, i.e., the network of membranous tubules within the cytoplasm of a cell, connected to the nuclear membrane) thereby offering a cytosolic and an endoplasmic reticulum pathway from cell to cell (Fig 6 (c)). Apoplast and symplasm are continuously extended during plant growth, by cell division, cell expansion and cell wall deposition.

In cross sections of stems, vascular bundles form discrete structures and are often arranged on a circle inside the cortex (Fig. 7). Phloem elements differentiate in the outer part of the bundles and xylem elements in the inner parts (Fig. 7). Leaves, developing as lateral protrusions from the shoot, consistently contain the phloem in the lower (abaxial) part of the bundles and the xylem in the upper (adaxial) part, respectively (Fig. 8(d)).

Even though stem and leaves appear as separate units of the shoot, the development of their vascular system shows a tight relationship between them. Vascular bundles are not independent from each other, but are connected in a complex manner in the stem *nodes*, i.e. the positions where leaves are attached to the stem. Actually, each stem bundle is the continuation of *leaf traces*, i.e. vascular bundles connecting leaf and stem through the petiole. If one follows the median and lateral bundle traces of a given leaf down the shoot by carefully analyzing serial cross and longitudinal sections, bundle fission and fusion events become evident at different nodes below the leaf insertion, leading to the eventually constant number of vascular bundles per stem segment between the nodes (Evert, 2006). In palms and several other monocots the vascular bundles are spread across the stem diameter leading to an even more complex interconnected bundle system, which was for the first time convincingly demonstrated by a cinematographic presentation of serial cross sections by Tyree and Zimmermann (2002); Zimmermann and Tomlinson (1965)

Fission and fusion of vascular bundles happen in the nodes, but there are also connections between the vascular bundles between nodes, which are called *anastomoses*. These can be individual strands, but also an extensive network of connections. Such anastomoses consist typically of phloem elements only and can serve as a bypass for assimilate transport when vascular bundles are inter-

rupted and/or as part of the defence system, when the phloem contains protective proteins (Aloni and Jacobs, 1977; la Cour Petersen *et al.*, 2005; Gaupels and Ghirardo, 2013).

In woody plants, the vascular bundles in the stem increase in thickness by secondary growth where the residual cell layer between phloem and xylem (i.e. the vascular cambium) is activated and produces additional phloem elements to the outside and xylem elements to the inside. Secondary growth results in an annual increase in thickness of root and shoot. Leaves and reproductive as well as storage organs rarely experience secondary growth.

Adjustment to light conditions and accessibility to water import and sugar export pathways are the primary determinants of the specific leaf anatomy. Light is captured by the mesophyll cells, which are typically only a few cells away from a vascular bundle, releasing xylem sap and absorbing phloem sap. Each vascular bundle is encircled by the bundle sheath (Fig. 8(d-e)), which controls the transport processes between bundle and mesophyll. The vascular bundles form parallel avenues only in leaves of e.g. grains, grasses, and palms. They are, at regular intervals, cross-linked by thin anastomoses (Fig. 8 (c)). In most angiosperm leaves, the vascular system does not form parallel veins but a complex reticulate network. Here the vascular bundles constitute a hierarchical vein system with several branching orders, the midrib being "class 1" veins and the veins branching off from the midrib "class 2" and so on (Fig. 8 (a) and (b)). The finest branches, typically class 5, 6 or even 7, called the minor veins, are pivots where water is leaving the xylem and assimilates are loaded into the phloem, (Fig. 8 (d) and (e)). Only the largest classes (1 to 3) enter the petiole, eventually forming the main and lateral leaf traces in the stem.

The beautiful bifurcation patterns formed by leaf veins have been widely studied (Prado and Maurel, 2013; Price and Weitz, 2014; Roth-Nebelsick *et al.*, 2001; Sack and Scoffoni, 2013), but due to their diverse functionality, there is currently no agreement on precisely how these patterns should be understood, in the sense of being optimal. One remarkable observation (Bohn *et al.*, 2002; Couder *et al.*, 2002) is that the bifurcations seem to satisfy a simple vectorial rule, in the form of a "force balance" akin to the patterns formed by drying gels. Thus a vein can bifurcate into two new veins of different radii in many different ways, but the angles that the new veins form with the old one depends on their relative radii. Bohn *et al.* (2002) write the relation between the three veins as

$$F(R_1)\mathbf{e}_1 + F(R_2)\mathbf{e}_2 + F(R_3)\mathbf{e}_3 = 0 \qquad (30)$$

where $\mathbf{e}_i$ is the unit vector pointing in the direction of vein i and F is a function only of the radius of the vein. As seen in Fig. 9, this function is amazingly close to linear, at least in the 7 species studied.
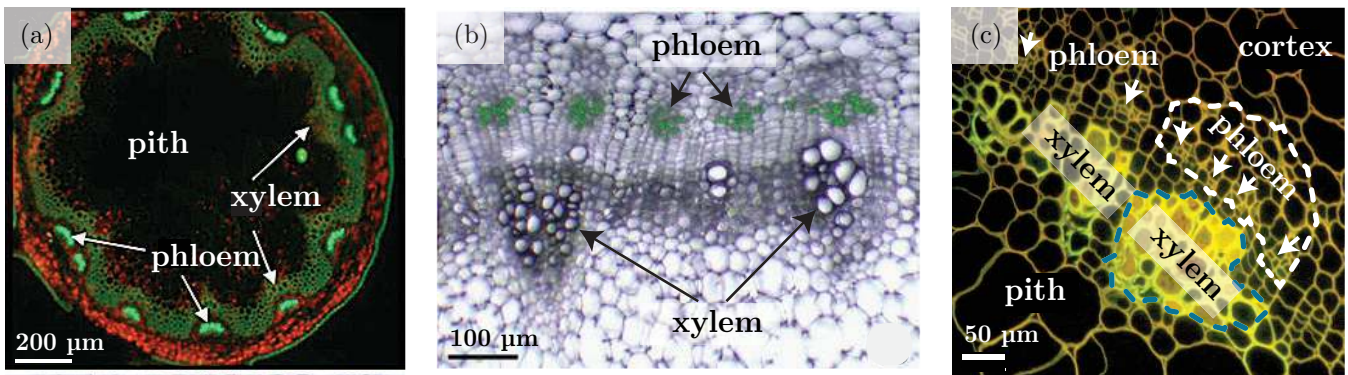
Figure 7 Vascular bundles in the plant stem. (a) Fluorescence micrograph cross section through the stem of *Arabidopsis* with dull green xylem (X), and bright green phloem (P), translocating water with inorganic ions and sugars, respectively. (b) Bright-field micrograph showing vascular bundles in cauliflower with xylem (X) and phloem (P) overlayed with green fluorescence of sieve elements. (c) Fluorescence micrograph of a young apricot tree stem cross section stained with Coriphosphine O (before the onset of secondary growth). The vascular bundles with phloem (P, white dashed line) and xylem (X, blue dashed line) are embedded in the cortex and pith. Arrows point to the small sieve-element companion cell complexes, responsible for sugar transport. Tracheary xylem elements show strong yellow fluorescence in their lignified cell walls. (a) and (b) adapted from (Khan *et al.*, 2007). (c) courtesy of Helle J. Martens, Department of Plant and Environmental Sciences, University of Copenhagen

Although such networks under quite general conditions can be shown to have minimal resistance or maximal efficiency when they form a "tree", i.e., have no loops (Durand, 2006), it has recently been pointed out that the loops, which are abundant in leaf venation networks, will be advantageous by inducing multiple connections, if damage occurs to the leaf (Katifori and Magnasco, 2012; Katifori *et al.*, 2010; Sack *et al.*, 2008). An entirely different understanding of the venation pattern comes from the analysis of how the leaf is folded in the bud, which to a certain extent can explain shapes and symmetries of leaves, and also how adaxial/abaxial asymmetry built up during growth induces curvature and folding (Couturier *et al.*, 2012, 2009). Recently, detailed 3D images of intact tomato leaves have been obtained by synchrotron X-ray radiation with a resolution of 750 nm (Verboven *et al.*, 2015) and this seems a promising technique, in particular if one can reduce the necessary scanning time (currently 10 min) (see also the review by Brodersen and McElrone (2013) and Fig. 35 in Section VI.A.3).

A. Phloem Anatomy

Phloem is a complex tissue containing different cell types: sieve elements, companion or Strasburger cells, parenchyma cells and sometimes also sclerenchyma cells. In this section, we will discuss the overall organization of the phloem and the size, structure and diversity of the conducting cells. Our emphasis is on the phloem of trees, which belong to two botanical taxa: angiosperms (flowering seed plants like most hardwood) and gymnosperms (non-flowering seed plants such as the conifers).

The function of the phloem varies between source (leaves) and sink (e.g. roots and fruits) tissues which is partially reflected in its anatomy. According to their function, the different phloem sections have been defined as collection phloem, transport phloem and release phloem (van Bel, 1996; Lucas *et al.*, 2013), found in leaves, stem and sink organs, respectively. The different functions are overlapping, and it is sensible to use the term *collection phloem* for the minor veins of the leaf only (class $4 - 7$). Major veins have dual functions: in the developing leaf they release sugars and amino acids towards the immature leaf regions, and in the mature leaf they contain the transport phloem and are thus responsible for the export from the minor veins to the petiole (Wright *et al.*, 2003). Transport phloem seems also to have a retrieval function allowing it to pump leaked assimilates back into the transport pathway. Release of assimilates from the phloem to sinks such as young leaves, roots, and seeds is generally a passive process which is facilitated by wide plasmodesmata as seen in the spreading behaviour of radioactive sugars, tracers and fluorescent macromolecules (Lalonde *et al.*, 2003; Schulz, 1995; Stadler *et al.*, 2005; Wright *et al.*, 2003).

The conducting cells of the phloem are the sieve elements as evidenced already more than 60 years ago by experiments with radioactive transport sugars and fluorescent markers (Christy and Fisher, 1978; Fritz and Eschrich, 1970; Knoblauch and van Bel, 1998; Schumacher, 1950). As all living cells, sieve elements are separated from the cell wall space by an intact plasma membrane that controls water and nutrient exchange. In contrast to other cell types, however, sieve elements change their structure dramatically when becoming functional
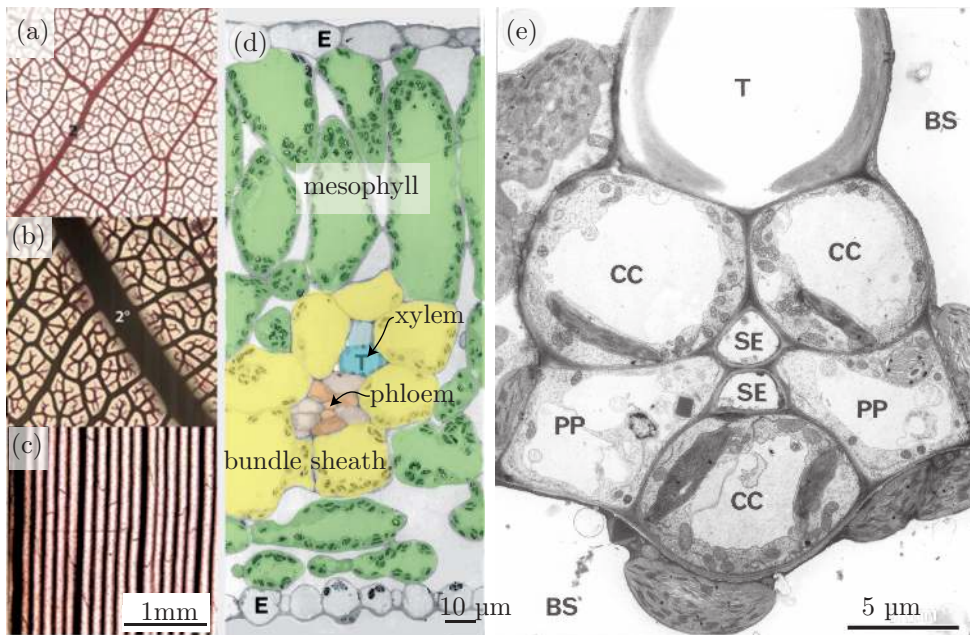
Figure 8 Structure of leaf veins. Venation patterns of (a-b) reticulate and (c) parallel veined leaves. Numbers indicate the vein class. Adapted from (Sack and Scoffoni, 2013). (d) Cross section through a potato leaf at a minor vein. The tissue types are photosynthetically active mesophyll (green) and the bundle sheath (yellow) encircling the vein. The vein has one xylem treachery element (T, blue), two phloem sieve elements (beige), and three phloem companion cells (beige). (e) Cross section through the smallest vein class (6) of a potato leaf consisting of one tracheary xylem element (T), two phloem sieve elements (SE), three phloem companion cells (CC), and two phloem parenchyma cells (PP). The bundle sheath (BS) surrounds the vein. Adapted from (Schulz et al., 1998).
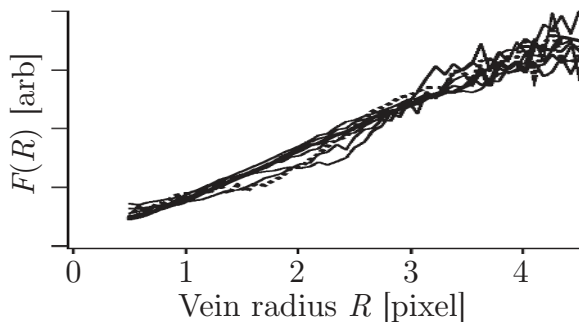

Figure 9 The function F computed from (30) for the seven leaves. As one can see, $F(R)$ is close to linear. Adapted from (Bohn et al., 2002).

and adapted for long-distance transport. The structure of active sieve elements has been a matter of dispute over decades, since the preparation necessary to visualize them with light or electron microscopy easily causes artefacts in the phloem system, which is pressurized when functional. Careful preparation methods and visualisation of functional sieve elements by using tracers and confocal laser scanning microscopy (Knoblauch and van Bel, 1998; Schulz, 1992) have led to the now generally accepted view of their structure, which is remarkably uniform in different plant taxa.

The end walls connecting one sieve element with the next are penetrated by many direct connections, the sieve pores, which are derived from plasmodesmata. The chain of sieve elements thus intimately connected is called a sieve tube (Fig. 10 (b)). The diameters of sieve pores found in different angiosperms span $0.1 - 7$ μm (Fig. 11 (a) and (c)). In gymnosperms, sieve elements have long-tapering end walls with numerous sieve areas connecting to the adjacent sieve element (Fig. 10 (d)). Their sieve pores are rarely wider than 0.3 μm (Fig. 11 (d)), suggestive of a higher flow resistance than in angiosperms. We return to this point in Section IV. The diversity of sieve element lengths, sieve plate areas and inclination of the end walls in higher plants is documented in Esau's classical handbook on the phloem (Esau, 1969). The cross section of sieve elements in angiosperms is generally more or less circular, while those in gymnosperm are rectangular (Fig. 10), which makes the "diameter" somewhat ambiguous (Jensen et al., 2012a). Sieve plates can be oriented perpendicular to the sieve tube, but are often more or less inclined (Fig. 10).

The organelles and other cellular constituents which could offer resistance to intracellular transport, like the nucleus, vacuole(s) and ribosomes, either disappear during cell maturation, or move to the cell periphery as can be seen in Fig. 10b. The mitochondria and a modi-
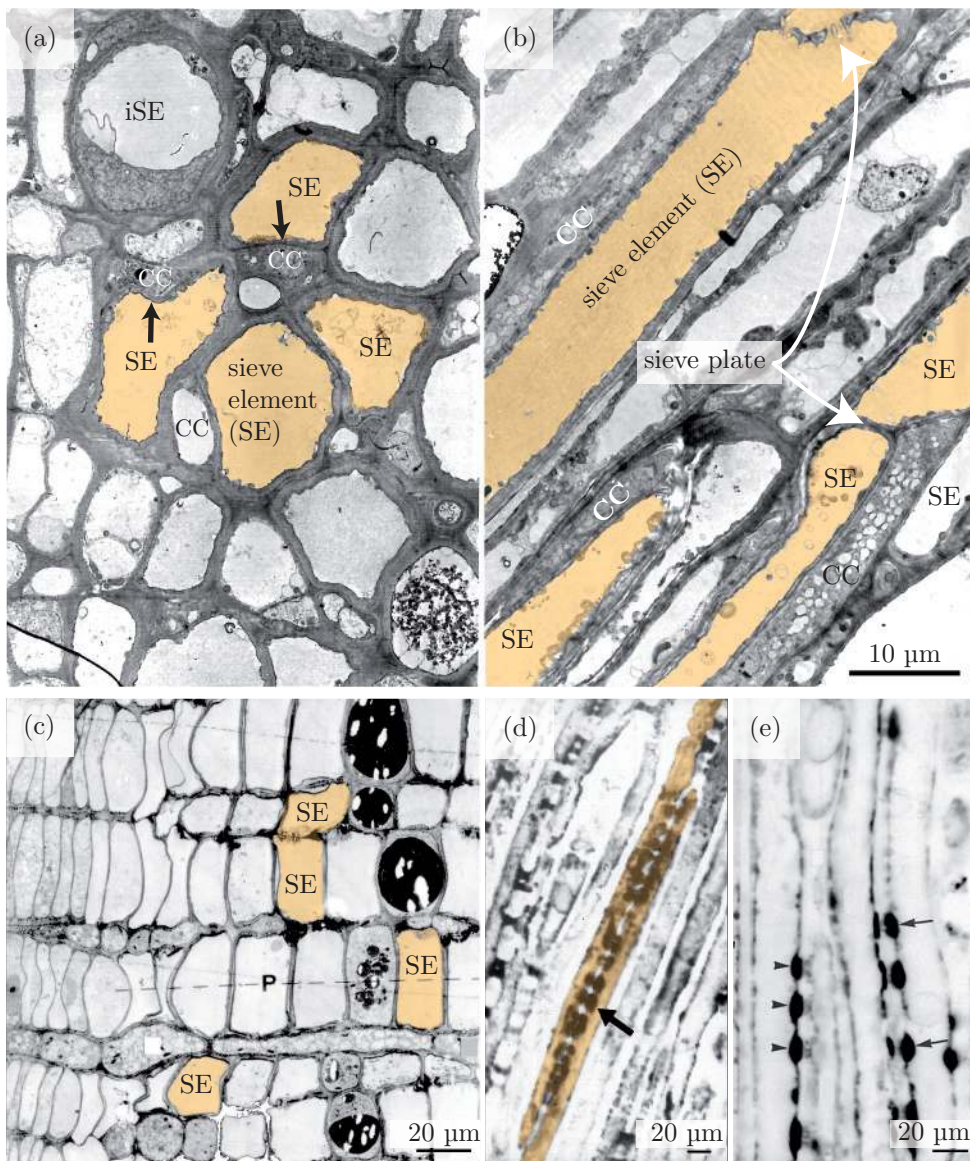
Figure 10 Electron microscopic comparison of the phloem of the flowering plant (angiosperm) beech (a-b) and the non-flowering seed plant (gymnosperm) spruce (c-e). Beige shaded areas are the conducting sieve elements. (a) Transverse cross sections of beech phloem with sieve elements (SE) that are neighbored by companion cells (arrow, CC). The immature sieve element (iSE) still contains a dense cytoplasm. (b) Longitudinal cross section of beech phloem sieve elements (SE) that are neighbored by companion cells (CC) with a dense cytoplasmic content. A sieve plate (SP) separates two adjacent sieve elements. (c) Transverse cross section of spruce phloem (P). Sieve elements appear empty, while parenchyma cells are filled with black tannic acid vacuoles. (d) and (e) Confocal micrographs of live phloem in tangential cross section view, stained with a endoplasmic reticulum specific dye (dark grey). (d) Arrow, end wall of two overlapping sieve elements marked by the many sieve areas, each of them covered on either side by endoplasmic reticulum. (e) Arrows pointing on the sieve areas between two parallel sieve elements. Arrowheads show plasmodesmal connections from a sieve element to a Strasburger cell, which is covered with endoplasmic reticulum on one side only. Adapted from: (a) - (c) (Schulz and Behnke, 1987), (d) (Schulz, 1990), (e) (Schulz, 1992).

fied endoplasmic reticulum system seem to be fixed at the plasma membrane via protein linkers (Ehlers *et al.*, 2000). Specific structural phloem proteins (P-proteins) occurring as filaments or persistent crystalline structures in the majority of sieve elements of angiosperms (Fig. 11) do not seem to have large influence on assimilate transport in intact sieve tubes (Froelich *et al.*, 2011; Knoblauch *et al.*, 2014). Wounding of the phloem by mechanical impacts and pathogen attacks is, however, thought to lead to the accumulation of such proteins on
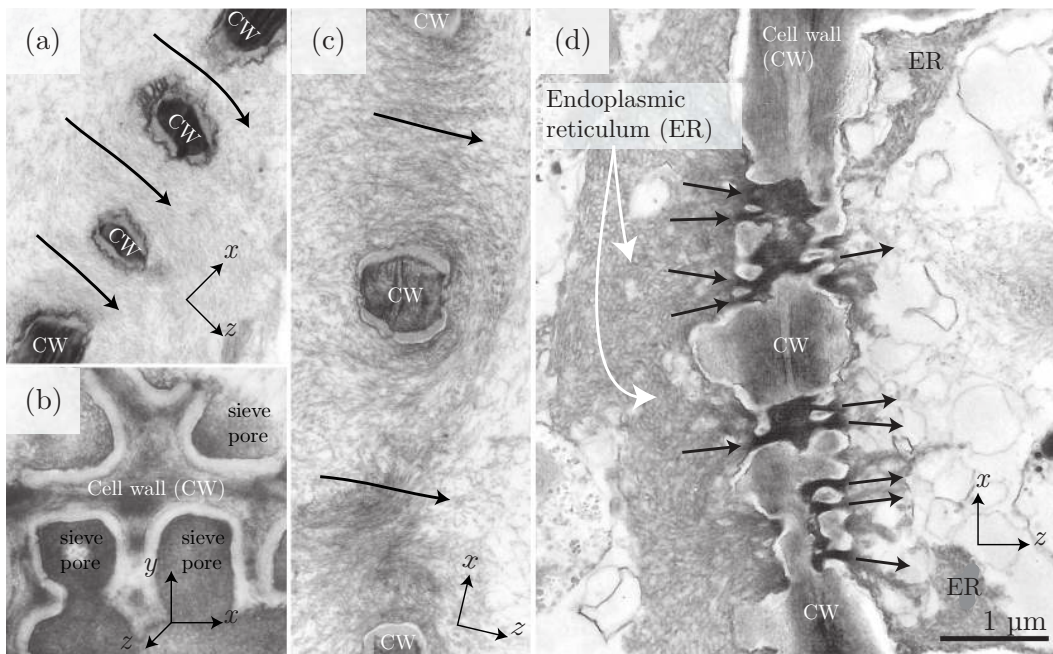
Figure 11 Comparison between phloem sieve plate pores in beech and sieve area pores in spruce, typical for angiosperms and gymnosperms, respectively. (a) Cross section of two sieve pores in a beech sieve plate (see face view of a sieve plate without cellular contents in Fig 1d). Arrows indicate flow paths which are only loosely occupied by hair-like protein filaments (grey). (b) Oblique view of beech sieve pores densely filled with protein filaments. (c) Cross section of sieve pores loosely filled with protein filaments. (d) Cross section of spruce sieve area pores. Arrows mark the orifices of the pores covered on either side with endoplasmic reticulum (ER). The pores form an extended cavity within the cell wall (CW). Scale bar for all panels 1 μm. Adapted from (Schulz and Behnke, 1987).

and in sieve pores. Together with the deposition of a specific wall polysaccharide found around sieve pores and plasmodesmata (callose), this leads to constriction and clogging of sieve tubes (Furch *et al.*, 2007; Knoblauch and Peters, 2004; Knoblauch *et al.*, 2012; Schulz, 1986). Gymnosperms do not have P-proteins (Schulz, 1990). However, their sieve areas are covered by extended complexes of tubular endoplasmic reticulum on either side of a sieve area (Fig. 11). Changes of these complexes after wounding were observed with electron and live confocal microscopy and indicate a similar clogging mechanism (Schulz, 1992).

Taken together, the sieve tubes in angiosperms are symplasmic low-resistance pathways that combine the low-resistant intercellular transport through wide sieve pores with the low-resistant intracellular transport through the reduced cytoplasm of sieve elements. The same is valid for gymnosperm phloem, although the smaller width and increased complexity of sieve pores seem to offer more resistance to the intercellular section of the pathway. This is indeed reflected in smaller transport speeds measured and theoretically calculated for gymnosperm trees (Jensen *et al.*, 2012a; Liesche *et al.*, 2015).

Reduction in cytoplasmic contents is a unifying feature in sieve elements across the higher plant taxa

(Behnke and Sjolund, 1990). However, the cytoplasmic structures persisting in sieve elements, in particular the plasma membrane, are dependent upon protein and lipid turnover as well as on molecular energy carriers which the mature sieve element cannot provide on its own. Therefore, sieve elements are strongly dependent on a fully equipped neighbour cell, the companion cells of angiosperms, and the Strasburger cells of gymnosperms (Fig. 10). The delivery of energy carriers and exchange of worn-out proteins and lipids most probably takes place through the particular contacts consisting of sieve pores on the sieve element side and branched plasmodesmata on the neighbour cell side.

B. Phloem Physiology

We have discussed above that the phloem forms a low-resistance pathway for assimilate transport from source to sink. The question to be treated in this section is the mechanism and the driving force of this transport. Phloem transport is mechanistically seen as an osmotically generated pressure flow driven by accumulation of sugars in mature leaves and consumption in sinks (Münch, 1930), see Fig. 1. The accumulation of sugars is the direct consequence of the photosynthetic ac-
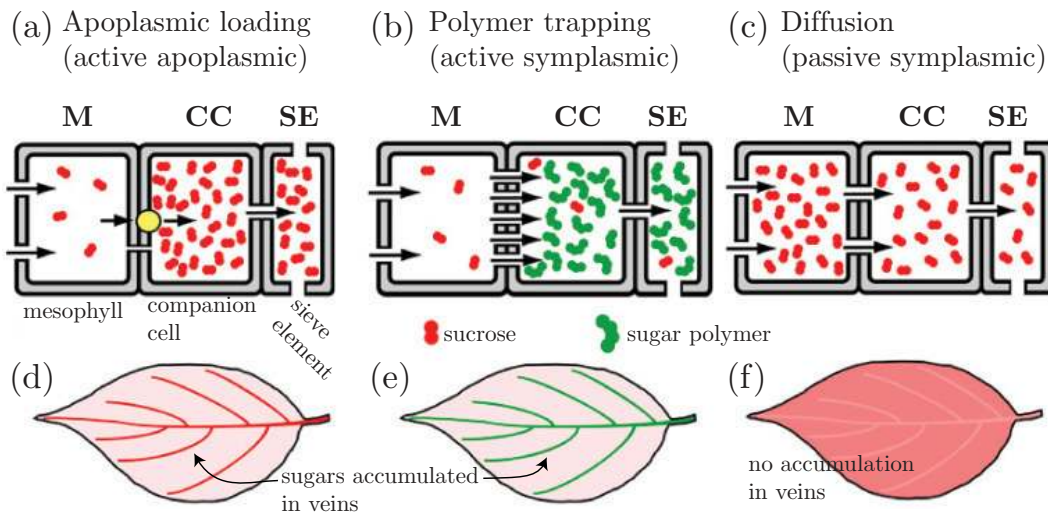
Figure 12 Models of phloem sugar loading strategies according to Turgeon (2010). Represented cell types are sieve element (SE), companion cell (CC), and mesophyll (M). (a) Active apoplasmic loading: sugar transporters (yellow circle) in the companion cell plasma membrane transfers sucrose (red dot) from the apoplast into the sieve element-companion cell complex, energized by a proton pump (not shown). (b) Active symplasmic loading (polymer trapping): Sucrose is transferred from the mesophyll to the companion cell via plasmodesmata gaps in the wall (4 arrows). Here, it is converted under investment of metabolic energy into larger raffinose oligosaccharide family sugar polymers (green dots) that are trapped in the sieve element-companion cell complex. They cannot move back, since the plasmodesmata are too narrow, but can move on into the sieve element through the wide plasmodesma-sieve pore contact. (c) Passive symplasmic loading: sugar diffuses from the mesophyll to the sieve element via plasmodesmata in the companion cell wall. (d), (e) and (f) visualizes the distribution of regions of high sucrose concentration under the the three loading strategies. Accumulation occurs in veins of active apoplasmic loaders and polymer trappers, but not in passive symplasmic loaders. Adapted from (Turgeon, 2010).

tivity of the leaf mesophyll. For the export of sugars from the mature leaf into other plant organs, it is decisive that the plasma membrane of the sieve elements remains intact. The sharp difference in solute potential across the plasma membrane leads to the osmotic uptake of water from the apoplast into the phloem, and thus to the development of pressure in the phloem system. The pressure in the leaf phloem drives a bulk flow of liquid through files of sieve elements towards regions of low hydrostatic pressure. Since the majority of sink sites allows for a passive release of nutrients, the decrease of the sugar concentration towards sink tissues establishes a pressure differential in the phloem system, driving the observed transport of sugars and other organic compounds from source to sink.

Münch's original hypothesis was that the sugars in the phloem accumulate due to photosynthesis in the mesophyll and subsequent loading into the sieve elements by diffusion. However, this hypothesis was established without the knowledge of active membrane transport systems. Currently we know that at least three principally different strategies of phloem loading have developed in evolution. The active ones show an accumulation of sugars in the leaf veins – and not the mesophyll – when leaf disks are incubated in radioactive sugar solutions (Turgeon and Wimmers, 1988). In contrast, leaf disks of passive sym-

plasmic loading plants do not accumulate sugars in the veins. This passive loading mode is typical for woody angiosperms and gymnosperms. The question why particularly the rapidly growing herbaceous plants have adopted active loading strategies seems to be related to their economic life strategy, which is focused on an efficient use of photosynthates (Turgeon, 2010).

1. Active apoplasmic loading

One of the driving forces for the sugar accumulation in the collection phloem emerged in the 1970ies to be an active sucrose-proton cotransport from the apoplast into the symplasm (see Giaquinta (1980); Komor (1977)). Uptake of sugars is fuelled by the activity of the plant proton pump which hydrolyses the energy carrier ATP. An important breakthrough for the understanding of this so called *apoplasmic loading mode* was the purification, characterization and localization of the sucrose transporter to the plasma membrane of the sieve element-companion cell (Kühn *et al.*, 1997, 1996; Stadler *et al.*, 1995). Since then several sucrose transporters were characterized in different plant taxa (for their evolution see (Peng *et al.*, 2014)) and, aside from sucrose, they transport sugar alcohols like mannitol and sorbitol (Rennie and Turgeon, 2009). Experimental removal of the sucrose

19

transporter protein led to reduction or loss of phloem transport (Gottwald *et al.*, 2000; Kühn *et al.*, 1996; Schulz *et al.*, 1998).

The localization of the sugar transporters and the measurements of osmotic pressures in different tissues of mature leaves confirmed that sugars do accumulate in the minor veins (Geiger, 1975; Geiger *et al.*, 1973), in agreement with the leaf disk experiments. Sugars and amino acids to be translocated long-distance in the phloem must first to be transported from mesophyll cell to mesophyll cell into the bundle sheath. This pre-phloem transport of assimilates, with sucrose as the most important representative of sugars, follows the distribution of plasmodesmata in the cell wall interfaces (Schulz, 2014). A simplified cartoon on active apoplasmic loading is shown in Fig. 12. Plant species exploiting apoplasmic phloem loading are characterised by an isolated phloem, i.e. only few plasmodesmata link the bundle sheath with the sieve element-companion cell complex (Fig. 8).

2. Active symplasmic loading by polymer trapping

In contrast to the closed minor vein configuration discussed above, a number of plant families however have numerous plasmodesmata in the interface between bundle sheath and sieve element-companion cell complex. This so-called open configuration (Batashev *et al.*, 2013; Gamalei, 1989) was a challenge for the understanding of active phloem loading through sugar transporters up to 1990, since the plasmodesmata would allow sucrose to flow back into the mesophyll, instead of accumulating in the phloem. At that time Robert Turgeon presented his polymer trap hypothesis for herbaceous flowering plants with an open minor vein configuration (Turgeon and Gowan, 1990), called *active symplasmic loading*. It combined different ultrastructural and physiological observations of a subgroup of plants with an open minor vein configuration, most importantly: (i) the plasmodesmata between bundle sheath and companion cells are branched and very narrow on the companion cell-side, (ii) chemical inhibitors of sugar transporters have no effect on phloem loading and, (iii) the main transport sugar found in the phloem of this subgroup are larger raffinose family oligosaccharides such as raffinose, stachyose and verbascose, in contrast to the disaccharide sucrose as used by the majority of plant families (Schmitz *et al.*, 1987; Turgeon and Hepler, 1989; Turgeon *et al.*, 1975; Turgeon and Wimmers, 1988; Zimmermann and Ziegler, 1975).

The polymer trap hypothesis assigns the branched plasmodesmata a filtering function: large enough to let sucrose pass from the bundle sheath into the companion cell, but too small for the larger sugars, synthesized in the companion cell (see Fig. 12). Synthesis of the larger sugars in companion cells leads to an accumulation of

sugars which again attracts water osmotically. Since the metabolic conversions from sucrose to raffinose and/or stachyose demand energy, this loading mode is denoted active symplasmic loading. Subsequent studies confirmed the feasibility of the hypothesis and annotated the relevant plant families within the flowering plants (van Bel *et al.*, 1993; Haritatos *et al.*, 2000; Holthaus and Schmitz, 1991; Kempers *et al.*, 1998; Turgeon *et al.*, 2001). The polymer trap mechanism is not associated with a specific growth form as it is found in herbaceous plants like pumpkin, but also in, for example, olive trees (Davidson *et al.*, 2011). Direct evidence for the capability of plasmodesmata to filter sugars with a very small difference in hydrodynamic radius from each other is still lacking. Modeling the plasmodesmal substructure and calculation of the plasmodesmal conductance at the crucial interface showed, however, that plasmodesmata might indeed be able to discriminate sucrose from the larger sugars if their cut-off is close to the hydrodynamic radius of stachyose (Dölger *et al.*, 2014; Liesche and Schulz, 2013). For more details of this mechanism, see Section VI.C.

3. Passive symplasmic loading

Over the last 15 years, Münch's original hypothesis experienced a renaissance for sucrose translocating trees. It was shown, first in willow, and then in other tree species, that leaf disks exposed to labelled sucrose did not accumulate radioactivity in the minor veins and inhibitors of sucrose uptake did not have any effect. At the same time, the global sugar concentration in the leaves was higher than in herbaceous plants (Davidson *et al.*, 2011; Fu *et al.*, 2011; Rennie and Turgeon, 2009). They had an open vein configuration and were accordingly called *passive symplasmic loaders* (Turgeon and Medville, 1998) and they appear to be in good agreement with Münch's original idea (Münch, 1930): that sucrose synthesized in the mesophyll moves down its concentration gradient to the minor veins, where it easily can enter the companion cells through the abundant plasmodesmata at the bundle sheath-companion cell interface (Zhang *et al.*, 2014) (see Fig. 12). Passive symplasmic loading seems in a way quite energy-efficient, since no additional energy is needed in the phloem itself, and the highest sugar concentration is where it is produced. For the overall transport process from mesophyll via the phloem to the sink organs, it is an interesting question where the purely diffusive sucrose transport starts to be converted into a bulk flow: already on the pre-phloem pathway, or only in the phloem (Schulz, 2014). Indications for passive symplasmic loading are given for many woody angiosperms and for all gymnosperms. The pre-phloem pathway of the latter is however much more complex (Canny, 1993; Liesche *et al.*, 2011; Schulz, 2014).

C. Xylem Anatomy

The principal role of the xylem is to replace water lost from leaves during transpiration with water from the soil (Tyree and Zimmermann, 2002). Up to 98% of the water moving through the xylem exits the leaves through the stomata pores as water vapor (Fig. 1(a)), with the remaining 2% being used in photosynthesis and volume growth (Kramer and Boyer, 1995). It is not uncommon for a large tree to lift as much as 100 liters every day (Vogel, 2012). For comparison, the fastest growing trees add around 100 kg dry mass per year (Stephenson *et al.*, 2014). To justify the plant's insatiable desire for water, consider the photosynthesis reaction:

$$\text{light} + 6H_2O + 6CO_2 \rightarrow C_6H_{12}O_6 + 6O_2. \tag{31}$$
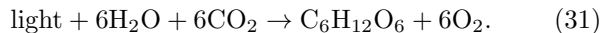
Six CO_2 molecules are needed to produce one glucose sugar molecule. This corresponds to approximately 1.4 kg CO_2 per 1 kg glucose. Plants obtain CO_2 from the atmosphere by diffusion through stomata pores. The pores expose the interior of the leaf to the atmosphere, and thus invariably also allow water vapor to escape. A conservative estimate of the relative water flux J_{H_2O} and carbon dioxide flux J_{CO_2} is

$$\frac{J_{H_2O}}{J_{CO_2}} = \frac{D_{H_2O}}{D_{CO_2}} \frac{\Delta c_{H_2O}}{\Delta c_{CO_2}} \tag{32}$$

$$\simeq \frac{2.4 \times 10^{-5} \text{ m}^2/\text{s}}{1.4 \times 10^{-5} \text{ m}^2/\text{s}} \frac{1 \text{ mol/m}^3}{10^{-2} \text{ mol/m}^3} \tag{33}$$

$$\simeq 1.7 \times 10^2 \tag{34}$$

where D is the diffusion coefficient in air and Δc are typical concentration gradients (Nobel, 2009; Thoning *et al.*, 1989). The plant thus loses around 200 water molecules for every CO_2 captured, or at least 100 kg water per 1 kg glucose synthesized. Apart from water, the xylem also transports dissolved nutrients, amino acids, hormones and other signaling molecules (Fisher and Cash-Clark, 2000); but – in contrast to the phloem – the solution is dilute (typically less than 10 mmol (Schurr, 1998; Siebrecht *et al.*, 2003)).

The large amount of energy needed to vaporize water means that transpiration also serves to cool leaves (Lambers *et al.*, 2008). Yet in considering the role of transpiration in leaf energy balance it is worth noting that transpiration cools leaves even when leaf temperatures are lower than optimum levels for photosynthesis. Furthermore, when soils are dry and stomata close, transpirational cooling will be lost. For this reason, other features, such as leaf angle, leaf reflectance and leaf size, play an important role in preventing sunlit leaves from reaching lethal temperatures.

The conduits through which water flows are formed from cells that (1) have thick cellulosic walls impregnated with a class of complex organic polymers ($C_9H_{10}O_2$, $C_{10}H_{12}O_3$, $C_{11}H_{14}O_4$) called lignin and (2) lack a
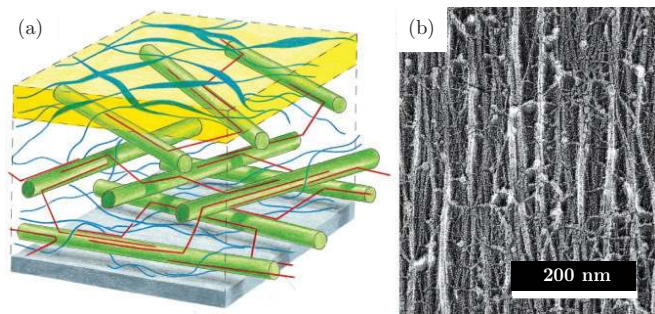

Figure 13 Structure of plant cell walls. (a) Plant cell walls comprise a network of cellulose microfibrils (green rods) linked by hemicellulose (red strands) and pectin (blue strands) to form a network. Lignin confers additional mechanical strength. (b) Electron micrograph of cell wall structure shows mainly cellulose microfibrils after extraction of pectin and hemicellulose. Adapted from (Alberts *et al.*, 2014)

membrane-bound protoplasm at maturity (Fig. 13). Both features contribute significantly to the ability of plants to pull water from the soil. Xylem conduits are of two basic types (Fig. 14): single-celled tracheids and multicellular vessels (Evert, 2006). The latter are formed from linear files of cells called vessel elements. As vessel elements mature, the cell wall between them is chemically broken down. This creates a continuous lumen that spans multiple cells. The degraded walls between vessel elements are referred to as *perforation plates*; these can be essentially open holes or retain parallel bars of cell wall material across the opening between vessel elements. The perforation plates approximately doubles the total hydraulic resistance of the conduit lumen (Christman and Sperry, 2010). Their functional role, either in terms of reinforcing conduits against implosion (Carlquist, 2001) or preventing gas from aggregating into larger bubbles following a freeze-thaw event (Tyree and Zimmermann, 2002), remains unresolved.

The major significance of vessels is that they can be of larger diameter and of longer length than tracheids (Sperry *et al.*, 2006). Tracheids are typically $10 - 20$ μm in diameter ($40 - 60$ μm maximum), and less than 10 mm in length (2 cm maximum). Vessel dimension vary substantially, but in some cases they can be up to 500 μm in diameter and multiple meters in length (Tyree and Zimmermann, 2002). As a result, plants with vessels can support higher rates of water flow and greater rates of CO_2 capture than a plant with only tracheids. Tracheids are found in all types of vascular plants, whereas xylem vessels occur in only some groups, most notably in the flowering plants (angiosperms).
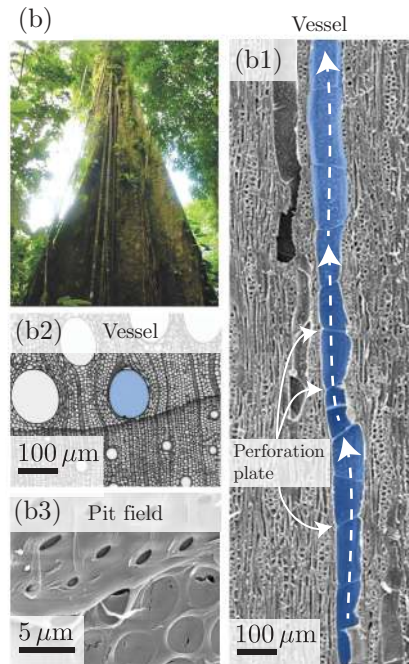
Due to the hydrophobic nature of lignin, the secondary walls of xylem conduits are relatively impermeable to water. Thus, all exchange of materials with both adjacent living cells and other xylem conduits occurs through pits,
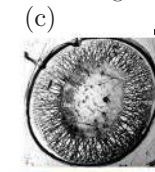
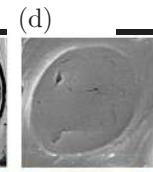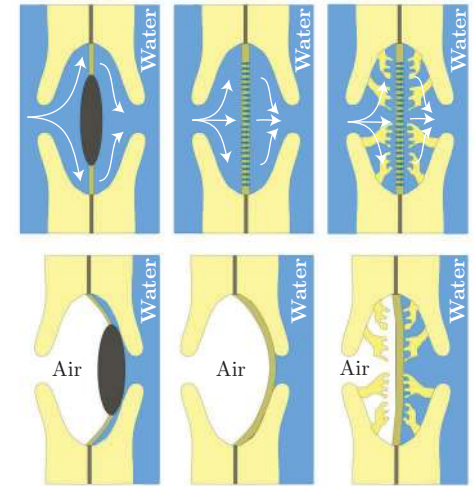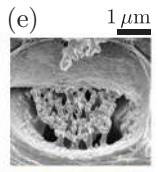# Structure and function of wood

Gymnosperm
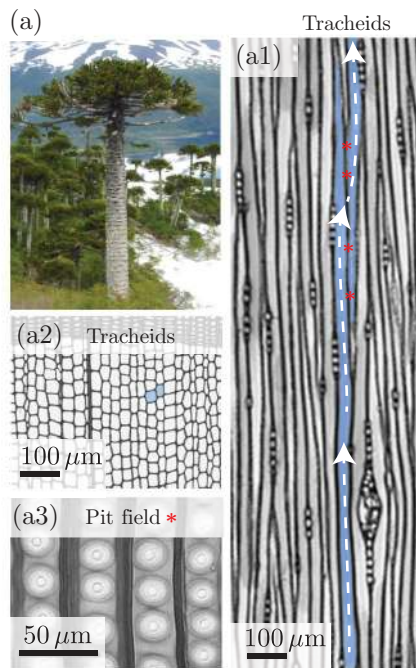
Angiosperm

Bordered pit

Figure 14 Principles of wood structure in gymnosperms (a) and angiosperms (b). (a1) and (b1) depict typical features of conductive wood (xylem). In gymnosperms, the longitudinal conducting elements (tracheids; (a1), cross section view (a2)) are connected via linearly aligned bordered pits (a3). In angiosperm wood vessels are composed from large cells that are vertically aligned and joined via per foration plates (b1), vessels are also seen as large ovals in cross section (b2). Vessels are connected via fields composed from tens to hundreds of bordered pits (b3). The structure and function of xylem bordered pit pores vary between species (c-e). (c) Bordered pits of gymnosperm with torus and margo, (d) typical angiosperm pit, and (e) angiosperm with vestured pits. Drawings below (c-e) represent cross-sections of bordered pits under normal non embolized conditions, and their potential function as protection from gas spread. (c) From (Core *et al.*, 1979), (e) courtesy of Steven Jansen, from (Jansen *et al.*, 2004).

circular to oval regions that lack a secondary wall (Evert, 2006), (see Fig. 14). The primary cell wall which is formed while the cell is actively increasing in size, remains intact and thus forms a porous barrier, referred to as the pit membrane. Unlike cellular (lipid) membranes, pit membranes are not selectively permeable, but their presence at the interface between adjacent vessels significantly impedes flow (Choat *et al.*, 2006). Overall, endwalls are thought to contribute $56 - 64\%$ of total xylem hydraulic resistance (Sperry *et al.*, 2006).

Pits are sentinel features of xylem that help maintain liquid continuity (Choat *et al.*, 2008). In the so-called bordered pits that form between xylem conduits, the secondary walls arch over the circular pit membrane, forming a chamber that is connected to the conduit lumen by a circular-to-elliptical hole (Fig. 14). When adjacent conduits are water-filled, the pressure difference across the pit membrane is small relative to its strength, such that there is little deflection of the pit membrane in the direction of water flow. However, when a gas-filled conduit (at atmospheric pressure) adjoins a water-filled con-

duit that remains under significant tension, the pressure difference across the pit membrane can be large. When this happens, the pit membrane deforms elastically and eventually comes to rest against the physical barrier created by the over-arching secondary cell wall. Capron *et al.* (2014) documented this process in *Populus* xylem by creating silicone moldings of the pit membrane at different pressure gradients (Fig. 15). In some species, outgrowths of the overarching secondary wall extend into the pit chamber, forming structures referred to as *vestures* (see Fig. 14(e)). Vestures restrict the deformation of pit membranes when exposed to large pressure gradients (Choat *et al.*, 2004). For reasons that are currently unclear, such vestured pits are most commonly found in species from warm, tropical climates (Jansen *et al.*, 2004).

Pit membrane structure is central to how pits prevent air from spreading between conduits (Jansen *et al.*, 2009). Pit membranes begin as primary cell walls, although they may be substantially modified during conduit maturation. Primary cell walls consist of dense layers of cellu-
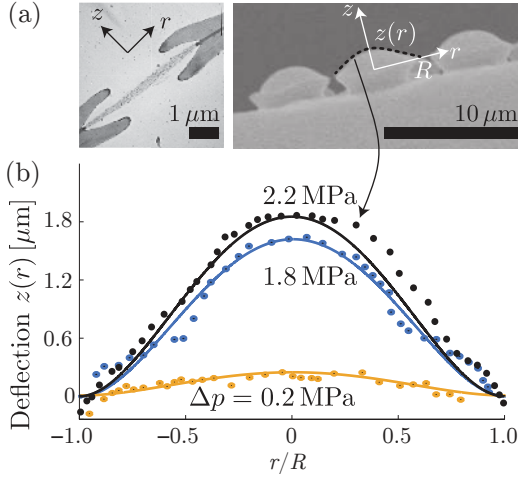
Figure 15 (Color online) Elastic deformation of a pit membrane. (a) Silicone molding of Populus pits at pressure gradient $\Delta p = 2.2$ MPa. (b) Data points show deflection of the pit membrane as a function of the normalized radial position r/R, measured from molding experiments at pressure gradients indicated in the plot. Solid lines are fits to the linear elastic deflection of a circular plate with clamped edges. Adapted from (Capron *et al.*, 2014).

lose microfibrils, which are crosslinked with other carbohydrate polymers, with the entire network embedded in a pectin hydrogel as shown in Fig 13. The characteristic distance between cellulose fibers have been reported in the range $10-100$ nm (Capron *et al.*, 2014; Choat *et al.*, 2004). In some species, the pit membranes are thick (up to 1 μm), while in others the thickness is similar to that of typical primary walls (≈ 200 nm). In most plants, the pit membrane appears relatively featureless, with atomic force microscopy indicating the presence of a soft surface layer that covers the cellulose network (Lee *et al.*, 2012). The presence of hydrogels in pit membranes is indicated by the effect of cations on hydraulic resistance (Santiago *et al.*, 2013; Zwieniecki *et al.*, 2001).

The pit membranes of many gymnosperms are highly modified into a thick central region (the torus) that is suspended in the middle of the pit chamber by cellulose microfibrils (the margo) (Fig. 14(c)). This differentiation creates a region of lower hydraulic resistance than in a homogeneous pit membrane, while at the same time retaining a thickened torus that can form a seal to prevent gas from spreading between conduits (Delzon *et al.*, 2010). The higher permeability to water of these pits helps explain how gymnosperms grow to form tall trees despite producing only tracheids (Pittermann *et al.*, 2005). Indeed, some of the tallest trees in the world (notably coastal redwood, giant sequoia, and douglas firs), reaching heights of 100 m, are also gymnosperms.

As illustrated in Fig. 13, wood cell walls comprise cellulose, hemicellulose, lignin, and pectin - in addition, a structural analysis indicates that particular geomet-

rical constructs are dominant. These include honeycomb, foam-like, and helical structures (Ali and Gibson, 2013; Carlquist, 2012; Gibson, 2012; Karam, 2005; Niklas, 1994; Tekoglu *et al.*, 2011; Wegst, 2011). The arrangement of the four basic building blocks in plant cell walls and the variations in cellular structure give rise to a remarkably wide range of mechanical properties: Young's modulus E varies from $E \sim 0.03$ GPa to $E \sim 30$ GPa, while the compressive strength σ varies from $\sigma \sim 0.3$ MPa to $\sigma \sim 300$ MPa (Gibson, 2012) (Fig. 16). Models based on the assumption that the mechanical strength of the wood depends on the geometrical structure and the density of the underlying polymer material – composing the cell wall – only, are quite successful in predicting the mechanical properties of the particular type of wood (Gibson, 2012). As an example, one may consider wood organized primarily in honeycomb structures with prismatic cells, i.e., the honeycomb structure of the shortest dimensions appears in the plane perpendicular to the xylem vessels and thereby also perpendicular to the direction of flow. With a density of the wood of value ρ, the model predicts that when loaded along the vessels, Young's modulus $E_{||}$ and the compressive strength $\sigma_{||}$ are related to the similar material properties of the cell wall, E_{cw} and σ_{cw} through the ratio of the densities, ρ/ρ_{cw},

$$E_{||} \sim E_{cw}\left(\frac{\rho}{\rho_{cw}}\right), \qquad (35)$$

$$\sigma_{||} \sim \sigma_{cw}\left(\frac{\rho}{\rho_{cw}}\right). \qquad (36)$$

When one accounts for the spacing between the walls in the symmetric structure, the density of the wall material, ρ_{cw} should be larger than the density of the wood ρ, as also apparent from Fig. 16, implying that the elastic moduli $E_{||}$ and $\sigma_{||}$ are smaller than the values for the cell wall itself, E_{cw} and σ_{cw}. The same is true for loading perpendicular to the xylem vessels, also referred to as perpendicular to the grain. In this situation, at sufficient loading, plastic hinges form between the wooden cell walls, and the relevant moduli are

$$E_\perp \sim E_{cw}\left(\frac{\rho}{\rho_{cw}}\right)^3, \qquad (37)$$

$$\sigma_\perp \sim \sigma_{cw}\left(\frac{\rho}{\rho_{cw}}\right)^2. \qquad (38)$$

The scalings in Eqns. (36)-(38) are in rough accord with observations from woody plants, cf. Fig. 16 (Gibson, 2012). The data for the perpendicular Young's modulus $E_\perp$ as a function of density ρ lie on a line closer to a slope of 2 than 3, with the data for loading in the tangential direction of the tree trunk closer to a slope of 3 and those for loading in the radial direction of the tree trunk closer to a slope of 2. It appears that in the radial direction, rays are formed in the tree trunk and act as
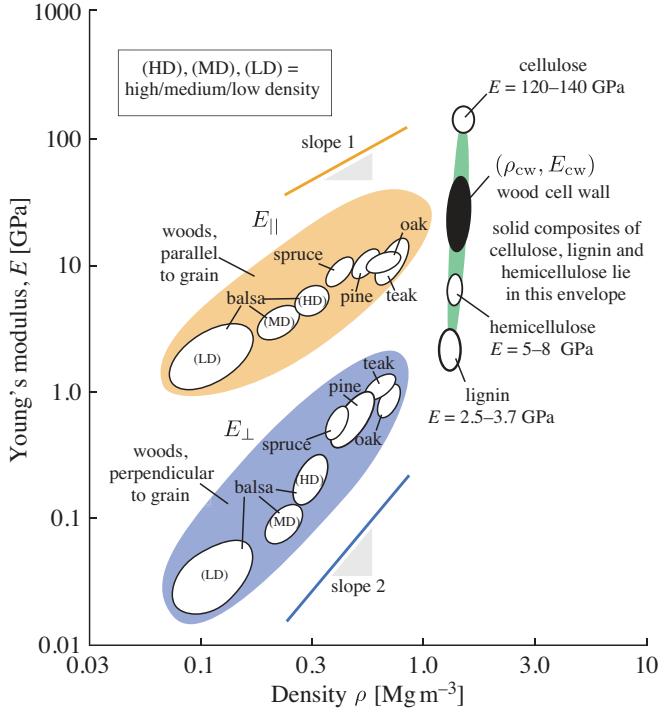
Figure 16 (Color online) Young's modulus E increases with wood density ρ, in rough accord with model Eqns. (38) and (36). Parameters for the pure materials are displayed in the right upper part of the figure, whereas parameters for the composite wood corresponds to the lower density in the yellow (loading parallel to the xylem vessels) and in the blue areas (loading perpendicular to the xylem vessels) of the figure. Adapted from (Gibson, 2012).

reinforcement (Easterling *et al.*, 1982). With radial loading, these rays are loaded along their axis and the loading therefore not only results in bending of the elements of the honeycomb, a fact that would explain a slope of a value less than 3.

D. Xylem Physiology

Having briefly outlined the basic structure of xylem conduits, we are now ready to consider what drives the flow of water through the xylem. Water transport in plants is often described as passive; meaning that no direct expenditure of metabolic energy is required. Instead, plants make use of an existing external gradient in chemical potential between wet soil and dry air (Stroock *et al.*, 2014). Yet to do this, they have to build structures that maintain liquid continuity such that the pathway of lowest resistance is through the plant, rather than through the much shorter distance to the soil surface. Thus, although water transport is passive in the strict sense, energy is required to build and maintain the xylem.

1. Cohesion-tension theory

The Cohesion-Tension theory, first articulated by Dixon and Joly (1895), unites two important ideas (Pickard, 1981; Stroock *et al.*, 2014). The first is that the driving force that pulls water through plants and, ultimately, from the soil, results from transpiration – specifically, a drop in chemical potential at the sites where water evaporates. The second is that intermolecular forces allow water to be pulled through the lumen of xylem conduits. The cohesion-tension theory differs from popular conceptions of water transport in plants in which the driving force is analogized to a mechanical (vacuum) pump. Plants lack the moving parts needed to decrease air pressure within the leaf and, even if they could, such a mechanism would limit plant height to less than 10 meters. By recognizing that the driving force is generated at the sites of evaporation, the cohesion-tension theory overcomes concerns that capillary forces within xylem conduit lumen are far too small to account for the movement of water through plants (Holbrook and Zwieniecki, 2008).

In developing a quantitative description of the forces involved in moving water through a transpiring plant, we express the chemical potential of water on a volumetric, rather than molar, basis (Nobel, 2009). This is the water potential Ψ, see Eq. (17), and it describes well regions within the plant where water exists as a bulk liquid phase, e.g., within xylem conduits or within the *protoplasts* of cells (i.e., the region inside the cell wall). However, in regions where surface interactions dominate and where hydrogels may be involved (e.g., soils and cell walls), the situation is more complicated and a simple separation into pressure and concentration terms is not possible. For simplicity (and without loss of utility), we rewrite Eq. (17) as

$$\Psi = \Psi_{\text{matrix}} + \rho g z, \qquad (39)$$

where Ψ_{matrix} represents the sum of capillary, gel-related and adsorptive forces that may occur in microporous materials (Stroock *et al.*, 2014).

Soils are the reservoir of water that plants draw on for growth, metabolism and transpiration. Soil water potentials are typically negative, corresponding with our common experience that water flows into (and not out of) soils. Soils are made up of irregularly shaped particles of a variety of sizes and, unless completely water-logged, have a substantial volume fraction of air (Kramer and Boyer, 1995). The major force that draws water into soils is thought to be capillarity, resulting from the curvature of air-water interfaces in the soil, as described by the Young-Laplace law (Eq. (26)). As soils dry out, these interfaces recede deeper into the spaces between soil particles, resulting in greater capillary forces and lower soil water potentials. This means that plants have to pull harder to obtain water from a drier soil (Kramer and

Boyer, 1995). In addition, as soils dry, the ease with which water flows through the soil falls precipitously as a result of both the smaller cross-section of the liquid-filled spaces and the increasingly tortuous pathway for water movement (Hillel, 1998). Thus, in dry soils, plants must contend not only with less water that is more tightly bound, but also with the fact that it can only be withdrawn at an ever-diminishing rate. The agriculturally relevant range of soil water potentials is generally considered to be greater than −1.5 MPa. Some plants can make use of water from even drier soils, but produce many more roots and have lower transpiration rates than a typical crop plant.

The air, at least during the day, is typically much drier than the soil. The water potential of liquid water in equilibrium with air is $\Psi = (RT/V_w)\ln(e/e_0)$, where e is the partial pressure of water vapor in the air and e_0 is the saturated vapor pressure. If the relative humidity $(100e/e_0)$ at midday is 50%, the equilibrium water potential is on the order of −100 MPa (Nobel, 2009). Living cells cannot remain metabolically active at such negative potentials. Thus even as leaves have to acquire CO_2 from the atmosphere, they also have to protect themselves from desiccation. Typical midday leaf water potentials are on the order of −1 to −2 MPa, indicating that the water status of leaves is more closely coupled to that of the soil than it is to the air (Kramer and Boyer, 1995). To maintain the hydration of leaves requires both an inflow of water into leaves via the xylem and the means to restrict water loss to the atmosphere via a waxy cuticle and stomata that can open and close. Stomata are the gatekeepers between the humid air spaces within the leaf and the much drier surrounding air. As a result, stomata control rates of transpiration and thus the movement of water from the soil.

Air spaces play a critical role in leaf function by providing a pathway for the inward diffusion of CO_2 (Byott, 1976; Pickard, 1982). The veins within leaves are surrounded by a ring of bundle sheath cells as shown in Fig. 8, which are impermeable to gasses, and thus xylem conduits do not directly come into contact with the air (Evert, 2006). Instead, the surfaces of leaf mesophyll cells, which obtain CO_2 from these air spaces, form the downstream end of the (liquid) transpiration stream. The interfacial forces that develop in these cell walls maintain their hydration and thus they serve as a seal that prevents air from entering into the xylem.

Traditionally the matrix potential of cell walls has been attributed to capillary forces arising within the network of cellulose microfibrils (Pickard, 1981; Rand, 1983; Tyree and Zimmermann, 2002). In this view, curved air-water menisci within cell walls work in opposition to their curved counterparts in the soil. This might be a simplified view. The cellular wall matrix is not a simple porous rigid structure but an elastic composite made of cellulose fibers, pectins and hemicelluloses, plus a small amount of
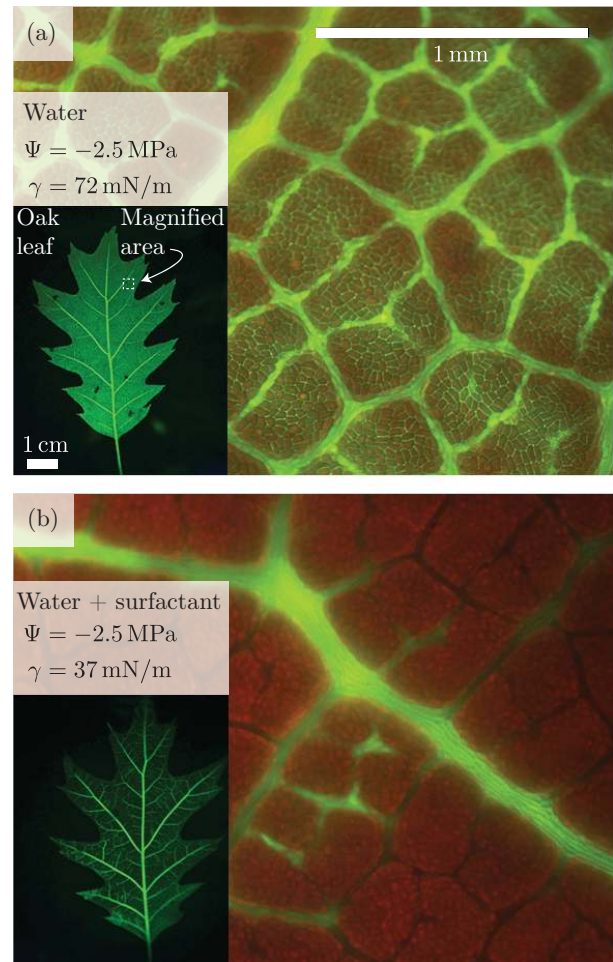
Figure 17 (Color online) Reduction of xylem sap surface tension in oak leaves influences distribution of water in the veins of trees experiencing significant water shortage. Transpiration stream of intact branches on a tree were supplied with either (a) water (surface tension = 72 mN/m) or (b) water mixed with surfactant (0.01% Tween 20, surface tension 37 mN/m). Branches were then cut and allowed to dehydrate to a water potential of −2.5 MPa. At the desired stress level, leaf petioles were cut from the branches while submerged in a fluorescent dye solution (Sulforhodamine G). Leaves infiltrated with water mixed with surfactant experienced significant reduction of dye infiltration to minor veins. Experiments by M. Zwieniecki (unpublished).

structural proteins. In short, the cell wall is a porous material infiltrated by a gel-like substance. Such structure may dry out but will not necessarily allow for retraction of the air-water meniscus into the wall space. Instead, the water holding capacity of gels originate from interactions between solvent and polymer as e.g., described by the Flory-Rehner equation (Hong et al., 2010, 2008; Wheeler and Stroock, 2008). However, a recent experiment (Fig. 17) aimed at studying the influence of surface tension on a leaf's ability to sustain water distribution to sites of evaporation under increasing water stress revealed that the presence of a surfactant (reducing the

surface tension from 0.072 N/m to 0.037 N/m) limited water access to minor leaf veins. This might suggest the retraction of water from minor veins, in support of the menisci hypothesis. However, alternative explanations might be possible, depending on what other effects the surfactant (Tween) could have on the leaf, e.g., closure of the stomata or inhibition of the cell aquaporins of the cell membrane.

At night, when stomata are closed, the plant will come into equilibrium with the soil. The water potentials in the plant, however, will not equal that of the soil; due to gravity the water potential decreases below that of the soil by $\rho g h = 0.1$ MPa for every 10 m increase in elevation. For plants that are on the scale of one to several meters in height, the impact of gravity relative to soil water potentials is small. The water potentials at the top of a 100 m tall tree, however, must be 1 MPa lower (more negative) than the water potential of the soil in order to support the water column. Thus even when a plant is not transpiring, capillary and osmotic forces develop within leaves to counterbalance the weight of the water column and to overcome the forces exerted by the soil. During transpiration even larger forces are needed to overcome the viscous losses associated with the movement of water through the plant (Tyree and Zimmermann, 2002).

2. Transpiration

Transpiration results from the gradient in water vapor concentration between a leaf's air spaces and the outside air. Due to the substantial contact with living cells, the vapor pressure of air spaces remains saturated with respect to the temperature and water potential of the cells (Nobel, 2009; Rockwell *et al.*, 2014b). Thus, as water molecules diffuse out of the leaf through stomata, other water molecules evaporate from the surfaces of interior leaf cells. In principle, water could evaporate from the surface of any cell in contact with an air space, however, the actual sites where water changes phase will be determined by both the flow of energy (heat) and liquid water needed to sustain evaporation. Solving the coupled heat and mass transport indicates that most evaporation occurs near the stomata, with a second region of evaporation occurring in the center of a leaf, in the same plane as where the venation is located (Rockwell *et al.*, 2014b).

Evaporation rates from leaves are highly variable and depend on leaf morphology (stomatal size, stomatal density, vein density, leaf size, leaf shape), physiological status of the leaf (stomatal aperture, internal CO_2 concentration, leaf hydration), and on environmental conditions (vapor pressure deficit, wind speed, temperature, light level) (Schuepp, 1993). The maximum transpiration rates reported per leaf surface area of angiosperm plants are in the range of 2×10^{-4} kg/m^2/s (Reported for *Acer macrophyllum* by Simonin *et al.* (2014)). It is interesting

to contrast this value with the evaporation rate J_{fs} from a free body of water into a dry atmosphere

$$J_{\text{fs}} \sim D \frac{\Delta c_{\max}}{\ell}, \qquad (40)$$

where $D = 2.4 \times 10^{-5}$ m^2/s is the diffusion coefficient of water vapor in air at 20°C (Nobel, 2009), $\Delta c_{\max} \simeq 1$ mol/m^3 (or 18 g/m^3) is the concentration gradient (Taiz and Zeiger, 2010), and ℓ is the boundary layer thickness. Assuming a wind speed of $u = 10$ m/s, we can estimate the boundary layer thickness as $\ell \simeq 4.9\sqrt{\nu l/u} \simeq 1.9$ mm, where $\nu = 1.5 \times 10^{-5}$ m^2/s is the kinematic viscosity of air, and $l = 0.1$ m is the leaf size. With these values we find $J_{\text{fs}} = 2.3 \times 10^{-4}$ kg/m^2/s. The most efficient plant leaves thus allow water to escape almost as quickly as from a free surface. This is remarkable given that stomata pores frequently cover only $1-10$ per cent of the leaf surface (Franks and Beerling, 2009). For an in-depth discussion of evaporation and gas diffusion problems related to water transport in plants, see Pickard (1981) and Rand (1983).

The loss of water molecules from the surfaces of cell walls decreases the cell's water potential. Initially, water is drawn towards the sites of evaporation from adjacent and nearby cell protoplasts. As water exits from mesophyll cells, their water potential also falls. Much of this is due to decreases in turgor pressure as the cell walls relax, with the remainder from increasing solute concentration and thus osmotic pressure (Nobel, 2009). Therefore, an important role of turgor pressure in leaf cells is to mitigate against changes in cell volume despite large variations in water potential. As transpiration continues, water will be drawn from cells increasingly further away from the sites of evaporation. Based on the hydration times of individual versus aggregates of cells, the movement of water through plant tissues is thought to occur predominately through the living interiors of cells, with a smaller contribution due to apoplasmic flow through the cell walls (Boyer, 1985). The major pathway for water movement from one cell interior to another involves traversing the membranes and walls separating adjacent cells. Plasmodesmata may also contribute to the movement of water between cells, although their hydraulic contribution is poorly quantified (Fisher and Cash-Clark, 2000). The movement of water across cell membranes is mediated by aquaporins, protein channels with a high selectivity for water (Maurel *et al.*, 2008).

Mesophyll cells can lose only a small amount of water before their cellular and metabolic functions become jeopardized. Without an inflow of water from the xylem, leaves would have to close their stomata within minutes of opening (Kramer and Boyer, 1995; Schymanski *et al.*, 2013). The xylem provides that inflow, replacing water lost via transpiration with water pulled from the soil. As water flows from xylem conduits towards the sites of evaporation, the water potentials in the xylem will de-

crease. How much depends on both the transpiration rate and the hydraulic conductance of the xylem, as the drop in xylem water potential is the result of viscous losses associated with water transport through the plant (Pickard, 1981; Tyree and Zimmermann, 2002). In the xylem close to the sites of evaporation (i.e., within a leaf), the water potential during transpiration can be on the order of 1 MPa more negative than when the water column is stationary (Rockwell *et al.*, 2014b).

3. Stability of water under tension in the xylem

Decreases in xylem water potential (Eq. (17)) can be entirely attributed to decreases in pressure. Because xylem conduits lack semipermeable membranes, there is no osmotic contribution to their potential, and, in any event, the concentration of solutes in the xylem is low. Thus, the pressure of the water within xylem conduits is negative and the liquid is under tension (Tyree and Zimmermann, 2002). This means that water is literally pulled through the xylem. However, it also means that water in the xylem is thermodynamically unstable with respect to its vapor phase (superheated) and thus prone to cavitation (boiling) (Debenedetti, 1996; Stroock *et al.*, 2014). Although cavitation renders xylem conduits useless for transporting water under tension, the activation energy needed to nucleate a phase change is large (Pickard, 1981). Stability limits for homogeneous nucleation, based on theoretical and experimental data, are on the order of -100 MPa (Azouzi *et al.*, 2013; Herbert and Caupin, 2005; Zheng *et al.*, 1991). Thus, water in the xylem is kinetically stable provided it does not come into contact with the vapor phase (Wheeler and Stroock, 2008).

In this review we use the term cavitation to refer to any process in which the local equilibrium of water under tension is replaced by the thermodynamically more stable state of water vapor. In this usage, cavitation can result from homogeneous nucleation as well as from the expansion of bubbles drawn in from a neighboring gas-filled conduit or produced during freezing. Embolism, as used here, refers to the gas-phase that replaces conduits formerly filled with metastable water.

Xylem conduits remain water-filled throughout their development and all of the water that enters the xylem in the roots has previously been forced to flow across endodermal plasma membranes. For these reasons, gas bubbles should be absent from the xylem (Pickard, 1981). Other mechanisms, however, can bring xylem into contact with air. Physical damage that breaches conduit walls, provides one such entry point for air. Freezing represents another mechanism as dissolved gases are segregated from the ice lattice, coalescing to form gas bubbles that can expand once the conduit thaws. The stability limit for bubbles depends both upon their dimension,

which dictate the forces due to surface tension that serve to push the gas back into solution, and any tensions in the xylem, which act in an outward direction on the bubble (Tyree and Sperry, 1989). Larger diameter conduits are more susceptible to freeze-thaw embolization due to the formation of larger air bubbles during freezing as dissolved gases and other impurities are excluded from the crystal lattice (Sevanto *et al.*, 2012).

Embolization is not solely an issue of losing the transport capacity of individual conduits. Once a conduit becomes air-filled, cavitation can spread like a disease to neighboring conduits as air is pulled through pit membranes, something that plant biologists refer to as "air-seeding" (Tyree and Zimmermann, 2002). The tiny bubbles pulled through pit membranes will be unstable in the water-filled conduit and thus will expand, such that the entire conduit becomes filled with water vapor, and eventually, as gases comes out of solution, with air. Thus, a plant's resistance to embolization lies both in the properties of its pit membranes (Choat *et al.*, 2008) and the architecture of its vascular network (Loepfe *et al.*, 2007). At both levels, the system is constrained in terms of its dual function of allowing water to flow easily through the xylem and preventing gases from spreading. We shall return to these issues in Section VI on water transport.

IV. SUGAR TRANSPORT IN PLANTS

A. Experimental Results

To obtain a mechanistic understanding of the physiological processes that drive and regulate sugar transport in plants, detailed measurements of transport speed, sugar concentration, and pressure are needed. Experimental investigations of the phloem, however, have to cope with several factors that limit the number of applicable tools and techniques. The cells in question are buried below several tissue layers, making them difficult to access, for example for live-cell microscopy (Fig. 7). In addition, it is difficult to extract phloem cells for molecular analysis, especially from the leaf, because it is composed of distinct cell types that are present only in low number. Furthermore, the pressurized phloem is very sensitive to manipulation. Any preparatory step that causes the loss of pressure, like incision with a blade, potentially changes the state of cells even though they might be several centimeters away from the site. In spite of these difficulties, methods and approaches have been developed to produce experimental data on the function of the phloem, which will be presented below.

1. Phloem sap sugar concentration

Knowledge of phloem sap composition is important for any quantitative understanding of resource alloca-
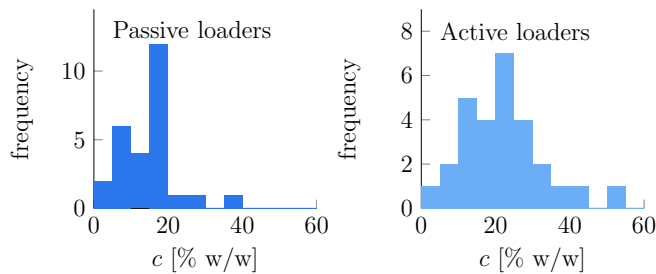
Figure 18 Histograms showing phloem sap concentration measured in plants that utilize passive and active phloem loading strategies (Sec. III.B). See also Fig. 26. Data from Jensen *et al.* (2013b).

Table II The composition of phloem sap from castor bean (Ricinus communis). Data from Hall and Baker (1972).

Component	Concentration (kg/m^3)
Sugars	80-106
Amino acids	5.2
Organic acids	2-3.2
Protein	1.45-2.2
Potassium	2.3-4.4
Chloride	0.355-0.675
Phosphate	0.35-0.55
Magnesium	0.109-0.122

tion within plants. The sugar concentration c is typically around $c \simeq 20\%$ weight (Fig. 18), but the sap also contains a variety of other organic molecules and ions (Table II). Assuming that sap viscosity has a simple dependence on sugar concentration thus suggests that the liquid is approximately twice as viscous as pure water (Fig. 26(a)). One of the first investigations carried out by Hartig (1860) after discovering and naming phloem sieve elements, was aimed at identifying the sap composition. He found that the phloem sap of various angiosperm trees, sampled by the stem incision method, contained 25% to 33% sugar, most of it in the form of sucrose. The question is still timely, as it remains difficult to obtain a complete and artifact-free sample of phloem sap (Jensen *et al.*, 2013b; Turgeon and Wolf, 2009). Phloem sap composition has been obtained from many trees, several of which bleed sap for several minutes after stem incision (Hartig, 1860; Münch, 1930). Only few herbaceous plants, however, bleed as readily. Castor bean (*Ricinus communis*) is one exception and is often used for phloem sap sampling (Hall and Baker, 1972) (Table II). In other herbaceous plants, the incision causes a wound reaction that stops phloem sap bleeding, usually within seconds. The wound reaction can be prevented by making the cut in solution containing Ethylenediaminetetraacetic acid (EDTA), which binds Ca^{2+}, effectively suppressing the signal for clogging(King and Zeevaart, 1974). While sufficient quantities of phloem sap can be collected from any plant with this method, it is prone to artifacts (van Helden *et al.*, 1994; Liu *et al.*, 2012). EDTA is known to soften tissue and can induce leakage of ions and metabolites, including carbohydrates (Hepler, 2005). A less invasive alternative is the sampling of phloem sap with the help of stylectomy. For many plants species, phloem-feeding insects, mostly aphids, can be found (Fisher and Frame, 1984). These insects penetrate the plant tissue with their stylets without severing cells until they reach a sieve element to feed on. To obtain phloem sap, the insect body can be removed and a drop of sap collected from the end of the stylet (Kennedy and Mittler, 1953). Most of the data on phloem sap composition in herba-

ceous plants is based on this technique. Nevertheless, also in this case there is a potential for artifacts, because aphids were shown to alter phloem sap composition by secreting saliva into the phloem to prevent a wound reaction (Furch *et al.*, 2015; Will *et al.*, 2007). Independent of the sampling techniques, the collected phloem sap is generally analyzed with chromatographic and spectrometric techniques in order to identify its components and quantify their abundance. The parallel use of different methods and control experiments to verify the phloem origin of the collected sap has resulted in the identification of its major components. These are sugars, amides and amino acids, secondary compounds, auxin, proteins, RNAs, potassium and other ions. The relative amounts of these components show only limited species-dependence and are shown in Table II for castor bean phloem sap. The sap sugar composition depends on the phloem loading type (see Sec. III.B). Castor bean, as an active apoplasmic loader, transports almost exclusively sucrose. In contrast, more than half of the sugars in the phloem sap of active symplasmic loaders are raffinose and stachyose (Ziegler, 1975; Zimmermann and Ziegler, 1975). Other species were shown to transport mainly sugar alcohols (Reidel *et al.*, 2009).

2. Phloem cell pressure

To this date, one of the most elusive parameters related to phloem function has been the pressure inside sieve elements. The formulation of the pressure-flow hypothesis by Ernst Münch was based on cryoscopic analysis of expressed tissue sap and plasmolysis experiments, which showed a gradient of osmotic pressure from leaves to the stem and roots in forest trees (Münch, 1930). A conclusive validation of Münch's hypothesis requires determining the viscous pressure gradient dp/dx associated with the flow. For a flow speed $u = 10^{-4}$ m/s in a cylindrical tube of radius $a = 10^{-5}$ m, the expected magnitude of the pressure gradient is $|dp/dx| \simeq 8\eta u/a^2 \simeq 10^4$ Pa/m, while for $a = 10^{-6}$ m, it is $|dp/dx| \simeq 10^6$ Pa/m.

One method for measuring phloem cell pressure has taken advantage of the aphid stylectomy approach de-

scribed above (Sec. IV.A.1). After removal of the insect body, pressure can be measured directly by sealing a micropipette over the stylet (Fisher and Cash-Clark, 2000; Wright and Fisher, 1980) or attaching a pressure sensor (Gould *et al.*, 2004, 2005). In trees, where the high number of sieve elements in the bark makes them more accessible, a needle with a narrow tip produced by pulling a glass capillary tube has been used (Hammel, 1968; Lee, 1981; Sovonick-Dunford *et al.*, 1981). This technique was also recently used to measure pressure inside translocating sieve elements in the herbaceous bean plant *Vicia faba* (Knoblauch *et al.*, 2014). The measured pressures lie in the range of $p = 0.6 - 1.4$ MPa for trees, while it can reach up to $p = 2.4$ MPa in herbaceous plants (Fisher and Cash-Clark, 2000; Lee, 1981; Sovonick-Dunford *et al.*, 1981; Wright and Fisher, 1980). This difference in absolute pressure could be related to the difference in phloem loading type (see Section III.B), which is active in herbs and passive in most trees. Furthermore, the high pressure in the phloem of herbaceous plants might have other functions than driving transport, for example in plant defense (Turgeon, 2010). The main quantitative question with respect to the pressure-flow mechanism of Münch – the size the pressure difference between source and sink - has not been answered conclusively, because of the technical difficulty of measuring pressure at different positions on the same plant, ideally on the same phloem strand (Fisher and Gifford, 1986; Pritchard, 1996). The limited available data shows pressure gradients of $\sim 10^5$ Pa/m in tobacco and sugar beet (Fellows and Geiger, 1974; Hocking, 1980), not inconsistent with the Münch hypothesis. Calculations based on pressure measurements in trees suggest that the pressure gradient is smaller in these organisms (Turgeon, 2010).

3. Phloem flow speed

Following the transport of photoassimilates from the leaf to the sink organs has always been of major interest to plant biologists trying to understand the dynamics and regulation of growth. Typical translocation speeds range in magnitude from 10^{-5} m/s to 10^{-4} m/s (Fig. 19). In some cases, like for maize or sugar cane, speeds of up to $\sim 5 \times 10^{-4}$ m/s have been measured (Hartt *et al.*, 1963; Wardlaw *et al.*, 1965). Much higher values that have been occasionally reported for stem phloem transport are most likely the result of experimental insufficiencies (Crafts and Crisp, 1971). Transport speed does not scale with plant height (Dannoura *et al.*, 2011; Liesche *et al.*, 2015; Windt *et al.*, 2006), instead depending primarily on sieve element geometry (Jensen *et al.*, 2011; Mullendore *et al.*, 2010). This can be clearly seen in trees, where a meta-analysis of all available experimental data showed a significant difference in phloem transport speed between gymnosperm and angiosperm species, which is
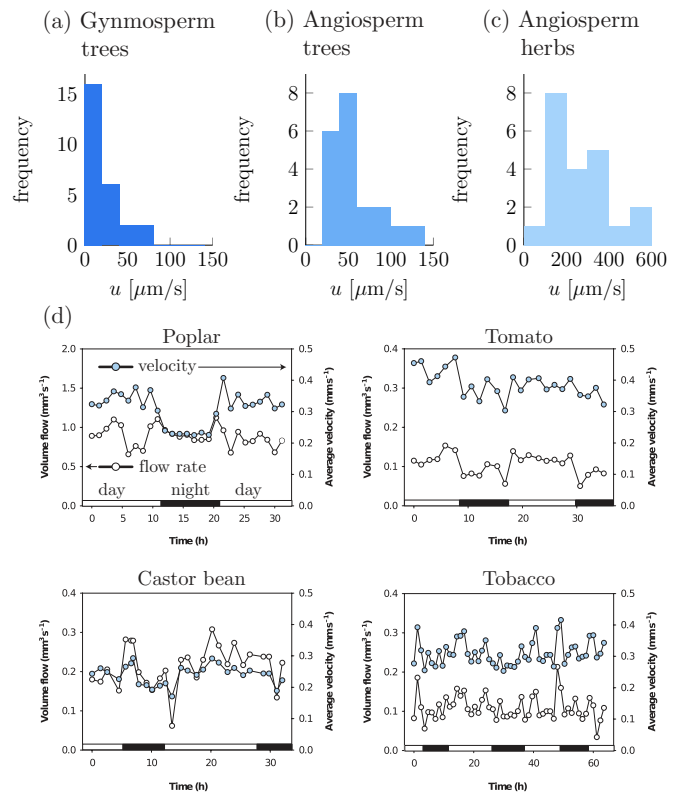

Figure 19 Phloem transport speeds u vary in the range 10^{-5} m/s to 10^{-4} m/s between (a) gymnosperm trees, (b) angiosperm trees, and (c) angiosperm herbs. Panel (d) illustrates the limited diurnal variation in phloem transport rates in four herbaceous angiosperms observed by Windt *et al.* (2006). Note the difference in abscissa scale between (a,b) and (c). Data from (Liesche *et al.*, 2015): (a,b) and (Hartt *et al.*, 1963; Hendrix, 1968; Jensen *et al.*, 2011; Kursanov, 1956; Moorby *et al.*, 1963; Mortimer, 1965; Mullendore *et al.*, 2010; Thompson *et al.*, 1979; Wardlaw *et al.*, 1965; Windt *et al.*, 2006; Ziegler and Vieweg, 1961): (c). Panel (d) adapted from (Windt *et al.*, 2006).

caused by the difference in sieve element and end-wall anatomy (Liesche *et al.*, 2015) as shown in Fig. 19.

The most straight-forward way to identify allocation patterns and measure the amount of carbon transported to different organs is to monitor the organ's increase in dry weight over time (Canny, 1973). More detailed quantifications can be achieved by using dyes or radioisotopes as tracers, or with magnetic resonance imaging.

The movement of substances in the phloem can be traced directly with the help of dyes. After cutting the tip of a leaf of a potato plant, Dixon and Ball (1922) applied a drop of the dye eosin and followed its spread to the shoot tip, the roots and the tuber (potato). Several authors have investigated phloem translocation speeds by further developing this dye tracing approach (see e.g. (Froelich *et al.*, 2011; Jensen *et al.*, 2011; Savage *et al.*, 2013; Schumacher, 1948)). Dyes have also been used to quantify the capacity of loading and unloading path-

ways (Liesche and Schulz, 2012; Oparka *et al.*, 1994), as well as the impact of wounding on sieve element function (Knoblauch *et al.*, 2001; Schulz, 1992).

Radioisotope tracers are considered less invasive than dye techniques, since little or no removal of tissue to access the phloem is necessary. The technique was instrumental in establishing the general principles of source to sink transport (reviewed by Crafts and Crisp (1971); Ho *et al.* (1989); Minchin and Troughton (1980)) and the measurement of key parameters of phloem transport, such as speed and volume. Typically, isotopic carbon, in the form of $^{11}CO_2$, $^{13}CO_2$ or $^{14}CO_2$ is applied to leaves, where it is fixed and built into sugars. The translocation of isotope-labeled sugars is subsequently tracked by detectors positioned outside the plant (Epron *et al.*, 2012; Liesche *et al.*, 2015).

In the last decade, magnetic resonance imaging velocimetry was adapted for measuring phloem transport speed and volume (Peuke *et al.*, 2001; Windt *et al.*, 2006) (Fig. 19(d)). Magnetic resonance imaging has the advantage of providing visual information of flow, i.e. the cross-sectional area of actively translocating sieve elements at the time of analysis (Windt *et al.*, 2006).

4. Molecular biology of phloem transport

Sucrose transporters transport sucrose either intercellularly across plasma membranes or intracellularly across the vacuole membrane (Ayre, 2011; Kühn and Grof, 2010). Sucrose transporters are essential to phloem function in active apoplasmic phloem loaders as they pump sucrose into the companion cell-sieve element complex in source leaves (Gahrtz *et al.*, 1994; Riesmeier *et al.*, 1994), thereby determining the phloem loading rate (Dasgupta *et al.*, 2014) (for loading modes, see Section III.B). They are also responsible for retrieval of leaked sucrose along the transport phloem (Gould *et al.*, 2012). In passive symplasmic phloem loaders, vacuolar sucrose transporters were shown to similarly influence phloem loading (Payyavula *et al.*, 2011). In active symplasmic loaders, described more quantitatively in Section VI.C, synthesis of the higher molecular weight sugars raffinose and stachyose, catalyzed by galactinol synthase in the companion cells, determines the phloem loading rate (Haritatos *et al.*, 1996; McCaskill and Turgeon, 2007). In symplasmic sinks, like growing roots, the unloading rate depends on sucrose utilization, either by starch synthesis or vacuole import for carbon storage or energy conversion for growth. Influence on the unloading rate might be exerted by proteins that control the effective diameter of plasmodesmata (Baluška *et al.*, 2001; Schulz, 1995, 1999). In apoplasmic sinks, like fruits or seeds, unloading is controlled in two steps: by cell wall invertases that break down sucrose and by monosaccharide transporters that import the resulting glucose and fructose molecules

into the storage cells (Patrick, 1997).

During phloem development, sieve pore formation is preceded by deposition of callose between the plasma membrane and the cell wall around each plasmodesma. The pore is formed by widening of the plasmodesma channel, a process that involves removal of some of the callose. A specific enzyme was found to be responsible for this process (Barratt *et al.*, 2011; Xie *et al.*, 2011). Furthermore, mutants lacking this protein were not able to perform a wound reaction, demonstrating that callose synthesis is needed in this process. Inside the sieve element lumen, a variety of proteins, referred to as P-proteins (Section III.A) are present that have been categorized as amorphous, crystalline, filamentous, tubular, or fibrillar. The main role of P-proteins is assumed to be clogging of the sieve tubes in response to wounding (Eschrich, 1975; Knoblauch and van Bel, 1998).

From a wealth of physiological experiments it is clear that phloem transport is finely regulated and adjusted to the environmental conditions. So far only few pieces of the molecular machinery regulating phloem transport have been identified, such as sensors for the sugar concentration in source and sink, or membrane transporters facilitating sugar release from the phloem. However, the emerging improvements of phloem sampling in connection with molecular biological approaches should soon lead to a better understanding of the subtleties of phloem transport (see e.g. Anstead *et al.* (2013); Doering-Saad *et al.* (2006)).

B. Biomimetic Models of Sugar Transport in Plants

Experimental systems designed to mimic transport processes in plants and animals alike have been used by several authors to test mechanistic hypotheses of vascular physiology (Wong *et al.*, 2012). Biomimetic models of xylem transport played an important role in validating the cohesion-tension theory, starting with the work of Dixon and Joly (1895). For an excellent overview of historical and technical aspects of this discussion, we refer the reader to Brown (2013) and Stroock *et al.* (2014). Here, we focus on phloem transport models and begin at the origin of this field; Münch's 1927 experiment (Münch, 1927, 1930). Münch's device to mimic phloem transport consisted of two flasks connected by a glass tube (Fig. 20(a)). Parts of the flasks were covered by a semipermeable membrane that allowed water, but not small molecules, to pass. He introduced a concentrated sugar solution into one of the flasks and submerged both in a water bath. From this experiment, he reported a mass flow through the glass tube connecting the flasks of high and low concentration. By equating the flasks to source and sink organs, Münch argued that similar flows occur in plants, since "same causes have same effects" ((Münch, 1930) p. 37, translation by Knoblauch
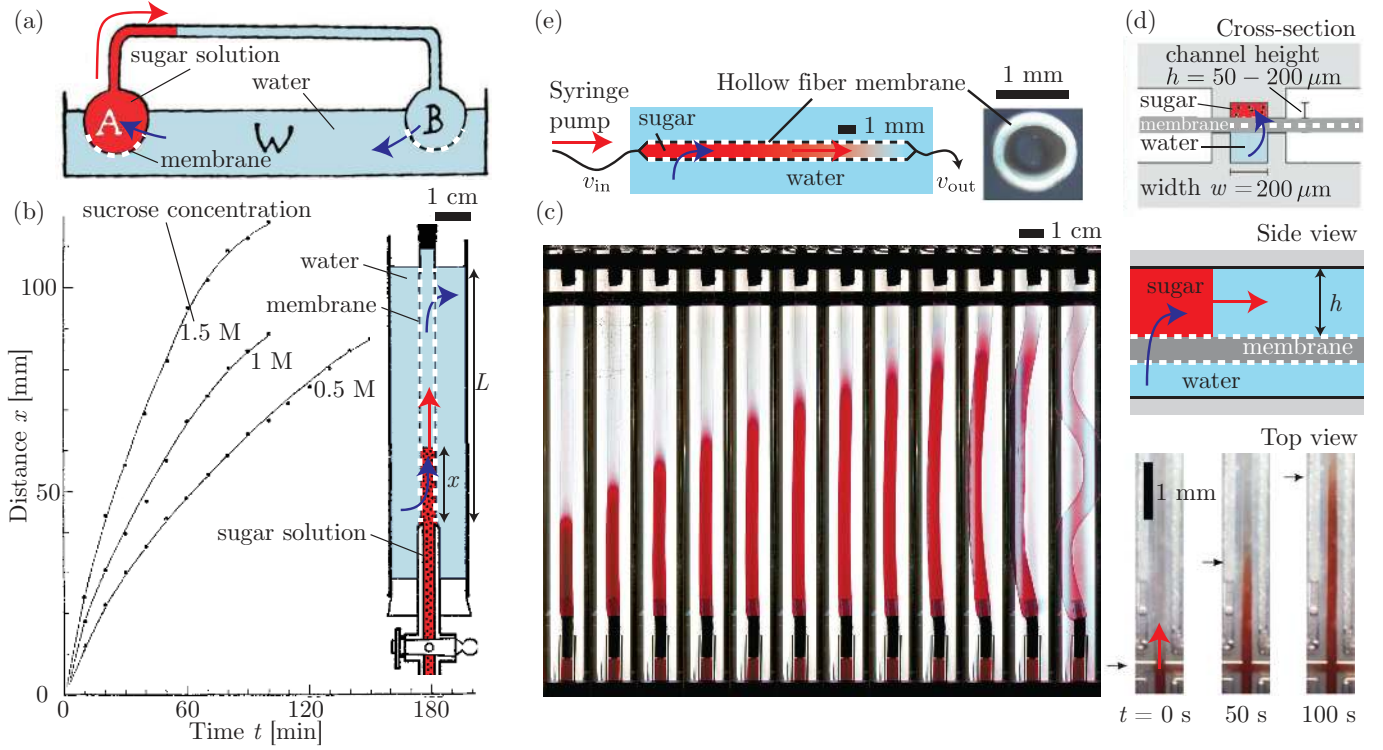
Figure 20 Biomimetic models of phloem transport. (a) Device used by Münch (1927) to demonstrate osmotically drive flows between flasks A (high sugar concentration) and B (negligible sugar concentration) submerged in a water bath W. (b) Osmotic pumping in Eschrich et al. (1972)'s cylindrical membrane tube, and (c) a similar more recent experiment (Jensen et al., 2009b). (d-e) Microfabricated osmotic pumps byJensen et al. (2009a) and Haaning et al. (2013). See details in text (Sec. IV.B). Adapted from (Eschrich et al., 1972; Haaning et al., 2013; Jensen et al., 2009a; Münch, 1927).

and Peters (2010)).

Following Münch's example, a number of workers have improved upon his basic setup to elucidate various factors that may influence plant transport characteristics. Eschrich et al. (1972) was the first to use a semipermeable cylindrical pipe to capture the effects of osmotic flow along the transport pathway (Fig. 20(b)). Eschrich's setup comprised a cylindrical membrane tube (7 mm diameter, $\sim$ 20 cm length) fitted inside a larger water-filled glass tube. At the beginning of the experiment, a small amount of sugar was introduced into the near end of the membrane tube. The group conducted experiments with the far end being either open or closed. They observed that the front velocity v increased in linear proportion to the initial concentration c_0, and that the speed was either constant in time or decayed exponentially, if the far end of the tube was either open or closed (Fig. 20(b)). To rationalize these observations, Eschrich et al. (1972) used the following conservation argument: for incompressible flow in a closed semipermeable tube of length L and radius a embedded in water, we imagine the part of the tube between the base and $x(0)$ initially filled with sugar solution and the rest with pure water. For a wide tube with slow flow, viscous effects and thus the pressure gradient along the tube is negligible and the pressure is sim-

ply equal to the osmotic pressure averaged over the tube, i.e., $p = RT\bar{c}$, where $\bar{c} = c_0 x(0)/L$ is the constant average sugar concentration. The water volume flow through the tube wall ahead of the sugar front x (where there is no osmosis) is $-2\pi a(L - x)L_p RT\bar{c}$, where L_p is the permeability of the tube and the flow is negative since water flows out. This will be equal to the rate of change of volume ahead of x and thus, due to incompressibility, to $-\pi r^2 dx/dt$. Putting these two expressions together we get

$$\frac{dx}{dt} = 2\frac{L_p RT\bar{c}}{a}(L - x) \qquad (41)$$

Thus, the instantaneous front position is $x(t) = L - (L - x(0))\exp(-t/\tau)$ where the characteristic time $\tau = 2L_p RT\bar{c}/a$. If by contrast the tube is open, the pressure is atmospheric everywhere in the liquid and the only driving force is the osmotic suction. This leads to an inflow behind the front of $2\pi a x(0)L_p RTc_0$ so in this case the velocity is constant

$$v_{\text{open}} = 2\frac{L_p RT x(0)c_0}{a}. \qquad (42)$$

The initial velocity for the closed tube is $v_{\text{closed}} = 2L_p RTc_0 x(0)(L - x(0))/(aL)$ and the ratio of the two

velocities is

$$\frac{v_{\text{closed}}}{v_{\text{open}}} = \frac{L - x_0}{L}. \tag{43}$$

The ratio approaches unity when $x_0 \ll L$, so the characteristic velocity scale for long tubes is in both cases $2L_pRTc_0x(0)/a$.

The experiments by Münch (1927) and Eschrich *et al.* (1972) were conducted in macroscopic setups with channel radii of around 5 mm. This is approximately 500 times greater than the typical phloem sieve element size (radius $a = 10$ µm). Aided by developments in microfabrication techniques (Stone *et al.*, 2004; Xia and Whitesides, 1998), Jensen and co-coworkers refined the Eschrich and Lang experiments in micro-channels of diameters $50 - 200$ µm (Jensen *et al.*, 2009a, 2011, 2009b) which are comparable in size to sieve elements of e.g. *Curcubita Maxima* (Jensen *et al.*, 2011). Their base device (Fig. 20(e)) comprised a semi-permeable membrane squeezed between shallow channels cut in two PMMA-plates. The upper channel of height $h = 50 - 200$ µm and width $w = 200$ µm carried the sugar solution, while the lower channel provided contact to a water bath held at atmospheric pressure. By varying the channel height and sugar concentration, Jensen *et al.* (2009a) found good agreement between Eq. (42) and experiments.

The experiments described thus far have dealt with transient flows where the system relaxes towards equilibrium from an initial state of osmotic imbalance (Fig. 20(c)). The prevailing situation in plant phloem, however, is likely closer to a steady-state where a continous influx of sugars at the leaf is consumed by metabolic and growth processes in distal parts of the plant. Lang (1973) modified Eschrich's experiment and used a long semipermeable tube ($L = 7.2$ m, $d = 6.35$ mm) to study steady-state osmotic flows by slowly injecting a 0.2 M sucrose solution at one end of the pipe. He carefully documented the approach to steady state and found that the flow speed increased from the inlet to the outlet by a factor $\gamma = v_{\text{out}}/v_{\text{in}} - 1 = 3$ due to osmotic inflow along the tube (from $v_{\text{in}} = 0.16$ cm/min to $v_{\text{out}} = 0.66$ cm). The time to reach steady state observed was set by $L/v_{\text{in}} \sim 75$ h. When performing a similar experiment in the aforementioned microfluidic device (Fig. 20(e)) Jensen *et al.* (2011) found similar values of the velocity increase γ in a 200 µm × 200 µm rectangular channel. Haaning *et al.* (2013) conducted the first systematic experimental study of the factors that influence the flow amplification factor γ. Their setup used a hollow-fiber-membrane (Fig. 20(d)), a cylindrical tube of length $L = 14$ cm, radius $a = 500$ µm with semi-permeable walls. Haaning *et al.* (2013) varied the inlet velocity, inlet concentration, and channel length, and observed values of γ in the range $0.1 - 10$. Reasonable accord with theoretical estimates due to Aldis (1988b) and Thompson and Holbrook (2003b) were found: Taking the flow speed v

and concentration c to be averaged over the cross-section of the pipe, one arrives at the conservation equations for water volume and solute mass

$$\partial_x v = 2\frac{L_pRTc(x)}{a} \tag{44}$$

$$\partial_x(cv) = 0 \tag{45}$$

With boundary conditions $v(0) = v_{\text{in}}$ and $c(0) = c_0$ these can be solved to yield the speed profile

$$v(x) = v_{\text{in}}\left(1 + 4L_pRTc_0x/(v_{\text{in}}a)\right)^{1/2}. \tag{46}$$

In terms of the flow amplification factor $\gamma = v_{\text{out}}/v_{\text{in}} - 1$ is

$$\gamma + 1 = \frac{v_{\text{out}}}{v_{\text{in}}} = \sqrt{1 + 4\frac{L_pRTc_0L}{v_{\text{in}}a}} \tag{47}$$

In some cases, however, Haaning *et al.* (2013) found that this prediction overestimates the outlet velocity. To account for this discrepancy, they relaxed the assumption that the solute concentration $c(x)$ is uniform across the tube in Eq. (44) and derived an expression for γ which reduces to Eq. (47) when radial Péclet number is quite small, i.e. when the concentration is uniform across the tube. For further details see Sec. V.D).

C. Hydraulic Resistor Theory

To understand the basic rules for the long-distance translocation in the phloem, it is advantageous to start with a simple "resistor" model of a "one-dimension plant" as shown in Fig. 21. The plant's vascular system is viewed as a collection of parallel tubes of constant diameter that span the full length of the plant. In each tube, both ends are closed, but near each end, the walls are semipermeable (penetrable to water but not to sugar), representing the leaf and the root respectively. Such approaches have been used successfully in this field, e.g., by Daudet *et al.* (2002); Lacointe and Minchin (2008); Minchin *et al.* (1993), where more complex network configurations have been modeled. Here we follow Jensen *et al.* (2012b) in the treatment of a single tube, but with different resistivities coming from axial pressure driven flow along the tube and lateral osmotic flows. In reality, the tubes do not necessarily have the same diameter all the way, and the tubes do not just connect sugar producing leaves (sources) to the roots, but also to other sugar consuming sinks such as young leaves as in Lacointe and Minchin (2008). Thus, the ideal, globally optimal structure likely resembles the observed hierarchical network architecture of the plant body. However, as a simple representation for the longest pathway this analysis still turns out to be useful. The differences in concentration between source and sink tissues provides the driving force for the transport via the osmosis generated in the leaf section.

1. Optimization of phloem transport speed

Our aim is to determine how this tree translocates sugar most efficiently. Following Jensen *et al.* (2011), we shall argue that "most efficient" in this context should simply mean that the rate of sugar transport is maximal for a given investment in vascular tissue. If we assume that the total cross-sectional area for the phloem tubes is constant at a given position, this will be equivalent to maximizing the flow velocity (i.e. flux) in each tube. In addition a large flow velocity will allow the plant to respond rapidly to external perturbations. Finally, we note that phloem transport speed has been shown to influence photosynthesis, belowground respiration, and whole plant transfer and integration of information (Mencuccini and Hölttä, 2010). Of course, this simple system does not consider the possibility of branching architectures, as seen in real plants. It does, however, capture an important trade-off: a wide tube will allow rapid flow of sap since the resistance is low, but the water has to come in by osmotic pumping through the surface of the leaf part, and for a wide tube this will be inefficient, since the surface to volume ratio is small. For a narrow tube, the situation is reversed: now the osmotic pumping through the surface is efficient, but the flow will be blocked by the large resistance through the stem. Thus, there should be an optimal tube radius giving maximal flow velocity.

To determine this optimal radius, a^*, we consider each of the tubes separately. It has a radius a, a "leaf" segment of length l_1, a "stem" segment of length l_2 and a "root" segment of length l_3 through which fluid of flow rate Q is running, and, instead of directly solving the fluid dynamical equation, which will be done later in Section V, we shall only consider the basic driving forces in each section and assign a corresponding "resistance". The stem segment is simply treated as a solid tube with impenetrable walls through which the fluid is driven by the pressure difference Δp between the leaf and the root. We further assume that this pressure difference is primarily created by the difference in osmotic pressure $\Delta \Pi$ due to sugar loading in the leaf and unloading in the root. Due to the low Reynolds numbers, it is thus simply a Poiseuille flow with flux

$$Q = \frac{\Delta p}{R_2} \tag{48}$$

where Δp is the pressure drop along the stem and the resistance for a cylindrical tube and fluid viscosity η is given by (Eq. 4e)

$$R_2 = \frac{8\eta l_2}{\pi a^4} \tag{49}$$

All the osmotic water intake is assumed to take place in the semipermeable (leaf) part of length l_1 which we assume to be loaded with a sugar solution, such that there is a concentration difference Δc_1 between inside
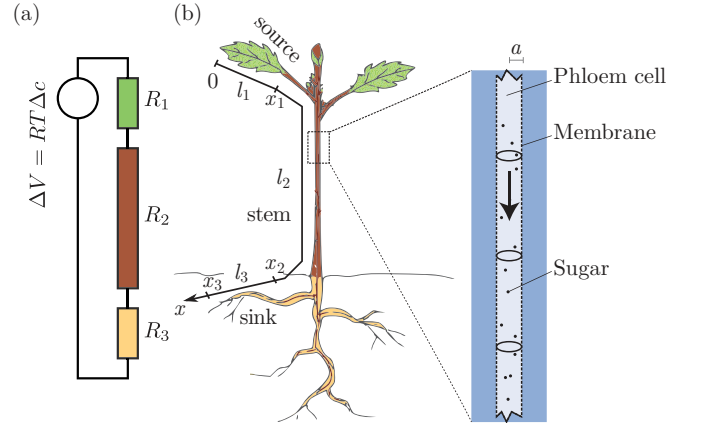

Figure 21 Resistor model of phloem sugar transport. (a) circuit diagram of with resistors representing hydraulic resistance in the source, stem, and sink regions of panel (b). Adapted from (Jensen *et al.*, 2011).

and outside, creating an osmotic pressure difference of $\Delta \Pi_1 = RT \Delta c_1$. The concentration difference Δc_1 is generated by phloem loading processes in which sugars produced in mesophyll cells are transferred into the phloem sieve elements (Sec. III.B, Fig. 12). Plants that use active loading generally appear capable of generating larger Δc's than species which use passive loading (Fig. 18). The difference in water potential, $\Psi = p - \Pi = p - RTc$ drives a trans-membrane water flux with the flow rate

$$Q = \frac{RT \Delta c - \Delta p}{R_1} \tag{50}$$

with the leaf-resistance

$$R_1 = \frac{1}{2\pi a L_p l_1} \tag{51}$$

which differs from Eq. (18) by the surface area $2\pi aL$ of the tube, and where we have assumed that the Poiseuille resistance in the leaf part is negligible since $l_1 \ll l_2$.

In the root, the situation is the reverse: here water is expelled so we obtain similarly the root-resistance

$$R_3 = \frac{1}{2\pi a L_p l_3} \tag{52}$$

and if we now assume that the pressure drops inside the leaf and root are small compared to the osmotic pressures (which corresponds to small Münch number for the leaf/root segments in the terminology of Sec. V) we can write the pressure in the entire leaf segment as p_1 and that of the root as p_3, and "Ohms's law" for the whole tube is

$$RTc_1 - p_1 = QR_1, \tag{53a}$$

$$p_1 - p_3 = QR_2, \tag{53b}$$

$$p_3 - RTc_3 = QR_3, \tag{53c}$$

Adding them, we get

$$RTc_1 - RTc_3 = RT\Delta c = QR_{tot} \qquad (54)$$

where Δc is the difference in concentration between leaf and root and the total resistance is

$$R_{tot} = R_1 + R_2 + R_3 \qquad (55)$$

as expected for resistance in series. The flow velocity will be

$$u = \frac{\Delta p}{\pi a^2 R_{tot}} = 2L_p \Delta p \frac{a^2 l_1 l_3}{V l_1 l_2 l_3 + a^3 (l_1 + l_3)} \qquad (56)$$

where we have used the notation Δp as a generic symbol (in the present case it should actually by a difference in *osmotic* pressure, $\Delta\Pi$) and

$$V = 16\eta L_p \qquad (57)$$

is a characteristic length scale - the "permeability length" to which we shall return below. The velocity (56) has, when varying only a, its maximum at

$$a^* = \left(2V \frac{l_2}{l_1^{-1} + l_3^{-1}}\right)^{1/3} = \left(2V \frac{l_1 l_2 l_3}{l_1 + l_3}\right)^{1/3} \qquad (58)$$

If the roots and the leaves are similar in size, we find

$$a^* = (V l_1 l_2)^{1/3} = (16\eta L_p l_1 l_2)^{1/3} \qquad (59)$$

It is perhaps more typical that the roots are considerably larger than the leaves – at least for trees. With $l_1 \ll l_3$ we get the result

$$a^* = (2V l_1 l_2)^{1/3} \qquad (60)$$

which differs from (Eq. 59) only by a factor $2^{1/3} \approx 1.26$.

The corresponding value of the flow velocity is

$$u^* = 2L_p \Delta p \frac{2^{2/3}}{3} \frac{l_1^{2/3} l_3^{2/3}}{V^{1/3} l_2^{1/3} (l_1 + l_3)^{2/3}} \qquad (61)$$

One can think about the condition (Eq. 58) as "impedance matching": inserting the expression for a^* into (Eqs. 49), (51) and (52) leads to

$$R_2 = \frac{1}{2}(R_1 + R_3) \qquad (62)$$

and thus the resistance of the stem has to be matched to the average of the resistance in the ends.

The flow velocity from (56) or (61) can be used to give an estimate of the transit time τ for sugar from the leaves to the root as $\tau \approx l_2/u$ which for optimised phloem tubes gives

$$\tau \approx \frac{l_2}{u^*} = \frac{3}{2^{5/3} L_p \Delta p} \frac{V^{1/3} (l_1 + l_3)^{2/3}}{l_1^{2/3} l_3^{2/3}} l_2^{4/3} \qquad (63)$$
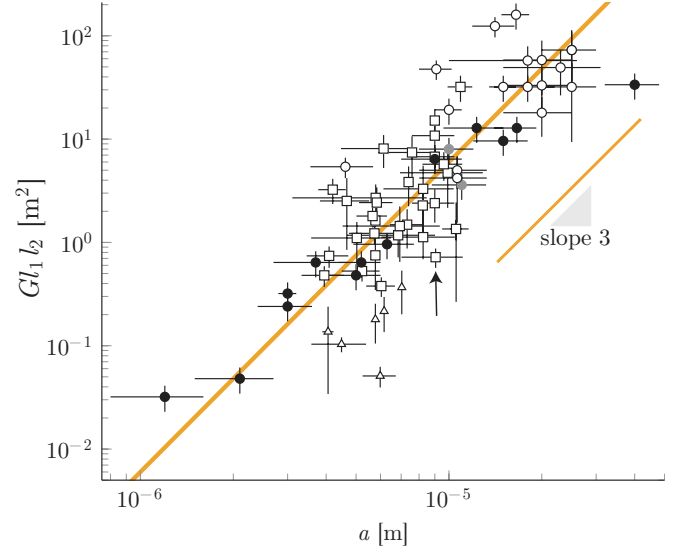

Figure 22 Evidence from field measurements that the radius of phloem sieve elements is optimized for rapid sugar translocation. Comparison between the predicted optimal radius $(a^*)^3 \sim l_1 l_2$ (Eq. (64)) and the measured radius a. Symbols indicate angiosperm herbs (dots), angiosperm trees (open circles), angiosperm shrubs (grey dots), gymnosperm trees (open square), and gymnosperm trees with scales (open triangle). All plants were mature. G is a geometrical factor depending on the cross-sectional shape of the tubes and similarly a is an effective radius. Data from (Jensen *et al.*, 2011, 2012a)

The scaling relation (Eq. 59) was first obtained by Jensen *et al.* (2011) and tested, as shown in Fig. 22a, against measured sieve tube radii a and the product of the lengths of stems and leaves for 20 plants ranging from 10 cm up to 40 m. In Jensen *et al.* (2012b) this study was extended by a large number of trees, 32 angiosperms and 38 gymnosperms (mostly conifers), up to 50 m in height. In gymnosperms, the cross-section of the sieve tubes are typically not circular, but closer to rectangular (see Fig. 10c), and the scaling relations have to be modified by a geometrical factor and a corresponding definition of the effective radius. As discussed in detail in (Jensen *et al.*, 2012b) (Appendix A), the scaling relation can in general be written (taking for concreteness the case of $l_1 \sim l_3$)

$$a^* = (G\eta L_p l_1 l_2)^{1/3} \qquad (64)$$

where a^* now is an effective radius depending on the shape of the tubes and G is a geometrical factor.

It is surprising that angiosperms and gymnosperms pretty much fall on the same scaling curve. Angiosperms are much younger, around 130 million years is the current estimate of their age, compared to the gymnosperms which are probably closer to 300 million years old, and they differ in many fundamental ways. In Section IV.A.3, in particular in Fig 19, it was shown that the typical flow

speeds in the phloem of gymnosperms are considerably smaller than that of angiosperms - but still they seem to be optimized in the same way.

As noted above, the optimality condition, e.g., Eq. (59) expresses the optimal radius as the cubic root of three lengths: the length of the stem, the length of the leaves and the quantity $V \sim \eta L_p$ with the dimensions of a length. Inserting typical numbers for sieve tubes, i.e., $L_p \approx 5 \times 10^{-14}$ m s^{-1} Pa^{-1} and $\eta \approx 2 \times 10^{-3}$ Pa s $= 2\eta_w$ (twice the viscosity of pure water) we find $\eta L_p \approx 10^{-16}$ m, which seems to be a length scale more relevant to particle physics than to biophysics. In fact, one should not think of it as a single length, but as involving several lengths having to do with the structure of the semipermeable plasma membranes producing the osmotic effects. Let us assume that the membrane has n pores pr unit area, for simplicity cylindrical, each with radius a_p and length d, the thickness of the membrane. The pore density n can be written in terms of the covering fraction ϕ of the pores as

$$n = \frac{\phi}{\pi a_p^2} \qquad (65)$$

and the flux pr. surface area passing the membrane is (if $a_p \ll d$) for a given pressure difference Δp

$$q = n\frac{\pi a_p^4}{8\eta_w d}\Delta p = \frac{\phi a_p^2}{8\eta_w d}\Delta p \equiv L_p \Delta p \qquad (66)$$

where we use η_w, since the sugar cannot penetrate the pores. Thus

$$\eta L_p \approx \frac{\phi a_p^2}{4d} \qquad (67)$$

If we take typical values for the membrane thickness $d \approx 5$ nm, we see that the values $a_p \approx 2$ Å and $\phi \approx 0.5 \times 10^{-4}$ will lead to the above value $\eta L_p \approx 10^{-16}$ m. The same value of a_p corresponds to the water being transported through aquaporins, but it implies also that our use of classical Poiseuille flow is at best suggestive. On the other hand, a typical value from the literature for the permeability of a single aquaporin is $l_p = 10^{-20}$ m^3 s^{-1} (Nielsen (2010) Table I) where

$$l_p = \pi a_p^2 \frac{RTL_p}{\phi V_w} \qquad (68)$$

where V_w is the molar volume of water. Inserting values above for L_p and a_p gives $l_p \approx 10^{-24}\phi^{-1}$ m^3 s^{-1}. A comparison of this number with the value of l_p from Eq. (68) gives $\phi \approx 10^{-4}$, in reasonable agreement with our earlier estimate.

In Fig. 23, a complementary scaling plot showing how the cross-sectional area of the sieve elements vary with the length of the stem. The cross-sectional area was used rather than the radius since the sieve elements of gymnosperms are typically not cylindrical (Fig 10). The plot
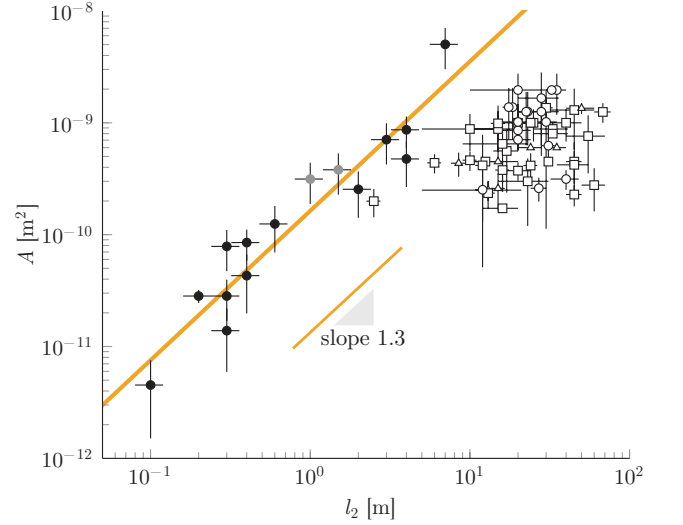

Figure 23 Sieve element cross-sectional area $A = \pi a^2$ is approximately proportional to stem length l_2 for stems shorter than ~ 10 m, and saturates above that height. Symbols indicate angiosperm herbs (dots), angiosperm trees (open circles), angiosperm shrubs (grey dots), gymnosperm trees (open square), and gymnosperm trees with scales (open triangle). Data from (Jensen *et al.*, 2012b).

shows that the width of the sieve tubes grow for small plants (up to around 10m in size), but for larger plants (trees) this growth basically stops. The sieve element radius ($\sim$ square root of the cross-sectional area) never exceeds a value of approximately 20μm. The reason for this is not known, but one has to keep in mind that the sieve elements are single living cells, and there might be good structural reasons for restricting its size.

We end this section by discussing the dependence of the velocity u, Eq. (56), on the geometric parameters of the problem. Since the sink length is difficult to ascertain, we proceed in the simplified case where the sink resistance is negligible: $R_3 \ll R_1, R_2$ (i.e., $l_3 \gg l_1, l_2$). In that limit, using the terminology $l_1 = l$ and $l_2 = h$, the velocity (Eq. (56)) is

$$u = \frac{2a^2 L_p l}{a^3 + 16\eta L_p lh}\Delta p \qquad (69)$$

and the optimal radius is now $(a^*)^3 = 2Vlh$ as in Eq. (60) with V given by Eq. (57). The general scaling with the geometric parameters is illustrated in Fig. 24. At constant h and l, the speed as function of conduit radius a can be expressed in terms of the relative conduit size $\alpha = a/a^*$

$$\frac{u(a)}{u(a^*)} = \frac{3\alpha^2}{1 + 2\alpha^3} \qquad u(a^*) = \frac{2^{1/3}}{3}\frac{(lL_p)^{2/3}}{(h\eta)^{1/3}}\Delta p, \quad (70)$$

where $u(a^*)$ is the speed at the optimal radius. As a

function of leaf length l, the speed is

$$\frac{u(l)}{u(l \to \infty)} = \frac{\lambda}{\text{Mü}^{-1} + \lambda} \qquad u(l \to \infty) = \frac{a^2}{8h\eta}\Delta p \quad (71)$$

where $\lambda = l/h$ and $\text{Mü} = 16\eta L_p h^2/a^3$ is the Münch number, which characterizes the ratio of viscous to membrane flow resistance (discussed in Sec. V), based on the leaf geometry. Considering only variations in the stem length h we finally have

$$\frac{u(h)}{u(h \to 0)} = \frac{1}{1 + \text{Mü}'\lambda^{-1}} \qquad u(h \to 0) = 2\frac{lL_p}{a}\Delta p \quad (72)$$

where the parameter $\text{Mü}' = l^2/h^2\text{Mü} = 16\eta L_p l^2/a^3$, is the (much smaller) Münch number, based on the leaf geometry.

The dependence of the speed u on the length-scales $a, l,$ and h, Eqns. (70)-(72), are plotted in Fig. 24. Panel (a) illustrates the optimality criterium, Eq. (60), and that the speed is reduced by up to 35 % for radii in the interval $a^*/2 < a < 2a^*$. Panel (b) shows an initial linear growth with leaf size followed by an asymptotic approach to a constant level. A larger leaf leads to a greater flow speed because the flow rate increases along the vasculature in the leaf due to osmotic exchange of water, acting as tributaries to a river. As the leaf grows very large, however, the leaf resistance becomes small compared to the stem resistance $R_1 \ll R_2$, and ultimately the flow speed can never exceed the value $a^2\Delta p/(8\eta h)$. Finally, panel (c) demonstrates a monotonic decrease in speed as function of plant height h due to viscous friction in the stem.

It is amazing that a model as simple as the one proposed here can say anything useful. We all know the complicated network structure of leaves, and we would thus assume that a model treating each phloem path as a simple tube of constant radius is nonsensical. One should, however, keep in mind that many of the vein bifurcations seen in a leaf are actually points where the vascular bundle is split, whereas the number and size of the individual sieve tubes is constant. In pine needles it has thus been seen that the area of each individual sieve element is approximately constant along the length of a pine needle (Ronellenfitsch et al., 2015). Whether the same is true for the truly two-dimensional leaves of angiosperms with their characteristic reticulate networks is not known at present. Variations in the diameter of the sieve tubes with height along the stem of trees (pines, ashes and willows) were recently investigated in (Petit and Crivellaro, 2014). The results were fitted to power laws $a \sim h^b$, where h is the height along the stem, with very low powers $b \approx 0.1 - 0.2$ and correspondingly very slow variation. This corresponds well with the lack of variations of the radius of sieve tubes (or their cross-sectional area) with the height of the tree shown in Fig. 23.
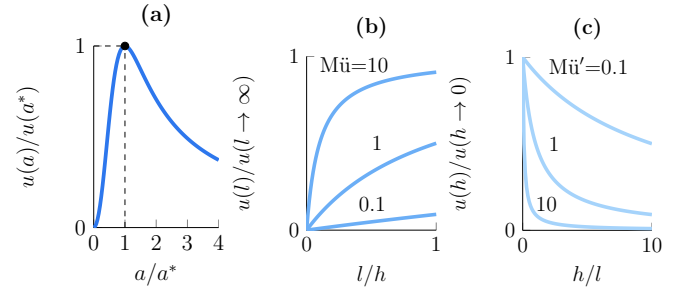
Figure 24 Scaling of the osmotic pumping velocity u (Eq. (69)) with geometric parameters according to Eqns. (70), (71), and (72).
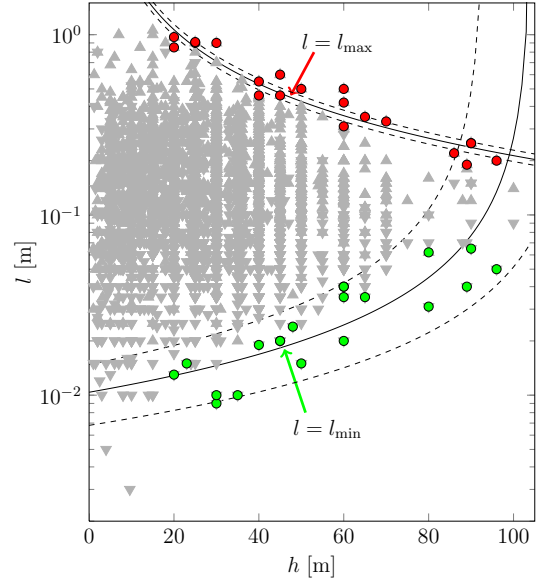
Figure 25 The variability of leaf sizes decreases with plant height, forming upper and lower boundaries (solid lines). Gray triangles show the reported range of leaf sizes for particular species as the longest and shortest leaf lamina length l plotted as a function of tree height h. Solid lines show fits to theory (Eqns. (73) and (74)). Adapted from (Jensen and Zwieniecki, 2013).

2. Limits to leaf size

Leaf sizes in angiosperm trees vary by more than 3 orders of magnitude, from a few mm to over 1 m (Fig. 25). Leaf morphology is influenced by a number of factors, including photosynthesis, gravity, wind, herbivores, and vascular transport efficiency (Onoda et al., 2011). For instance, the leaf must be kept more of less in the horizontal plane to maximize photosynthesis. This imposes mechanical constraints on the length of the petiole and size and mass of the leaf (for a detailed discussion, see Niklas (1994)).

Remarkably, the large diversity in leaf size is only expressed in small trees, and the observed leaf size range declines with tree height, forming well-defined upper and

lower boundaries (solid lines in Fig. 25). Jensen and Zwieniecki (2013) hypothesized that this could be rationalized based on considerations related to sugar export from the leaf. The fact that large trees should have small leaves can be understood on the basis of the scaling relation Eq. (59) or Eq. (64) combined with the experimental finding (Fig. 23) that the sieve tube radius in large trees apparently approaches a constant value ($a_{max} \approx 20\mu m$) leading to the scaling $l \sim 1/h$. To obtain the *maximal* leaf length Jensen and Zwieniecki (2013) used an expression for the energy flux $E = kcu$, where k is a metabolic constant and u is given in terms of leaf size l and tree height h by Eq. (69). Since the plant invests considerable amounts of energy in constructing and maintaining photosynthetic tissue, they argued that it will curtail the construction of still larger leaves once the energy flux E approaches the maximum energy output $E_{\max} = kca^2\Delta p/(8\eta h)$. At this point, the gain in energy output from increasing the leaf size is too small to offset the cost of building and maintaining the leaf, in accord with Charnov (1976)'s marginal value theorem. Further, leaf growth will cease once the energy output E has reached a fraction $E \sim (1-\tau)E_{\max}$ of the maximum obtainable, where the constant number $\tau \ll 1$. It follows that the maximum allowed leaf length $l_{\max}$ at a given height h is

$$l_{\max} = \frac{1}{16}\frac{a_{max}^3}{\tau L_p \eta}\frac{1}{h}. \tag{73}$$

While the leaf size derived in Eq. (73) provides a link between energetic constraints and the maximum leaf size, it does not account for the apparent lower limit to leaf size (Fig. 25). Based on the rationale that vascular systems are formed because cell-to-cell diffusion is insufficient as a transport mechanism over long distances, Jensen and Zwieniecki (2013) argued that the lower limit to leaf size represents a minimum flow phloem speed (LaBarbera, 1990; Vogel, 2004). With typical plant cell sizes in the range of $d = 10\,\mu m$ – $100\,\mu m$, diffusion and advection of sugars are equally effective over these length scales when the Péclet number Pe $= vd/D = 1$, where v is the flow speed and D is the diffusion coefficient ($D = 0.5 \times 10^{-9}$ m^2/s for sucrose (Haynes, 2012)). It follows that $v \simeq D/d = 5\,\mu m/s$ – $50\,\mu m/s$ provides a lower estimate of the minimum flow speed $u_{\min}$. Assuming a velocity equal to this and solving Eq. (69) for leaf length l leads to the leaf size $l_{\min}$ at which this speed is first obtained:

$$l_{\min} = \frac{1}{16}\frac{r^3}{L_p\eta}\frac{1}{(h_{\max} - h)}. \tag{74}$$

In Eq. (74), we have expressed the minimum leaf size in terms of $h_{\max} = r^2\Delta p/(8\eta u_{\min})$, the tree height at which it is no longer possible to obtain the flow speed $u_{\min}$ due to resistance to flow in the stem. Jensen
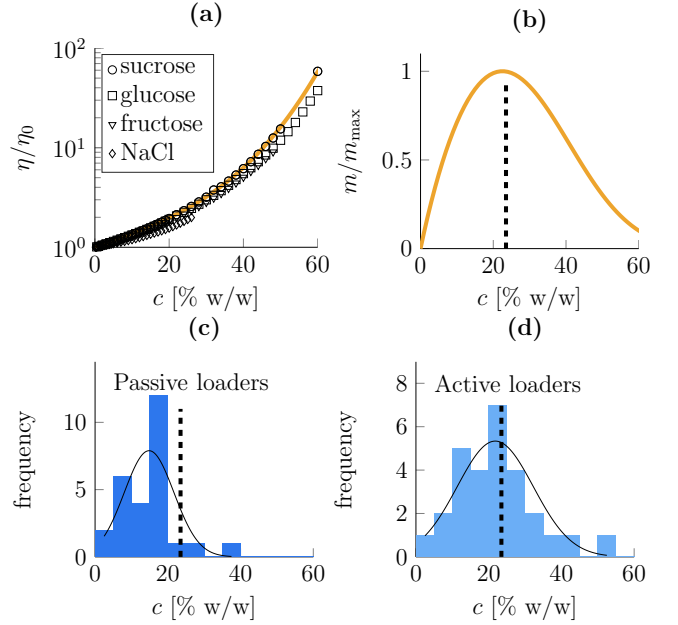

Figure 26 (a) Viscosity increases with concentration by almost two orders of magnitude between $c = 0$ %wt and $c = 60$ %wt. Viscosity η/η_0 plotted as a function of solute concentration c for the substances indicated in the legend. $\eta_0 = 1$ mPas is the viscosity of water and the solid line is a fit to the sucrose data. (b) The mass flux for sucrose (Eq. (75)) is optimal around $c = 23$ %wt (dashed line). Mass flux m normalized by the maximum value $m_{\max}$ plotted as a function of solute concentration c. (c-d) Histograms showing phloem sap concentration measured in plants that utilize passive and active phloem loading. Solid line is a gaussian fit to the frequency distribution. Dashed line shows the optimal concentration, cf. panel (b). Data from Haynes (2012): (a) and Jensen *et al.* (2013b): (c-d).

and Zwieniecki (2013) fitted Eqns. (73)-(74) to outliers of the data in Fig. 25, and found that the data suggests an efficiency $1 - \tau \simeq 0.9$ and a minimum speed $u_{\min} \simeq 100$ μm/s for parameter values $\Delta p = 1$ MPa, $L_p = 5 \times 10^{-14}$ m/s/Pa, and $\eta = 5$ mPas. The minimum flow speed 100 μm/s is in rough accord with experimental data from angiosperm trees (Fig. 19(b)) which has a strong peak around ~ 50 μm/s.

In summary, this suggests that in addition to effects related to e.g. photosynthesis, gravity, wind, and herbivores, efficiency of phloem transport may influence the size of plant leaves.

3. Optimal sugar concentration

In the preceding sections we have seen examples of how purely geometric factors influence the speed of sugar transport in plants. Further, we have found evidence that plants, on average, are inclined to favor geometric configurations that maximizes this speed (Fig. 22). The underlying assumption is of course that the speed u is a proxy

for the sugar mass flux $u\,c$, where c is the phloem sap sugar concentration, which implies that m is optimized if $u\,c$ is. The proportionality factor c, however, gives rise to additional dynamics in the flow problem which is independent of geometry. To see this, consider the case where the flow resistance is dominated by viscous resistance along the stem

$$u\,c = \frac{r^2}{8}\frac{\Delta p}{L}\frac{c}{\eta(c)}. \tag{75}$$

The geometric factor r^2 and pressure gradient $\Delta p/L$ are unchanged, but the ratio of concentration to viscosity $c/\eta(c)$ reveals that the mass flux $u\,c$ is directly influenced by properties of the sap. It is apparent (Fig. 26(a)) that viscosity increases rapidly with sugar concentration and that the function $c/\eta(c)$ has a maximum around $c \simeq 23$ %wt (Fig. 26(b)). The existence of an optimum sugar concentration derived from Eq. (75) and Fig. 26(a-b) was first proposed by Passioura (1976). Similar models have been used to rationalize observed concentrations in, for instance, blood flow (Birchard, 1997; Murray *et al.*, 1963; Stark and Schuster, 2012), nectar drinking animals (Kim and Bush, 2012; Kim *et al.*, 2011) and traffic-flows (Jensen *et al.*, 2013a). Passioura (1976) argued that efficient transport of sugar requires concentrations in the range $14-35\%$ based on increased viscous friction at high concentrations. Later, Lang (1978) conducted a theoretical comparison of different sugars and sugar alcohols, and concluded that the disaccharide sucrose at $c = 25\%$ is the most advantageous substance to transport, since it is chemically stable, highly soluble and only generates a modest osmotic pressure compared with other sugars, like its component parts, the monosaccharides glucose and fructose. An experimental test of the hypothesis that plants favor the optimum sugar concentration was performed by Jensen *et al.* (2013b), who collected data from 41 plant species (Fig. 26(c-d)). The optimal concentrations discussed above provide a rationale for the observation that the mean sugar concentration in the phloem sap of the plants found by Jensen *et al.* (2013b) was 18.2 %. At this concentration the flux $u\,c$ is less than 5 % from the maximum value. When considering active sugar loaders separately, the trend is even more clear: the average concentration is 21.1 % (Fig. 26(d)). By contrast, passive loaders (Fig. 26(c)) average at 15.4 %, which corresponds to 10 % less than the optimum mass flux.

Loading type appears to impact the sugar concentration and transport efficiency of the phloem: data suggest that active loaders achieve more optimal concentrations for transport than passive loading species. Several caveats are in order, however, as summarized by Jensen *et al.* (2013b): The concentration observed in nature may deviate from the theoretical optimum due to the limited availability of light, water and nutrients. Although some plant species maintain fairly constant sugar concentrations in their phloem, other species appear to exhibit

diurnal and seasonal changes in sap chemistry. Higher sugar concentrations may also prevent desiccation during extracellular freezing and facilitate supercooling during the winter. Therefore, some of the variation observed in phloem sugar concentration could be the result of differences in growth and sampling conditions.

D. Final remarks

In this section we have presented experimental data on sugar transport in plants. We have discussed attempts to use biomimetic models and scaling theory to rationalize some observations. Several of these have provided insights into the physical mechanisms that limit the range of observed anatomical and physiological features. However, a multitude of questions concerning long distance flow patterns of sugars, hormones, and other substances remain. Some of these arise from the difficulty in obtaining experimental data. Cell turgor pressure, for instance, is notoriously difficult to quantify, and no systematic study of pressure gradients in a plant has been made. This data is critical to an evaluation of the Münch osmotic pressure flow hypothesis. Remarkably little data exist on the global translocation patterns, i.e. on the flow speed and concentration of phloem sap at various positions in the plant body. Again, this is because the measurements are demanding, but it should be noted that the gain from better data on sugar transport would be considerable, especially if we are to take full advantage of emerging breeding and gene technology platforms to increase plant yield by reallocating resources via the phloem.

Our understanding is even further confounded by the lack of data on the phloem cell network architecture. We introduced a class of models inspired by electric circuits, and used a simple 1-dimension model of a tree to obtain information about the conduit sizes in the phloem, the leaf sizes for different tree heights and the sugar concentration in the phloem - based on optimising the flow speed. Here the entire leaf was replaced by a segment of a tube, characterised only by its radius and length. In reality we know that the phloem network in the leaf is a complicated, hierarchical structure, and it is a major question for future research to determine how the effective parameters (like resistance) are determined for these networks.

V. FLUID DYNAMICS OF SUGAR TRANSPORT IN PLANTS

To obtain a more reliable description of the osmotically driven flows, even in a single tube, like those making up the "one-dimensional tree" of last section, we now employ hydrodynamic equations taking explicitly into ac-
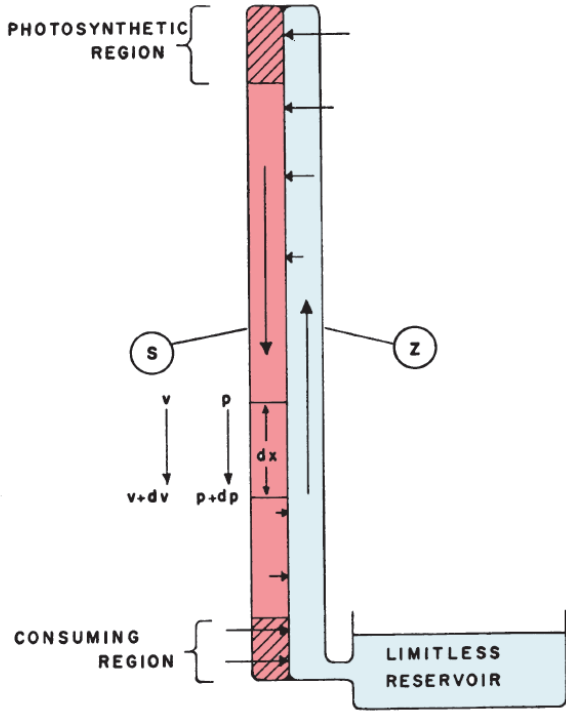
Figure 27 A "1-dimensional tree" according to Horwitz: a tube (S) with semipermeable walls, in contact with another tube (Z) containing pure water, connected to a water reservoir. From Horwitz (1958), reprinted with permission of the American Society of Plant Biologists

count the variations of flow velocities and concentrations along the tube. We make a number of simplifying assumptions, which, however, will allow us to expose the important features without too many confusing details. Still, the material presented in this section is intended for the mathematically inclined reader who wants to know the state of the art of the mathematical modeling of long distance flow in the phloem. Other readers can safely proceed to Sec. VI.

The starting point is the Aldis-flow of Sec. II.C: a cylindrical tube along the x axis of length L ($0 < x < L$) and radius a, with a side-wall consisting of a semipermeable membrane with permeability L_p. The tube contains an aqueous sugar solution with pressure $p(r, x, t)$, concentration $c(r, x, t)$, and velocity field $\boldsymbol{v}(r, x, t)$. A water reservoir at constant pressure $p = 0$ surrounds the tube. We neglect variations in density ρ and viscosity η induced by the presence of sugar, and assume rotational symmetry of velocity, concentration, and pressure. If low-Reynolds-number conditions prevail, the governing equations are the Stokes equation Eq. (3a) and the advection-diffusion equation Eq. (11). The boundary conditions at the membrane interface ($r = a$) are (see Sec. II.D) tangential no-slip of the water, radial inflow of water, and

zero flux of the solute,

$$v_x(a, x) = 0, \qquad \text{no slip,} \quad (76a)$$

$$v_r(a, x) = L_p\big[RTc(a, x) - p(a, x)\big], \quad \text{osmosis,} \quad (76b)$$

$$D\left.\frac{\partial c}{\partial r}\right|_{a,x} = c(a, x)\, v_r(a, x), \quad \text{no solute flux.} \quad (76c)$$

To our knowledge, no general solution to these coupled velocity-concentration equations has been found. Aldis (1988b) provided numerical solutions for the limit $p \ll RTc$, while Haaning et al. (2013) found analytical solutions for small deviations between the membrane concentration $c(a, x)$ and mean concentration.

The system complexity, however, can be reduced considerably by seeking equations for the radially averaged concentration $c = \langle c \rangle_r$ and axial flow speed $u = \langle v_x \rangle_r$ in the lubrication approximation (introduced after Eq. (23b)) valid when $a \ll L$. The governing equations for u and c are obtained from the radial average of the Aldis-equations Eqs. (24a) and (25) and of the advection-diffusion equation (10). Note that the latter can not be replaced (11) since the velocity field cannot be divergence free in this one-dimensional setting, which would imply a constant velocity u. Assuming that the solution is well-stirred, we have $c(x, t) = \langle c(r, x, t) \rangle_r$ such that $\langle v_x c \rangle_r = uc$ and (76b) leads to

$$\frac{a}{2L_p}\frac{\partial u}{\partial x} = RTc - p \qquad (77)$$

which together with Darcy's law (5)

$$\frac{\partial p}{\partial x} = -\frac{8\eta}{a^2}u \qquad (78)$$

give the final radial-averaged equations

$$\frac{a}{2L_p}\frac{\partial^2 u}{\partial x^2} = RT\frac{\partial c}{\partial x} + \frac{8\eta}{a^2}u, \qquad (79a)$$

$$\frac{\partial c}{\partial t} + \frac{\partial uc}{\partial x} = D\frac{\partial^2 c}{\partial x^2} + \Upsilon, \qquad (79b)$$

These equations, known as the Münch-Horwitz equations for osmotically driven pipe flows, first appeared in Horwitz (1958). An overview of the associated literature can be found in Thompson and Holbrook (2003b), and we give a brief summary here. Horwitz (1958) used a control-volume approach to derive equations for the steady flow problem in the form

$$A\frac{du}{dx} = \alpha c - \beta p, \qquad (80a)$$

$$\frac{d}{dx}\left(Auc\right) = \Upsilon, \qquad (80b)$$

$$\frac{dp}{dx} = -\epsilon u, \qquad (80c)$$

where $A = \pi a^2$ is the cross sectional area of the tube and α and β are physical parameters which in our terminology are $\alpha = L_p RT$, $\beta = L_p$, and $\epsilon = 8\eta/a^2$. His model divided the plant into three zones, a photosynthetic region, a stem region, and a consuming region, see Fig. 27. He discussed three different forms of the loading term Υ

$$\Upsilon = 0, \qquad \Upsilon = -kc, \qquad \text{and} \qquad \Upsilon = -\text{const}, \quad (81)$$

which correspond to either no loading in the stem region or concentration dependent or constant unloading in the consuming region. Horwitz (1958) did not provide solutions to Eqns. (80a)-(80c), but noted that (p. 87): *In general one would expect from the simple pressure flow theory that the rate of flow varies with distance along the tube, according to equation (80a). The size of this effect, however, depends on the difference between terms involving concentration in the phloem and pressure. If the pressure dissipation down the tube is paralleled by a corresponding decline in concentration (as by loss to adjacent tissue), there may be only a small variation in flow rate over long distances.* Subsequent analyses (Fig. 28 and e.g. (Christy and Ferrier, 1973; Thompson and Holbrook, 2003b)) have shown that most of the flow acceleration in Horwitz's model occurs in the photosynthetic (leaf) region. Work by Eschrich *et al.* (1972) and Young *et al.* (1973) continued the mathematical analysis of Münch flow by including an arbitrary position-dependent loading function $\Upsilon(x)$, noting that a physiologically relevant loading function must (in a steady state) ensure that the net transport of solutes into the tube is zero, i.e. $\int_0^L \Upsilon(x)\,\mathrm{d}x = 0$. They also performed an analysis of transient flow based on an integral form of Horwitz's equations (Sec. IV.B). Phloem flow models were further refined by Christy and Ferrier (1973) and Tyree *et al.* (1974) who found the first numerical solutions to the equations of motion using a discretised version of Horwitz's equations using constant loading rates in the source and sink regions constrained by the Young *et al.* (1973) criteria (Fig. 28(a)). They also took into account the molar volume of sugar solutions and xylem pressure gradients. To our knowledge, Ferrier *et al.* (1975) were the first to transient effects, though equations are not given explicitly and only numerical solutions were undertaken. Frisch (1976) found an analytical solution of time dependent system (including explicitly the term $\partial c/\partial t$ in Eq. (79b)) in the limit where viscous contributions to the pressure gradient is small. by relating it to the Burgers equation as described below. Phillips and Dungan (1993) presented an analytical approach based on the Stokes and advection-diffusion equations similar to that leading to Eqns. (79a) and (79b), finding two coupled equations for concentration c and pressure p by eliminating the velocity u. Thompson and Holbrook (2003b) criticized Phillips and Dungan (1993) for claiming that correct predictions can be achieved in no other way than through direct solution of the Stokes equation, pointing out that Horwitz's

control volume approach assumes local Poiseuille flow, thus giving the same predictions. More recently, Thompson and Holbrook (2003b) studied the approach to steady flow by numerical solutions to the Münch-Horwitz equations, Fig. 28(b).

The derivation of the Münch-Horwitz equations assumed that the water reservoir was all at the same pressure. In fact the phloem moves basically in parallel with the xylem and the osmotic flow thus depends on the local external pressure, i.e., the pressure in the xylem, mitigated through the intervening cambium. Denoting this pressure by $p_{ext}(x,t)$, it would enter into the radial inflow (76b) changing it into

$$v_r(a,x) = L_p \big[RTc(a,x) - (p(a,x) - p_{ext}(x,t)) \big], \quad (82)$$

where we have assumed that the solute concentration in the xylem is negligible. Such coupling terms have been included in some studies (Daudet *et al.*, 2002; Holtta *et al.*, 2006; Lacointe and Minchin, 2008) showing that e.g., the daily variation in the xylem can indeed influence the phloem translocation. Here one needs to model the cambium separating the xylem and the phloem, the elastic properties of the tissue as well as loading functions for the sugars. In the model of Holtta *et al.* (2006) a sufficiently strong transpiration (gradient in p_{ext}) can actually stop the phloem, but for a large range of transpiration below this value, the sugar flux is practically unaffected (Holtta *et al.* (2006) Fig. 4). We shall not discuss these models further here, but it is clearly an important area for future research. For more definite modelling of the xylem-phloem interactions one needs a better understanding of the complex coupling processes in the leaf, the mathematical modelling of which we shall return to briefly in section VI.C.

The Münch-Horwitz equations are difficult to solve numerically due to imminent shocks (as described below), and various ways of handling them with different loading mechanisms have been proposed in the literature (Christy and Ferrier, 1973; Goeschl *et al.*, 1976; Henton *et al.*, 2002; Jensen *et al.*, 2009b, 2012a; Thompson and Holbrook, 2003b). In (Thompson and Holbrook, 2003b), a non-symmetrical slope-limiting total variation diminishing (TVD) method is used to obtain results like Fig 28b. In their Appendix D, the method is described in detail as well as the differences with earlier studies. A simpler form of non-symmetric differentiation was used in (Jensen *et al.*, 2012a), the standard "upwind" technique, where only the point in question and its upwind neighbors are used. In our case the "wind" always comes from the loading zone (leaf), and therefore the upwind neighbors are those with smaller x. As well known in gas theory, this gives a simple approximative way of handling shocks (LeVeque, 1992) and it works well for the Münch-Horwitz equations as documented in Fig. 30, where the method is used.

(a) Source · Stem · Sink

Concentration [10^2 mol/m^3]

Velocity [10^{-4} m/s]

Distance x [cm]

(b)

Concentration [mol/m^3]

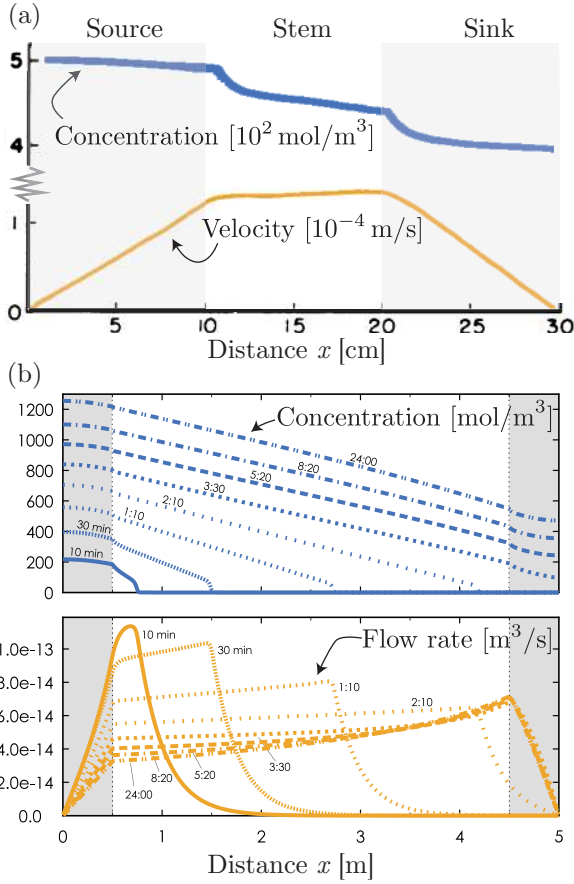Flow rate [m^3/s]

Distance x [m]

Figure 28 Numerical solutions of the Münch-Horwitz equations by Tyree *et al.* (1974) and Thompson and Holbrook (2003b) illustrates how the flow velocity increases in the source region, remains approximately constant in the stem, and approaches zero in the sink. The concentration decreases along the plant axis. (a) Shows steady solution by Tyree *et al.* (1974), while (b) illustrates the flow transient found by Thompson and Holbrook (2003b). Adapted from Thompson and Holbrook (2003b); Tyree *et al.* (1974). (a) is reprinted with permission of the American Society of Plant Biologists.

Several studies have reported analytical solutions to Eqns. (79a)-(79b), see e.g. Frisch (1976); Jensen *et al.* (2011, 2009b, 2012a); Phillips and Dungan (1993); Pickard and Abraham-Shrauner (2009); Thompson and Holbrook (2003a), and Hall and Minchin (2013). We proceed to discuss general approaches and some details of these solutions in the following sections.

To simplify the notation in the following mathematical treatment, we non-dimensionalize Eqs. (79a) and (79b) by using the system length L and inlet concentration c_0 as characteristic scales together with the osmotic pressure, velocity, and time scale p_0, u_0 and t_0, respectively,

$$p_0 = RTc_0, \qquad u_0 = \frac{2L}{a}L_p\,p_0 \qquad t_0 = \frac{L}{u_0}, \qquad (83)$$

to get non-dimensional variables C, U, P, X, and τ as

$$c = c_0 C, \ u = u_0 U, \ p = p_0 P, \ x = LX, \ t = t_0\tau, \quad (84)$$

Table III Values of the parameters M and $\bar{D}$ in various positions in a plant, based on the typical parameters $a = 10$ μm, $\eta = 2$ mPa s, $L_p = 5 \times 10^{-14}$ m/(Pa s), $D = 5 \times 10^{-10}$ m^2/s and $c = 0.5$ M, which yields $RTc = 1.22$ MPa.

Position in plant	Mü	$\bar{D}$
Single Sieve element ($L = 1$ mm)	1.6×10^{-6}	4×10^{-2}
Leaf ($L = 1$ cm)	1.6×10^{-4}	4×10^{-4}
Branch ($L = 1$ m)	1.6	4×10^{-8}
Small tree ($L = 10$ m)	160	4×10^{-10}

where L has been chosen such that $0 < X < 1$. Furthermore, we introduce the dimensionless parameters Mü (Münch number, hydraulic resistance divided by transmembrane resistance), $\bar{D}$ (inverse Péclet number), and $\bar{\Upsilon}$ (loading rate divided by radial diffusion rate),

$$\text{Mü} = \frac{16\eta L^2 L_p}{a^3}, \qquad \bar{D} = \frac{D}{u_0 L}, \qquad \bar{\Upsilon} = \frac{2t_0\Upsilon}{c_0 a}. \quad (85)$$

Using this, the non-dimensional radially-averaged form of the Horwitz equations (79a)–(79b) become

$$\frac{\partial^2 U}{\partial X^2} = \frac{\partial C}{\partial X} + \text{Mü}\,U, \qquad (86a)$$

$$\frac{\partial C}{\partial \tau} + \frac{\partial(UC)}{\partial X} = \bar{D}\frac{\partial^2 C}{\partial X^2} + \bar{\Upsilon}, \qquad (86b)$$

with the relations

$$\frac{\partial U}{\partial X} = C - P, \qquad (87a)$$

$$\frac{\partial P}{\partial X} = -\text{Mü}\,U. \qquad (87b)$$

for the pressure.

Typical values of Mü and $\bar{D}$ in different situations are listed in Table III. The scaling introduced in this way is most appropriate for small Münch numbers, and intermediary length scales, as it is based on the velocity scale u_0, Eq. (83), set by the osmotic pressure, the membrane permeability and the full length L of the system (e.g, the tree). Typical observed flow rates are of the order of 1 m/h $= 2.7 \times 10^{-4}$ m/s, but our u_0 varies from 0.044 m/h for the single sieve element to 440 m/h for a 10 m tree, whereas a "leaf" of length 2 cm would give $u_0 \approx 1$ m/h. This reflects the fact that the real velocity is set by the length scale where important water inflow takes place, and the appropriate pressure drop for the system. For large Mü, the dominant resistance comes from the stem, and using Eq. (79a), without the second derivative and setting $\partial c/\partial x \approx c_0/L$ and $r^2 \approx a^2$, the characteristic velocity u_1 in this case would be

$$u_1 = \frac{a^2}{8\eta}\frac{RTc}{L} = \text{Mü}^{-1}\,u_0. \qquad (88)$$

A. Solutions of the Time Dependent Equations with No Sugar Loading

We move on to analyze the Münch-Horwitz Equations (86a)–(87b). The first question to answer is whether they are well-posed. As discussed in Sec. II.B, the very different time scales for molecular and momentum diffusion has allowed us to discard the time dependence in the Navier-Stokes equation, i.e., in Eq. (86a). Thus, like the incompressibility condition in an incompressible fluid, the dynamics comes from Eq. (86b), whereas Eq. (86a) is in the nature of a constraint. One possible set of initial conditions for Eqs. (86a)–(87b) is to specify the entire concentration field $c_0(x) = c(x, t = 0)$. Then, since Eq. (86a) is linear in u, one can write

$$u(x,t) = \int_0^1 G(x,\xi) \frac{\partial c(\xi,t)}{\partial \xi} d\xi, \qquad (89a)$$

where the *Green's function* satisfies

$$\frac{\partial^2 G}{\partial x^2} - \text{Mü}\, G = \delta(x - \xi). \qquad (89b)$$

and where $G(x,\xi) = G(\xi,x)$. Further, $G(x,\xi)$ is continuous at $x = \xi$, whereas its derivatives are not. Integrating (89a) over x from $\xi - \epsilon$ to $\xi + \epsilon$ and letting ϵ tend to 0 we find $G'_x(\xi^+,\xi) - G'_x(\xi^-,\xi) = G'_\xi(x,x^+) - G'_\xi(x,x^-) = 1$.

To determine this Green's function, one has to specify the boundary conditions on u, i.e., whether the ends are open or closed. Often we are particularly interested in the case of close ends $u(0) = u(1) = 0$ since this is close to the situation in leaves or roots. Then the pressure (or more correctly: the pressure difference across the membrane) is determined by Eq. (87a), and cannot be specified independently. Inserting the expression (89a) for $u(x,t)$ into (86b) yields and integro-differential equation for $c(x,t)$, which can be solved by straight forward numerical techniques. The details of this method can be found in Appendix B of (Jensen *et al.*, 2009b) (note that the function $K(x,\xi)$ used there is $K(x,\xi) = -G'_\xi(x,\xi)$).

We begin by looking at the transient behaviour of an initially localized sugar distribution appropriate to many biomimetic applications, but perhaps less so for real plants. In particular, we shall show that the equations, in the limit Mü $= 0$ become equivalent to variants of the Burger's equation (Frisch, 1976; Jensen *et al.*, 2009b; Weir, 1981). Such equations can develop shocks (discontinuous gradients, but only true shocks for $D = 0$), as seen in the velocity field in Fig. 28(b) but as far as we know, the equations never actually do develop shock under biologically relevant conditions.

In the following, we take the loading function to be zero, $\Upsilon = 0$, since we assume, as typical in the biomimetic applications, that the sugar is present from the outset, and no sugar is added or taken out subsequently. In the limit of vanishing Münch number, the equations become particularly simple, and when also the molecular diffusion is neglected ($D = 0$), they can be solved by the method of characteristics. For an arbitrary initial condition, this method will generally yield an implicit solution. For arbitrary values of Mü and $\bar{D}$, we cannot solve the equations analytically and thus have to incorporate numerical methods. Due to the large derivatives which can develop, as shown in Fig. 28(b)), great care has to be taken in the numerical analysis, as discussed by Thompson and Holbrook (2003b) and Jensen *et al.* (2009b, 2012a). In the analysis in the remainder of this subsection, we employ the dimensionless equations, but drop the capital letters, and use t for τ, hoping thereby to make the reader more at ease without adding too much confusion.

Let us consider a tube closed at one end ($x = 0$) and open at the other ($x = 1$) with an initial sugar distribution, given as $c_0(t) = c(x = 0, t)$ concentrated near the closed end—a case discussed in Section IV.B and shown in Fig. 20(d). When Mü $= 0$, there is no variation in the pressure along the tube, and we can take $p = 0$ everywhere. Thus Eq. (87a) becomes

$$c = \frac{\partial u}{\partial x}. \qquad (90)$$

Inserting this into the advection-diffusion equation (86b) with $\bar{\Upsilon} = 0$, interchanging the derivatives with respect to t and x in the first term and integrating over x gives

$$\frac{\partial u}{\partial t} + u \frac{\partial u}{\partial x} - \bar{D} \frac{\partial^2 u}{\partial x^2} = A(t), \qquad (91a)$$

where A is independent of x. The two first terms on the left-hand side will vanish at $x = 0$ at all times due to the boundary condition $u(x = 0, t) = 0$. In addition, if we prescribe an initial $c_0(x)$ with $c'_0(0) = 0$, the last term will remain zero at $x = 0$ as long as $\frac{\partial^2 u}{\partial x^2}|_{x=0} = \frac{\partial c}{\partial x}|_{x=0} = 0$. We thus obtain the Burgers' equation (Whitham, 1974)

$$\frac{\partial u}{\partial t} + u \frac{\partial u}{\partial x} = \bar{D} \frac{\partial^2 u}{\partial x^2} \qquad (91b)$$

for the velocity. In the limit $\bar{D} = 0$ this is particularly simple and instructive. The solution is easily obtained by the method of characteristics, where the characteristics satisfy

$$\frac{du}{dt} = 0, \qquad \frac{dx}{dt} = u. \qquad (92)$$

i.e., that u is constant along the trajectory $\big(x(t),t\big)$, if $x(t)$ moves with the local speed u. Thus the solution can be parametrized as

$$u(\xi,t) = u_0(\xi), \qquad x(\xi,t) = \xi + u_0(\xi)t, \qquad (93)$$

where $u_0(\xi) = u(\xi,0) = \int_0^\xi c_0(x)\,dx$. If we assume that the sugar initially has the uniform concentration $c_0 = c_I$

in the interval $0 \leq x \leq \lambda$ of the tube, the initial velocity must increase linearly as $u_0(\xi) = c_I \xi$ for $x \leq \lambda$ and become constant $u_0(\xi) = c_I \lambda$ for $x \geq \lambda$. Solving the characteristic equations then gives

$$u(x,t) = \begin{cases} (c_I x)(1 + c_I t)^{-1}, & \text{for} \quad 0 \leq x \leq \lambda(1 + c_I t), \\ \text{const.} = c_I \lambda, & \text{for} \quad \lambda(1 + c_I t) \leq x \leq 1, \end{cases} \tag{94}$$

and the front $x_f(t) = \lambda(1 + c_I t)$ moves with the constant speed $u_f = x_f'(t) = c_I \lambda$ set by the total amount of sugar present in the tube, in agreement with Eq. (42). The solution only works as long as this amount is fixed, i.e., up to the time $t = (1 - \lambda)/(c_I \lambda)$ where the front reaches the open boundary. It is seen that the flow velocity *increases* up to the front position, which is typical of osmotically driven flows through a region of constant concentration difference as e.g., through a leaf.

In the other case treated in Section IV.B and shown in Fig. 20(c), the tube is closed in both ends, and the Münch-Horwitz equations (86a)–(87a) with Mü = 0 leads to a slight generalization of Eq. (90), as the pressure now increases in the tube,

$$\frac{\partial u}{\partial x} = c - p(t). \tag{95}$$

Using the boundary conditions $u(0,t) = u(1,t) = 0$, the (dimensionless) pressure becomes

$$p(t) = \int_0^1 c \, dx \equiv \bar{c}(t), \tag{96}$$

i.e., the mean concentration in the tube. Inserting Eq. (95) into Eq. (86b) (with $\bar{D} = \bar{\Upsilon} = 0$) gives

$$\frac{\partial}{\partial x}\left[\frac{\partial u}{\partial t} + u\left(\frac{\partial u}{\partial x} + \bar{c}\right)\right] = -\frac{d\bar{c}}{dt} = 0, \tag{97}$$

where the last equality expresses that $\bar{c}$ is constant in time since the tube is closed. Integrating with respect to x and using the boundary conditions on u to obtain

$$\frac{\partial u}{\partial t} + u\frac{\partial u}{\partial x} = -\bar{c}u. \tag{98a}$$

again a Burgers' equation, but this time a damped one (Gurbatov *et al.*, 1991). The characteristic equations are now

$$\frac{du}{dt} = -\bar{c}u, \qquad \frac{dx}{dt} = u. \tag{98b}$$

with solutions

$$u = u_0(\xi)\, e^{-\bar{c}t}, \tag{98c}$$

$$x = \xi + \frac{1}{\bar{c}}u_0(\xi)\left(1 - e^{-\bar{c}t}\right), \tag{98d}$$
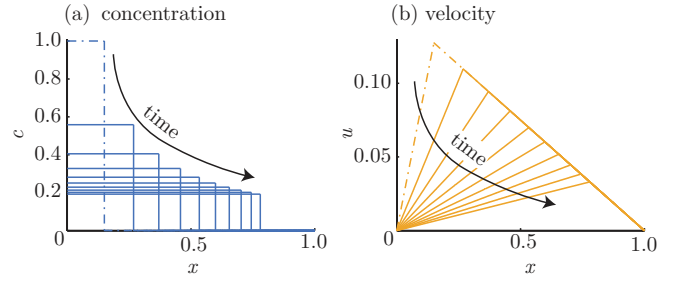
where $\xi = x$ at $t = 0$.

Figure 29 Plot of the analytical solutions (102) for the concentration (a) and for the velocity (b) in a closed, semi-permeable tube with initial sugar concentration given as $c_0(x) = c_I = 1$ for $0 < x < \lambda = 0.1$ and zero elsewhere. The average concentration is $\bar{c} = 0.1$. Adapted from Jensen *et al.* (2009b). Copyright Cambridge University Press. Reprinted with permission.

Assuming as above, and corresponding e.g. to the experiments quoted in Section IV.B by Eschrich *et al.* (1972) and by Jensen *et al.* (2009b), that the sugar has the uniform concentration $c_0 = c_I$ in the interval $0 \leq x \leq \lambda$ of the tube, we can use Eqs. (95)-(96) together with $\bar{c} = c_I \lambda$ to find the initial condition for u as

$$u_0(\xi) = u(\xi, 0) = \int_0^\xi (c(x,0) - \bar{c}) \, dx \tag{99}$$

Then, solving Eq. (98d) for $\xi(x,t)$, we can insert this in Eq. (98c) and compute $u(x,t)$. The solution, derived in detail in Jensen *et al.* (2009b) and equivalent to the result obtained by Weir (1981), is displayed in Fig. 29. The instantaneous sugar front position x_f and front velocity u_f is

$$x_f(t) = 1 - (1 - \lambda)\, e^{-\bar{c}t}, \tag{100}$$

$$u_f(t) = \frac{dx_f}{dt} = \bar{c}\,(1 - \lambda)\, e^{-\bar{c}t}. \tag{101}$$

Similarly, $c(x,t)$ is given by

$$c(x,t) = \frac{\bar{c}}{1 - (1 - \lambda)\exp(-\bar{c}t)}\, H(x_f - x). \tag{102}$$

Going back to dimensional variables, equations (100) and (101) become

$$x_f(t) = L - (L - l)\, e^{-t/t_0}, \tag{103a}$$

$$u_f(t) = \frac{L}{t_0}\, e^{-t/t_0}, \tag{103b}$$

where L is the length of the membrane tube, l is the initial front position and the decay-time t_0 is in accordance with the simple argument given in the Sec. IV.B and Eq. (41) for the front.

To some extent, one can include diffusion in this analysis, as recognised by Frisch (1976). Indeed, the diffusive

Burgers equation (91b) can be transformed to the linear diffusion equation by first noting that the substitution

$$u = \frac{\partial \psi}{\partial x}, \tag{104a}$$

yields the nonlinear phase equation

$$\frac{\partial \psi}{\partial t} + \frac{1}{2}\left(\frac{\partial \psi}{\partial x}\right)^2 = \bar{D}\frac{\partial^2 \psi}{\partial x^2}, \tag{104b}$$

where we, in analogy with Eq. (91a), have discarded an integration constant $A(t)$. Then the Hopf-Cole transformation (Whitham, 1974)

$$\psi = -2\bar{D}\frac{\partial}{\partial x}\log\phi, \tag{104c}$$

leads to the diffusion equation

$$\frac{\partial \phi}{\partial t} = \bar{D}\frac{\partial^2 \phi}{\partial x^2}. \tag{104d}$$

However, this transformation does not work for the more general cases like the damped Burgers equation (98a).

It is also hard to generalize these results to nonzero Münch numbers. For Mü $\gg$ 1, one can show (Jensen *et al.*, 2009b) that there is an asymptotic solution valid for intermediate times, where the sugar concentration is nonzero only in a finite interval $[0, x_f(t)]$ and the sugar front propagates like $x_f(t) \sim (t/\text{Mü})^{1/3}$. The central concentration decays like $c^* \sim t^{-1/3}$ and the solution remains valid only as long as $c^*(t) \gg \text{Mü}\bar{D}$, which becomes invalid at very large Mü and very large times, where we return to normal diffusive behavior.

B. Solutions for the Stationary Equations

Returning to our one-dimensional plant shown in Fig. 21 or Fig. 27, the time-dependent equations, starting e.g., with a localized sugar distribution, evolve into a steady state as shown in Fig. 28. The equations for the stationary flow are found from Eqs. (86a) and (86b) by omitting the time dependence. In the two next subsections, we shall also neglect molecular diffusion. The stationary equations have been investigated e.g., by Christy and Ferrier (1973); Goeschl *et al.* (1976); Henton *et al.* (2002); Thompson and Holbrook (2003a). Here, we follow Jensen *et al.* (2011, 2012a), where attempts were made to simplify the models and the boundary conditions as far as possible.

For large tube lengths, the non-dimensional diffusion constant $\bar{D}$ becomes very small as discussed above. Thus we have to solve the two equations (writing prime for d/dx),

$$u'' - \text{Mü}\,u = c', \quad (uc)' = \bar{\Upsilon}(x). \tag{105}$$

The precise form of this stationary state depends on how the boundary conditions are chosen and how the sugar is assumed to be loaded and unloaded, i.e., the choice of the function $\bar{\Upsilon}$. There have also been solutions where the loading and unloading zones were not taken explicitly into account, but replaced by boundary conditions at the ends, see e.g., Pickard and Abraham-Shrauner (2009). However, we stick to models with explicit loading and unloading, since, as we shall see, potential singularities are lurking at the entrance and exit of the central translocation zone, which make this replacement difficult. We shall use the dimensionless variables defined above, but in this case take $L = l_2$, which (in particular for trees) is the dominant length scale. Thus the borders of the different zones are at $x = x_1 = l_1/L$ and $x = x_2 = (l_1 + l_2)/L = 1 + l_1$ and the end of the roots are at $x_3 = (l_1 + l_2 + l_3)/L = x_1 + 1 + l_3/L$.

We always assume no outflow in the ends of the phloem tube, i.e., take $u(0) = u(x_3) = 0$ (for the dimensionless variables): Since we are considering the entire length of the tree/plant, water should flow in and out only through the semipermeable membranes and sugar should be explicitly loaded or unloaded, and not flow through the ends. This description is accurate in the case of plants that use apoplasmic (active) loading. In symplastic loaders, however, the phloem is radially connected to the mesophyll by plasmodesmata channels. Sugar loading is believed to occur by molecular diffusion through these narrow conduits. It is worth noting, however, that an osmotic flow of water from the xylem to the mesophyll may induce a bulk flow of water (and sugars) through the plasmodesmata. In passive loaders, sugar loading may thus be accompanied by a bulk flow of liquid (see further Sec. VI.B).These effects will not be considered here, where the long-distance translocation is in focus.

The simplest way of treating the leaves is to assume (Jensen *et al.*, 2011) that the loading function $\bar{\Upsilon}$ is adjusted so that the concentration in the leaf remains constant (i.e., $c = 1$). This is probably not true in detail, but might be a good first approximation. In the roots, a simple possibility (Jensen *et al.*, 2011) is to assume that whatever sugar is present at the inlet is decaying linearly to zero through the root. With these assumptions the equations for the leaf, translocation part and root reduce to

$$u'' = \text{Mü}\,u, \qquad\qquad \bar{\Upsilon} = u', \ 0 < x < x_1, \tag{106a}$$

$$u'' = \text{Mü}\,u - \frac{u(x_1)}{u^2}u', \quad (cu)' = 0, \ x_1 < x < x_2, \tag{106b}$$

$$u'' = \text{Mü}\,u - \beta, \qquad\quad c' = \beta, \ \ x_2 < x < 1. \tag{106c}$$

where we have used $c = 1$ in the leaf segment ($0 < x < x_1$). In the translocation part ($x_1 < x < x_2$), we see that $u(x)c(x) = \text{const} = u(x_1)c(x_1) = u(x_1)$, and thus $c(x_2) = u(x_1)/u(x_2)$. In the root part ($x_2 < x < x_3$), where by assumption c' is a constant, we find
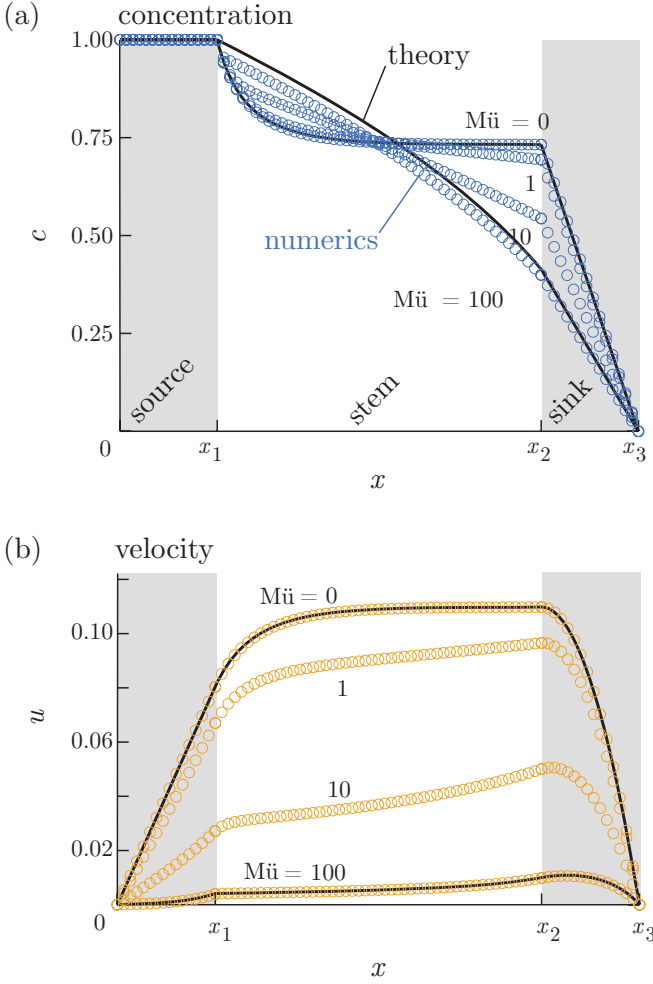
Figure 30 Solutions of the stationary Münch -Horowitz equations for a single tube with "leaf", "stem" and "root". Adapted from (Jensen *et al.*, 2011)

$c' = -c(x_2)/(1 - x_2)$ and thus

$$c' = \beta = \frac{u(x_1)}{u(x_2)(1 - x_2)}. \tag{107}$$

In this approach, the second derivative of u changes discontinuously at the borders x_1 and x_2 between the different zones, but we should be able to construct solutions which are continuous in u and it first derivative u'.

The nature of the solutions to the stationary flow equations depends strongly on the value of the Münch number. Below, we shall briefly look at the form in two limiting cases Mü $\ll 1$ and Mü $\gg 1$ following (Jensen *et al.*, 2011).

Case 1: Mü $\ll 1$. Here, the equations take the form

$$u'' = 0 \text{ for } 0 < x < x_1 \tag{108a}$$

$$u'' = -\frac{u(x_1)}{u^2}u' \text{ for } x_1 < x < x_2 \tag{108b}$$

$$u'' = -\beta \text{ for } x_2 < x < x_3 \tag{108c}$$

with β given in Eq. (107). The solutions are linear in the leaf section $0 < x < x_1$ and quadratic in the root section $x_2 < x < 1$. In the stem section $x_1 < x <_2$, (for Mü $= \hat{\Upsilon} = 0$) Eq. (105) (or (108b)) can be integrated once. to the form $u' = u_1/u + A$. The solution can be expressed implicitly as

$$x(u) = \frac{u_1}{A}\left[\frac{u}{u_1} - \frac{1}{A}\log\left(1 + Au/u_1\right)\right] + B \tag{109}$$

for $u_1 < u < u_2$, where $u_1 = u(x_1)$ and $u_2 = u(x_2)$. This means that it becomes almost constant near the end of a long stem, where u would approach the value $u^* = -u_1/A$ (possible for negative A). By matching u and u' at x_1 and x_2 one obtains the solution shown in Fig. (30b) top (Mü $= 0$). Note that the square root solution in Eq. (46) (i.e., $(u^2)'' = 0$) can be obtained from Eq. (109) in the limit $A \to 0$.

Case 2: Mü $\gg 1$. Again the solutions are simple in the leaf and root sections. For $0 < x < x_1$, using Eq. (106b) with $u(0) = 0$, we find $u = A_1 \sinh(x\sqrt{\text{Mü}})$ and for $x_2 < x < 1$ we get $u = A_2 \sinh((x - x_2)\sqrt{\text{Mü}}) + A_3 \cosh((x-x_2)\sqrt{\text{Mü}}) + \beta/\text{Mü}$. To match these solutions correctly in the stem zone $(x_1 < x < x_2)$, we have to remember, as discussed above, that the scaling chosen for u is not appropriate for large Mü. Indeed, from Eq. (88), we should expect $u = v(\text{Mü})^{-1}$, where v is of the order of unity. Inserting this into Eq. (106b) gives

$$v' = \frac{v^3}{v_1} - \frac{1}{\text{Mü}}\frac{v^2}{v_1}v'' \approx \frac{v^3}{v_1} \tag{110}$$

where $v_1 = v(x_1)$. For large Mü and small v'' we neglect the $O(\text{Mü}^{-1})$-term, and obtain $(v^{-2})' = -2/v_1$, so that

$$v(x) = \frac{v_1}{\sqrt{1 - 2v_1(x - x_1)}} \tag{111a}$$

or, returning to the usual scaling,

$$u(x) = \frac{u_1}{\sqrt{1 - 2\,\text{Mü}\,u_1(x - x_1)}} \tag{111b}$$

which would diverge, when $x \to x^*$ where

$$x^* - x_1 = \frac{1}{2\,\text{Mü}u_1} = \frac{1}{2\,v_1} \tag{112}$$

As long as $v_1 < 1/2$, $x^* - x_1 > 1$ and the divergence will not occur in the physical interval $0 < x < 1$. The coefficients A_2 and A_3 can be found by matching u and u' at x_2, but since we have neglected the highest order term, u'' in Eq. (105), we cannot ensure continuity of both the u and u' at x_1 without introducing additional boundary layers. Comparing with numerics shows that simply matching u while allowing a small discontinuity of u gives excellent results, as can be seen by the fits in Fig. (30).

Using these solutions and boundary conditions, we can now compute the average flow velocity, the quantity which we optimized in the resistor model of Section IV.C.1. As shown in detail in Jensen *et al.* (2011), the results are, for small Mü,

$$\bar{u} = \frac{\sqrt{3}-1}{2}x_1 - \frac{9-5\sqrt{3}}{8}x_1^2, \quad \text{for } \text{Mü} \ll 1, \quad (113a)$$

or $\bar{u} \approx 0.366x_1 - 0.042x_1^2$, while for large Mü,

$$\bar{u} \approx \frac{1}{\text{Mü}}, \quad \text{for } \text{Mü} \gg 1, \quad (113b)$$

where we, for simplicity have used the simplifying assumption $l_1 = l_3$. In the limit $l_1 \ll l_2 = L$, appropriate for a tree, the low Mü result simplifies to

$$\bar{u} = \frac{\sqrt{3}-1}{2}x_1, \quad (114)$$

with the corresponding dimensional value

$$\bar{u} = \left(\frac{\sqrt{3}-1}{2}\right)\frac{RTc_0L_p}{a}l_1 = \left(\frac{\sqrt{3}-1}{4}\right)x_1u_0 \quad (115)$$

where u_0 is given by Eq. (83). Aside from the pre-factor $(\sqrt{3}-1)/2$, this result corresponds to the flow predicted by the simple resistor theory of Section IV.C.1. in the case where the surface resistance R_1 in Eq. (51) dominates. The dimensional result for large Mü is

$$\bar{u} \approx \frac{RTc_0a^2}{8\eta l_2} \quad (116)$$

again in accordance with the results of Section IV.C.1, when the bulk resistance R_2 in equation (49) dominates. With this model, we can now verify the predictions made there, based on the coupled resistor model, i.e., the result Eq. (56) for the flow velocity and Eq. (59) for the optimal tube radius. We have already seen that the asymptotic behaviour agrees (within a factor $(\sqrt{3}-1)/2$ for the low Mü case). This behaviour, is shown in Fig. 31 together with direct numerical solutions in the whole interval for varying Münch number. As can be seen there, the optimal value of a agrees quite well with the simple estimate obtained by equating the asymptotic curves and, in fact the entire shape of $\bar{u}$ agrees well with a slightly modified version of Eq. (56) using $l_3 = l_1$, i.e.,

$$u = 2L_p\Delta p\frac{a^2l_1}{Vl_1l_2 + 2ma^3} = \frac{u_0}{2m\,l_2/l_1 + \text{Mü}} \quad (117)$$

where $V = 16\eta L_p$ (from (57)), $u_0 = 2L_p\Delta p\,l_2/a$ as in (83) and $m = 2/(\sqrt{3}-1) = \sqrt{3}+1 \approx 2.73$ instead of unity. The optimal radius is then,

$$a^* = \left(m^{-1}Vl_1l_2\right)^{1/3} = \left(8\left(\sqrt{3}-1\right)\eta L_pl_1l_2\right)^{1/3}, \quad (118)$$
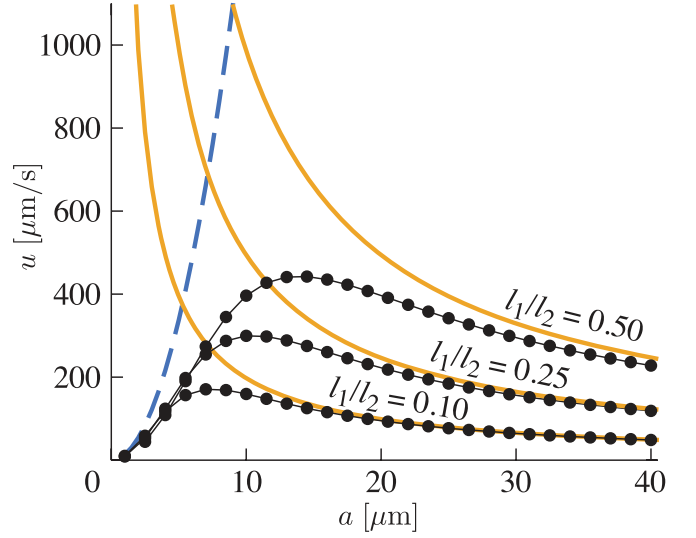

Figure 31 Numerically computed mean velocity $\bar{u}$ as a function of radius a (dots connected by lines) compared to the analytical results for Mü $\ll 1$ (Eq. (115), solid lines) and Mü $\gg 1$ (Eq. (116), dashed lines). These curves clearly show that $\bar{u}$ grows as a^2 for small a while it decays as $1/a$ for large a. At the intersection between the two lines given by equation the transition between the two types of flow occurs and the velocity is at a maximum. This is shown also by the dotted curve showing the slightly modified coupled resistor result, Eq. (117). The plots are made with $L_p = 5 \times 10^{-14}$ m(Pa s)$^{-1}$1, $l_1 = (0.1, 0.25, 0.50)$ m, $l_2 = 1$ m, $RTc_0 = 0.54$ MPa, and $\eta = 5 \times 10^{-3}$ Pa s. Adapted from Jensen *et al.* (2011)

in close agreement with the earlier result, Eq. (59).

The factor m which appears in Eq. (117) can be at least roughly understood within the framework of the resistor models of Sec. IV.C. It corresponds to replacing the resistance, Eq. (51), by

$$R_1 = \frac{m}{2\pi aL_pl_1} \quad (119)$$

i.e., increasing it by a factor of m. But one has to keep in mind that the velocity u, treated as constant in the resistor model is not really the average velocity through the loading zone (leaf). The flux Q that enters Eq. (50) should really be the water coming in through the outer surface of the tube due to osmosis and thereby accelerating the flow as Eq. (87a). If the inflow is roughly constant this means that the flow velocity increases linearly and thus that the mean value in the loading zone is roughly half of the total inflow, giving a factor $m = 2$.

C. Target Concentration Models

The details of the solutions presented above depend on the particular assumptions about the nature of the loading and unloading zones. The assumption of constant concentration in the leaf and linearly decreasing concentration in the root. To make more specific assumptions

would require a more detailed knowledge of loading and unloading, which, as discussed in the Sec. III.B depends strongly on the particular plant in question and is actually not known in detail, in particular because the sugar transport into the phloem cells carries with it a significant water flow, as we shall briefly discuss later (Sec. VI.C). From a more formal point of view, the asymmetry introduced between the treatment of the source and the sink also has drawbacks. In our formulation above, we have so far concentrated on the sugar transport from leaf to root, since it is the longest stretch for the plant to overcome. However, a large part of the sugar transport targets new shoots, fruits or immature leaves. The young leaves are particularly interesting, because they will, at some point, switch from sugar sinks to sugar sources. It would thus be nice to have a model which treated the sources and the sinks in the same way.

One possibility might be to use a constant concentration in both ends, and then simply let the direction of the sugar flow be governed by the relative strengths of the concentrations in the two ends. However, as was shown in (Jensen et $al.$, 2012a), this is not possible, since this kind of model will not allow a local maximum for u, which is necessary since $u = 0$ in both ends. In this case, the equations would take for form

$$u''(x) = \text{Mü}\, u, \qquad \text{for} \quad 0 < x < x_1, \qquad (120a)$$
$$u''(x) = c'(x) + \text{Mü}\, u, \quad \text{for} \quad x_1 < x < x_2, \qquad (120b)$$
$$u''(x) = \text{Mü}\, u, \qquad \text{for} \quad x_2 < x < x_3 \qquad (120c)$$

where in the stem ($x_1 < x < x_2$), there is conservation of sugar $u(x)c(x) = \text{const}$. It is easy to see that the velocity u must be monotonic in both the leaf and the root sections, since $u = 0$ in the two ends. Thus the maximum must occur in the stem. Integrating this equation from x_a to x_b both in the stem gives (using sugar conservation)

$$u'(x_a) - u'(x_b) = c(x_a) - c(x_b) + \text{Mü} \int_{x_a}^{x_b} u(x)\,dx$$
$$= c(x_a)\left(\frac{u(x_a)}{u(x_b)} - 1\right) + \text{Mü} \int_{x_a}^{x_b} u(x)\,dx. \quad (121)$$

If there is a maximum point at x_m we can choose x_a and x_b such that $x_a < x_m < x_b$ and $u(x_a) = u(x_b)$, which, inserted into (121), gives

$$u'(x_a) - u'(x_b) = \text{Mü} \int_{x_a}^{x_b} u(x)\,dx. \qquad (122)$$

For a positive flow, the right-hand side is positive, but around the maximum, the left-hand side is negative. Thus there can be no maximum.

Another possibility that retains the symmetry is to use a $target$ $concentration$ model, as done e.g., by (Lacointe and Minchin, 2008), where the local loading strength depends linearly on the difference between the local concentration and its target value. We thus choose to write the loading function appearing in (105) as $\Upsilon_i = \alpha_i(\sigma_1 - c_i)$, whereby these equations in the loading and unloading zones become

$$\frac{d^2u}{dx^2} - \text{Mü}\, u = \frac{dc}{dx}, \qquad (123a)$$

$$\frac{d(uc)}{dx} = \alpha_i(\sigma_i - c), \qquad (123b)$$

where σ_1 is the target value of the concentration in the leaf and σ_3 is the value for the root. No σ_2 is defined since the stem does not load or unload sugar in this model. Similarly, α_1 is the rate constant for the sugar loading and α_3 the one for the unloading. In the loading zone, we have $u(0) = 0$ and in the unloading zone we have $u(x_3) = 0$, and to make close symmetry between those two zones, we can change the variables in the unloading zone as $u \to -u$ and $x \to x_3 - x$ which leaves the equations unchanged, but gives the boundary condition the form $u(0) = 0$ also in the unloading zone.

In (Jensen et $al.$, 2012a) these equations are solved in the limits of Mü very small and very large. For Mü $\ll 1$ the solution is implicit, of the form

$$x\left|\frac{u(x)}{x} - v_+\right|^{\nu}\left|\frac{u(x)}{x} - v_-\right|^{1-\nu} = K \qquad (124a)$$

where

$$\nu = \frac{\nu_+}{\nu_+ - \nu_-} \qquad (124b)$$

$$\nu_\pm = -\frac{1}{2}(K_1 + \alpha \pm \sqrt{(\alpha - K_1)^2 + 4\alpha\sigma}) \qquad (124c)$$

where the constant $K_1 = p/(RTc_0)$ is the pressure in the tube, which is constant for Mü $\to 0$. This can also be expressed as

$$\nu_+ = -(c(0) + \alpha) \qquad (125a)$$
$$\nu_- = u'(0) \qquad (125b)$$

From the signs of u' (positive in the loading zone and negative in the unloading zone) one can infer that Eq. (124a) degenerates to a linear solution $u = A_1 x$ in the loading zone (since both ν_+ and ν_- are negative) whereas it cannot in the unloading zone. Correspondingly, the concentration $c = u'(x) + K_1$ becomes constant in the loading zone, but not in the unloading zone in agreement with the above discussion.

For Mü $\gg 1$ one finds, again in the loading and unloading zones, that the concentrations become almost constant, equal to their target values. We know from the arguments above that they cannot be absolutely constant, but the variation is concentrated in narrow boundary layers, in particular at the entrance of the unloading zone $x \gtrsim x_2$. Thus Eq. (123a) becomes

$$\alpha(\sigma - c) = \frac{d(cu)}{dx} \approx c\frac{du}{dx}, \qquad (126)$$
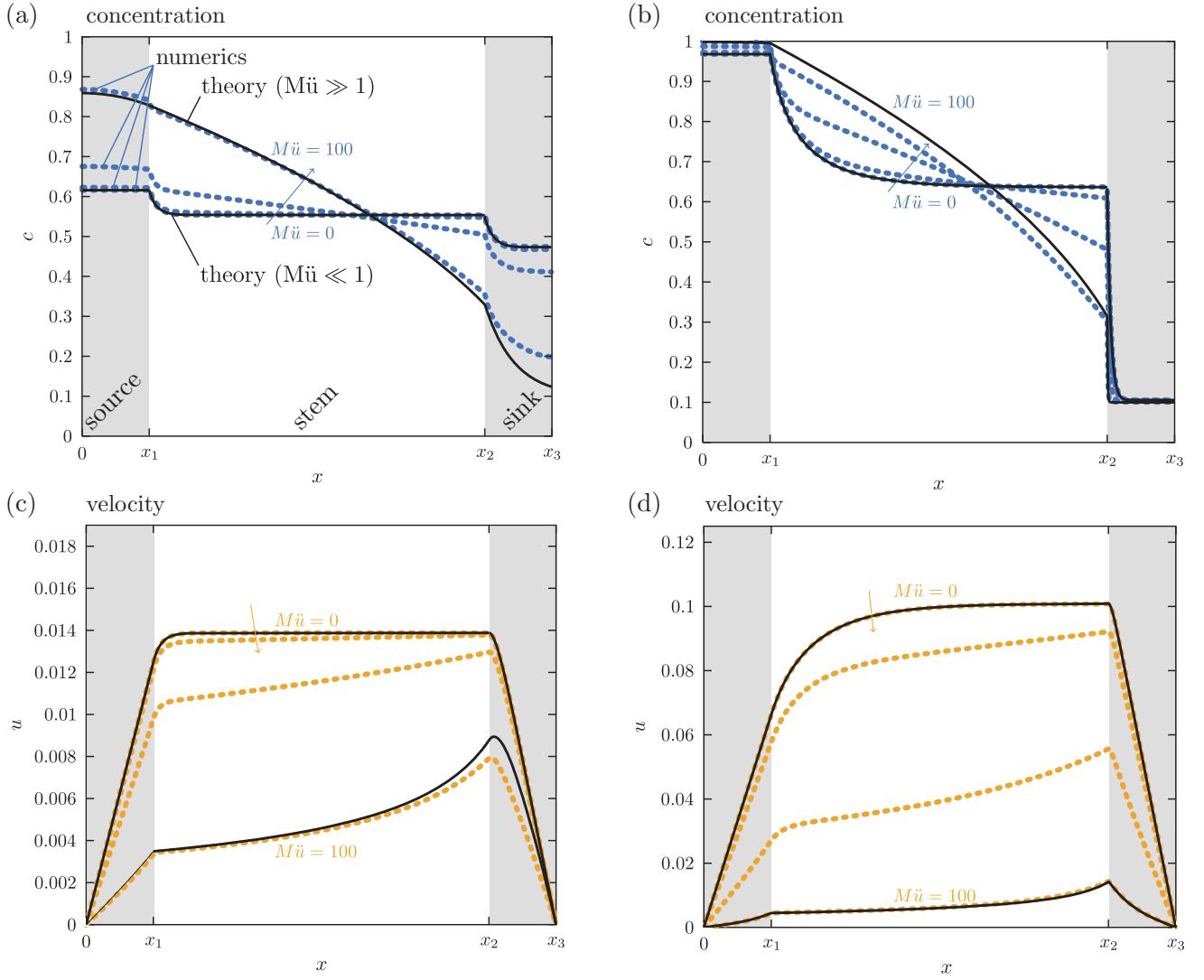
Figure 32 Solutions of the stationary Münch -Horowitz equations for a single 1-dimensional tree with target concentrations. Numerical solutions (thick grey lines) and analytical solutions for Mü = 0 (thin dashed lines) and Mü ≫ 1 (thin solid lines) are shown for target concentrations $\sigma_1 = 1$ and $\sigma_3 = 0.1$. In (a,c) $\alpha_1 = \alpha_3 = 0.1$ and in (b,d) $\alpha_1 = \alpha_3 = 10$. From (Jensen *et al.*, 2012a)

whereby

$$\frac{dc}{dx} \approx -\frac{\sigma}{\alpha}\frac{d^2u}{dx^2}, \qquad (127)$$

and Eq. (123a) becomes

$$\left(1 + \frac{\sigma_i}{\alpha_i}\right)\frac{d^2u}{dx^2} = \text{Mü}\,u, \qquad (128)$$

with the solution (given $u(0) = 0$)

$$u(x) = B \sinh x \sqrt{\text{Mü}\,(1 + \sigma/\alpha)^{-1}}. \qquad (129)$$

This is actually only appropriate in the loading zone. In the unloading zone, a boundary layer forms near the entrance, since the velocity has its maximum there, as seen in Fig. 32(c). The large Mü solutions all have order

1/Mü as expected and combining the results for large and small Mü one finds an interpolation formula for the average flow velocity of the form Eq. (117), in this case with $m = 2/(\sqrt{5} - 1) \approx 1.62$, confirming the basic ideas of the resistor model of Section IV.C.

D. Concentration Boundary Layers

The analysis of osmotic flows presented in Sec. V assumed perfect radial mixing of the solutes, thus presuming that the sugar concentration c does not vary over the cross-section of the channel. From the no-solute-flux boundary condition at the membrane interface (Eq.

(76c))

$$D \left.\frac{\partial c}{\partial r}\right|_{a,x} = c(a,x)v_r(a,x), \qquad (130)$$

however, it is apparent that such an assumption leads to an inconsistent relationship between concentration and velocity at the membrane interface: $c(a,x)v_r(a,x) = 0$. A finite, though possibly small, concentration gradient near the membrane interface must therefore be accounted for to make accurate predictions.

A substantial literature exists on membrane concentration boundary layer problems, which are of importance in several other biological and technical fields (Aldis, 1988a,b; Dainty, 1963; Jensen *et al.*, 2010; Pedley, 1980a,b, 1983; Pedley and Fischbarg, 1978). In the vicinity of an arbitrary perfect osmotic membrane, the concentration c_a is lowered compared to the bulk value, c_0, because sugar is advected away from the membrane by the influx of water. This, in turn, results in a lower influx of water than anticipated under conditions of perfect mixing. In order to explain water permeabilities in experiments exploring water transport through the cell walls of algae (*Nitella flexilis* and *Chara australis*), Dainty (1963) suggested that the formation of boundary layers was responsible for the differences observed between osmotically driven transport from the extracellular to the intracellular side versus an assay exploring the opposite direction of water transport. To determine how the concentration c changes with distance r from the membrane, Dainty (1963) considered the flux equation (Eq. (130)) in the bulk liquid and found $c(r) = c_0 \exp\left(v_r(r-\delta)/D\right)$ where δ is the distance at which the bulk concentration is reached $c(\delta) = c_0$. Note that the boundary layer thickness δ will generally depend on both geometry and the flow itself. In Dainty (1963)'s model, the concentration c_a at the membrane interface is

$$c_a = c_0 \exp\left(-\frac{v_r\delta}{D}\right). \qquad (131)$$

Equation (131) suggests that $c_a \simeq c_0$ when the radial Péclet number $\mathrm{Pe}_r = v_r\delta/D \ll 1$. While correct, the situation at hand is further complicated by the interdependence between concentration and velocity. The normal velocity is approximately proportional to the membrane concentration $v_r \simeq L_p RT c_a$, which is exact in the limit when the pressure p is significantly smaller than the osmotic pressure $RT c_a$ (Pedley and Fischbarg, 1978). This implies a transcendental equation for c_a

$$c_a = c_0 \exp\left(-\frac{L_p RT\delta}{D}c_a\right). \qquad (132)$$

As discussed by e.g. Pedley (1983), Dainty's simple model of a boundary layer neither allows for the variation of the normal flow component v_r with the distance

from the membrane, nor does it account for any type of stirring in the osmolyte solution. In a series of papers, several possible modes of stirring were investigated to determine the parameter range for which the unstirred boundary layer description would still be useful, but with an effective value of the boundary layer thickness (Pedley, 1980a,b; Pedley and Fischbarg, 1978). If a stagnation point stirring is included, for a large permeability and/or a small diffusion constant, the time dependent solution of the boundary layer problem indicates the appearance of damped oscillations in the osmolyte concentration. The oscillatory solution, however, corresponds to parameter values quite far from the diffusion coefficient of the osmolytes of interest in phloem (simple sugars), for typical permeabilities and typical concentrations in phloem cells. An important outcome of the detailed modelling of the stirring motion is the identification of the relevant effective boundary layer thicknesses δ (Table I in (Pedley, 1983)).

In plants, however, there is no reason to consider an external stirring mechanism - the stirring (i.e. advection) is caused by the bulk flow, which is also driven by the osmosis. In this self-consistent problem, entire flow can be treated in the Stokes approximation (i.e. as a lubrication flow) and there are no well-defined boundary layers, but one can find an expression for the lowered membrane concentrations (i.e., the lowered osmotic pumping) in the form

$$c_a = c_0 \frac{\sqrt{1+4\,\mathrm{Pe}}-1}{2\,\mathrm{Pe}} \qquad (133)$$

valid quite generally when the Péclet number is rescaled in a geometry dependent way (Jensen *et al.*, 2010).

We now return to the discussion of how concentration boundary layers affect the predictions made by the Münch-Horwitz theory. The basic situation in a cylindrical pipe is sketched in Fig. 33. Close to the membrane, the concentration c_0 is lowered compared to the value at the channel center, c_0, because sugar is advected away from the membrane by the influx of water. This, in turn, results in a lower influx of water since the radial velocity depends on the local concentration $v_r(a) = L_p(RTc_a - p)$, see Eq. (76b). Adapted from (Haaning *et al.*, 2013).

In the following, we restrict ourselves to conditions relevant to the experiments by Haaning *et al.* (2013), i.e. steady state flow in a cylindrical tube initiated by a syringe pump which delivers a solution of velocity u^* and concentration c^* at $x = 0$ (see Fig. 20(e)). The governing equations are the Münch-Horwitz equations (79a)-(77) with Mü $= 0$ and since the tube is open, the pressure can be neglected as in Eqs. (44)-(45) and (90) giving

$$\frac{\partial u}{\partial x} = 2\frac{L_p RT}{a}\,c(a,x), \qquad (134a)$$

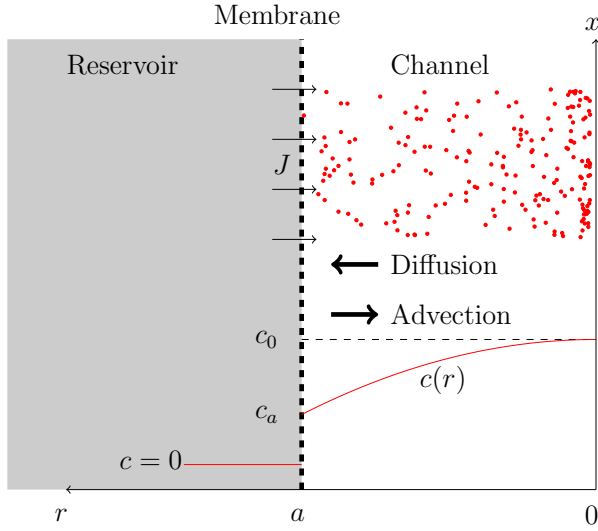$$\frac{\partial \langle cu \rangle}{\partial x} = 0. \qquad (134b)$$

Figure 33 (Color online) Sketch of the solute concentration $c(r)$ [solid red curve and density of dots] in a cylindrical tube of radius a in contact with a reservoir containing pure solvent ($c = 0$). The semipermeable membrane separating the two solutions is indicated by the thick dashed line. The concentration difference between the reservoir and channel drives an osmotic flow of solvent $J \propto c_a$ across the membrane. This dilutes the solution next to the membrane, and the concentration of solute in contact with the membrane c_a is therefore lower than the value c_0 at the center of the tube. The concentration profile $c(r)$ is set by the relative magnitude of diffusive and advective fluxes (thick arrows). At the membrane interface ($r = a$), there can be no net flux of solute molecules $J_s = -D\partial_r c + Jc_a = 0$, which determines the relative magnitude of c_0 and c_a; see Eq. (136). Adapted from (Haaning et al., 2013).

In the absence of boundary layers, these can be solved to yield the speed profile $u(x) = u^* (1 + 4L_pRTc_0x/(u^*a))^{1/2}$ with boundary conditions $u(0) = u^*$ and $c(0) = c^*$. In terms of the flow amplification factor $\gamma = u(L)/u^* - 1$ (i.e. the ratio between inlet and outlet flow speeds), this is

$$\gamma + 1 = \frac{v_{\text{out}}}{v_{\text{in}}} = \sqrt{1 + 4\frac{L_pRTc_0L}{v_{\text{in}}a}}. \qquad (135)$$

When the local radial Péclet number $Pe_r = v_r(a,x)a/D = LpRTc_a(x)a/D$ is small, the difference in concentration across the tube will be small. In this limit, it reasonable to assume that the concentration gradient at the membrane is of the order $(c_a - c_0)/a$. To solve the averaged advection-diffusion equation, we approximate the concentration profile by a parabolic function, $c(r) = c_0 + (c_a - c_0)\frac{r^2}{a^2}$. The boundary conditions Eq. (130) and no-flux across the channel centerline ($\partial c/\partial r = 0$ at $r = 0$) sets a relation (similar to Eq. (133)) between the concentration at the channel center c_0 and

wall c_a

$$c_0 = c_a + \frac{L_pRTa}{2D}c_a^2 = c_a + \frac{Pe_r}{2}\frac{c_a^2}{c^*}, \qquad (136)$$

where $Pe_r = L_pRTc^*a/D$ is the radial Péclet number. With this parabolic concentration profile, and using the velocity profile $v_r = r(r^2 - 2a^2)L_pRTc_a/a^3$ (Eq. (24b)) for the radial averaging, $\langle cu \rangle$, Eqns. (134a)-(134b) can be written in non-dimensional form

$$\left(\frac{\partial U}{\partial X} + \beta \left(\frac{\partial U}{\partial X}\right)^2\right) U = \Gamma, \qquad (137a)$$

where $X = x/L$ and $U = u/u^*$ and where

$$\Gamma = 2\frac{L}{a}\frac{L_pRTc^*}{v^*}, \qquad (137b)$$

is the ratio of the largest obtainable purely osmotic flow velocity $2\pi aLL_pRTc^*/(\pi a^2)$ and the inlet velocity u^*. The parameter

$$\beta = \frac{1}{6}\frac{a}{L}\frac{v^*a}{D} = \frac{1}{3}\frac{Pe_r}{\Gamma}, \qquad (137c)$$

is proportional to the ratio of the radial Péclet number Pe_r and the maximum flow gain Γ. Equation (137a) can be solved analytically (Haaning et al., 2013), and experiments show close agreement with theory (Fig. 34).

In the limit of strong concentration boundary layers, the concentration profile in the tube is no longer uniform and the magnitude of the parameter β can exceed unity. In the limit of $\beta \gg 1$, the solution of Eq. (137a) for the flow rate gain γ is

$$\gamma + 1 = \left[\frac{3}{2}\left(\frac{\Gamma}{\beta}\right)^{1/2} + 1\right]^{2/3} \qquad (138)$$

$$= \left[\frac{3}{2}\left(\frac{12L_pRTc^*L^2D}{a^3(v^*)^2}\right)^{1/2} + 1\right]^{2/3}. \qquad (139)$$

which should be compared with Eq. (135), valid when $\beta \ll 1$. Eq. (138) provides a simple approximation to the solution to Eq. (137a) for large values of β/Γ, where the flow rate gain scales as $\gamma \propto (\Gamma/\beta)^{1/2}$. For $\beta \geq 1$ and $\Gamma \geq 1$ Haaning et al. (2013) found that the error in Eq. (138) is typically less than 10% when compared to Eq. (137a).

In the experiments by Haaning et al. (2013), both β and Γ were of moderate magnitude and the boundary layer contributes significantly to the flow (Fig. 34). In plants, however, we can estimate the parameter $\beta = a^2u/(6LD) \simeq 3 \times 10^{-6}$ for $a = 10^{-5}$ m, $u = 10^{-4}$ m/s, $L = 1$ m, and $D = 5 \times 10^{-10}$ m^2/s. This analysis thus confirms the validity of the Münch-Horwitz equations under conditions relevant to flow in the phloem since the non-linear term $\beta(du/dx)^2$ in Eq. (137a) can be safely neglected in this limit.
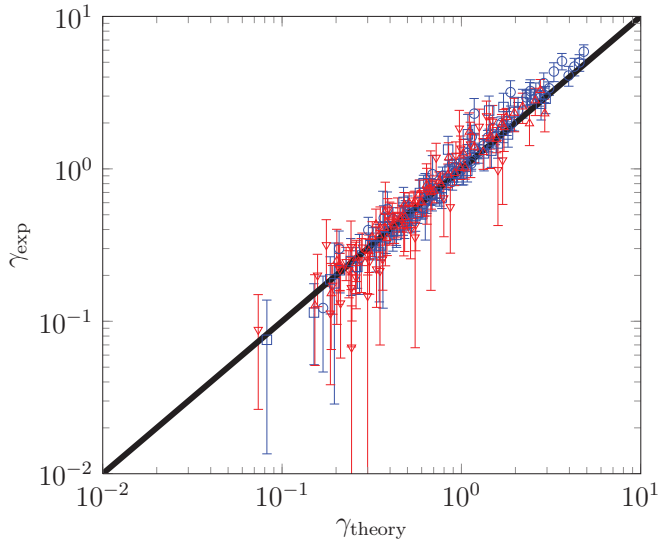
Figure 34 (Color online) Comparison between experimental and theoretical values of the flow rate gain $\gamma = u_{out}/u_{in} - 1$ obtained using Haaning *et al.* (2013)'s setup (Fig. 20(e)). Measured values of γ plotted as a function of the predicted values using Eq. (137a). Dark blue squares and circles are measurements with NaCl as the solute, for two different lengths of the semi-permeable membrane in the setup, whereas red triangles indicate measurements with sucrose as the solute. Adapted from (Haaning *et al.*, 2013).

.

E. Final remarks

In this section we have derived the basic equations for osmotically driven flows in a one dimensional system resembling a plant with leaf, stem and root. These Münch-Horwitz equations were obtained via the Aldisflow: a simple pipe flow perturbed (and driven) by osmotic inflow. Compared to the full hydrodynamic equations, they present an enormous simplification, but, due to their strong nonlinearity (from the coupling between velocity and concentration), the subtle matching at the border between the different segments, and the treatment of the loading function, they still remain challenging.

Osmotically driven flow is not a subject covered in present day textbooks on hydrodynamics, so we have presented simple and conceptually important solutions of both transient and stationary states, the latter including different types of loading. The use of constant concentration in the leaf (Sec. V.B) is very simple, but leads to an asymmetry between source and sink. The target concentration models (Sec. V.C) are more complicated, but probably also more physical and allow symmetry between source and sink. They seem to be good candidates for further work, e.g., including more complicated architectures and flow reversals, as when a young leaf is coming of age and turns from a sink to a source. Finally, we have described some of the effects that have been left

out in the simple one-dimensional description, i.e., the boundary layers that form near the tube walls and lead to a reduction of the osmotic strength (Sec. V.D). These effects are more important in the current biomimetic devices than in the real phloem due to the small sizes and low velocities in the sieve tubes.

The detailed prediction of velocity and concentration profiles through a "tree" as presented in e.g., Fig. 30 cannot at present be sensibly compared to any available data. Hopefully, this will change over the coming years, when we will be able to expand the theory to more realistic architectures than the single tube and when measurements of pressures, flow velocities and concentrations will be possible with high resolution in an active phloem. Until then the models should serve as inspiration and backing for simpler modelling, e.g., in the style of Sec. IV.C.

VI. WATER TRANSPORT IN PLANTS

A. Experimental Results

The experimental study of water transport in plants involves the measurement of only a few physical properties, of which the flow rates, and the gradients of pressure and solute concentrations that are responsible for generating the flows, are the most important. While the determination of such properties is trivial for man-made hydraulic systems, the mere fact that the water in the xylem is under tension, and, furthermore, that the system of transport is enclosed in both ends and along its path by living cells, and that the conduits have thick and optically opaque cell walls, make their direct determination difficult if not impossible. In general, any direct pressure measurement in a functional xylem system results in the formation of embolism and thereby changes both the pressure gradient and the flow. Thus plant biologists are left with indirect methods for estimating flow parameters. An important difference between xylem and phloem transport is that water movement through the xylem is coupled to an external driving gradient (evaporation), which means that flow rates and pressure gradients are not stationary. Flows approach zero at night and are typically maximal at midday, and pressure gradients follow the same pattern although they are also affected by soil conditions. For the characterization of xylem transport, we focus on maximal flow rates and minimal xylem pressures as these determine the nature of the flow regime and the potential for conductivity loss due to embolization.

1. Xylem flow rates

Historically, flow (volume flux) was determined from rates of transpiration, rather than actual measurements of flow in the xylem. Methods range from analysis of

gas exchange between leaves and ambient air conducted at the level of single leaves using hand-held devices (Mc-Dermitt, 1990) up to the scale of entire tree canopy using eddy correlation or heat balance methods (Hogg *et al.*, 1997; Jarvis and McNaughton, 1986). These methods only provide approximations of real fluxes as they either disturb the transpiration environment by enclosing leaves in gas chambers (thus perturbing the energy balance and boundary layers) or - in the case of fluxes observed on the canopy level - not of sufficient resolution to determine the contribution from single plants. Thermal sensors inserted into stems overcome, to certain degree, these limitations (Granier, 1987; Granier *et al.*, 1996; Swanson, 1994). This approach uses a heat pulse as a tracer to determine the speed of water passing by the sensor (Čermák *et al.*, 2004). Limitations relate to problems with calibration, as each plant has different heat transfer properties (Lundblad *et al.*, 2001). The most direct method for measuring flow rates relies on changes in weight to determine water loss from the plant/soil system. However, this is possible only for small plants growing in containers or in the field where *lysimeters* (devices that measure transpiration in the field) can be used(Liu *et al.*, 2002).

Estimates of volume flow rates through plants or stems cannot be directly translated to flow velocities. The reason for this is that xylem conduits make up only a fraction of the cells within the xylem tissue. In addition, the diameter of xylem conduits varies, often markedly. Larger diameter conduits will have the highest flow rates and carry most of the flow, with smaller diameter conduits hypothesized to play a role in permitting water to flow around gas-filled conduits (Ford *et al.*, 2004). The speed at which water moves through xylem conduits is estimated to fall within the range of $1-10$ m/h, indicative of low-Reynolds-number-flow (Table I, (Maier and Clinton, 2006)). Novel methods for flow estimation include the use of MRI with field gradients, allowing for observation of not only the spatial concentration of water but also the spatial distribution of velocity fields (Köckenberger *et al.*, 1997; Windt *et al.*, 2006). This promising method, however, requires special equipment and expertise and has so far only had limited application.

2. Xylem Pressure

Measuring the pressures in functional xylem is perhaps the *holy grail* of plant hydraulics, connected to the longstanding questions about the reality of negative pressures in plants and the stability of water under such conditions. This skepticism has been fueled by the fact that, until recently, the ability to transport water under large negative pressures has not been reproduced in the lab (Wheeler and Stroock, 2008). The challenge, of course, is that anything that breaks the integrity of xylem walls has the potential to form embolism or changes in pressure distribution (Jansen *et al.*, 2015; Rockwell *et al.*, 2014a). Only a few direct measurements of xylem pressure have been made successfully, all carried out using a cell pressure probe with capillary tip manipulated into the xylem conduit. All of these were made in plants in which the tensions were low, since the liquid in the capillary tends to form an embolus around -0.7 MPa, and only in relatively translucent tissue (excluding woody stems) (Pockman *et al.*, 1995; Tomos and Leigh, 1999; Wegner and Zimmermann, 2002; Wei *et al.*, 2001). Thus, most estimates of xylem pressure are based on determining the water potential of tissues assumed to be in equilibration with the xylem. Three major techniques are used (Boyer, 1995): (1) pressure chamber (Scholander *et al.*, 1965); (2) psychrometers (Boyer and Knipling, 1965); and (3) tensiometers. These methods give accurate estimates of xylem tensions as shown in their ability to capture the gradient in gravitational potential in tall trees (Scholander *et al.*, 1965), when measured at night (no transpiration), or on material in which xylem tensions have been experimentally generated using a centrifuge (Holbrook *et al.*, 1995). Under non-drought conditions, midday (i.e, minimum) xylem pressures fall in the range of -0.5 to -2 MPa. However, during periods of low soil water availability or in arid regions, xylem pressures can be much lower (Scholander *et al.*, 1965; Stroock *et al.*, 2014). For example, there are reports of gymnosperms in Western Australia having xylem pressures as low as -10 MPa. Equally impressive are mangroves, which grow in seawater and have xylem pressures in the range of -2 to -5 MPa. Mangroves exclude most of the salt at their roots and thus must develop substantial xylem tensions in order to carry out this form of reverse osmosis (Ball, 1988; Scholander, 1968; Tomlinson, 1994).

3. Cavitation

Xylem sap often experiences pressures well below atmospheric, and the liquid column is prone to fracture by the formation of bubbles. Critical to our understanding of xylem transport in plants are the stability limits for xylem – at what pressures does cavitation occur and spread between conduits? This problem was discussed recently in some detail by Stroock *et al.* (2014): for mildly reduced pressures, the liquid, which has been in contact with air at 0.1 MPa, becomes supersaturated with dissolved gases and thermodynamically unstable with respect to the formation of air bubbles. For larger reductions of pressure, the liquid also becomes thermodynamically unstable with respect to the formation of vapor bubbles or boiling. This doubly unstable situation need not be malignant because both these thermodynamically unstable states (supersaturation and superheat) can be kinetically stable (metastable) down to pressures below -100 MPa owing to the activation energy required to form

a gas nucleus in the liquid.

The basic experimental approach has been to determine the extent to which the xylem becomes gas-filled as xylem pressures are decreased. Xylem pressures can be manipulated by withholding water from plants or imposed using centrifugation, while the presence of gas-filled or embolized conduits can be measured hydraulically (i.e, as a reduction in xylem conductivity) or using imaging such as magnetic resonance imaging, cryo scanning electron microscopy or X-ray tomography (Brodersen *et al.*, 2013; Cochard *et al.*, 2013). Acoustic detectors have also been used to listen for ultrasound produced by cavitation events, and have the advantage that they can be attached to plants of any size (Kikuta and Richter, 2003). Some experiments suggest a correlation between ultrasound emission frequency and fraction of gas-filled conduits (Jackson and Grace, 1996), although many emission appear to occur from other types of events (Tyree and Dixon, 1983). Ponomarenko *et al.* (2014) observed cavitation events in a thin slice of gymnosperm wood embedded in a hydrogel and matched acoustic emissions to visual observation of emboli formation in tracheids, providing experimental support for using acoustic emission as a non-destructive way of monitoring embolism formation within trees.

Another approach is to determine the pressure needed to push air between conduits using a glass capillary glued to an embolized vessel blocked at the other end (Choat *et al.*, 2004; Zwieniecki *et al.*, 2001). This is a direct measurement of the propagation threshold between two conduits; the challenge is scaling these measurements so that they are relevant at the level of the xylem network. Despite the technical limitations of each method (MRI, X-ray, hydraulic resistance measurement, acoustic or single vessel), the general picture is that plants can tolerate xylem tensions that they normally experience in their natural environment, whether a wet tropical forest or a dry desert. Only extreme events such as prolonged droughts, changes in transpiration rates, or mechanical damage to stems result in plants being pushed to beyond their hydraulic limits, resulting in cavitation and the formation of air-filled or embolized xylem conduits.

The reversibility of embolism (Fig. 35), leading to the restoration of transport function in xylem conduits of trees is hotly debated (Brodersen and McElrone, 2013; Zwieniecki and Holbrook, 2009). While there is no doubt that the production of new xylem conduits can substitute for the ones lost to embolism, such growth is generally limited to specific periods of the year in temperate or semi dry climates. In some plants, restoration of xylem conductivity can be accomplished by root pressure in which, under conditions of limited transpiration (night), roots can accumulate solutes in xylem in concentrations exceeding those of the soil (Cochard *et al.*, 1994; Yang *et al.*, 2012). This results in the development of positive pressures within the xylem as water is
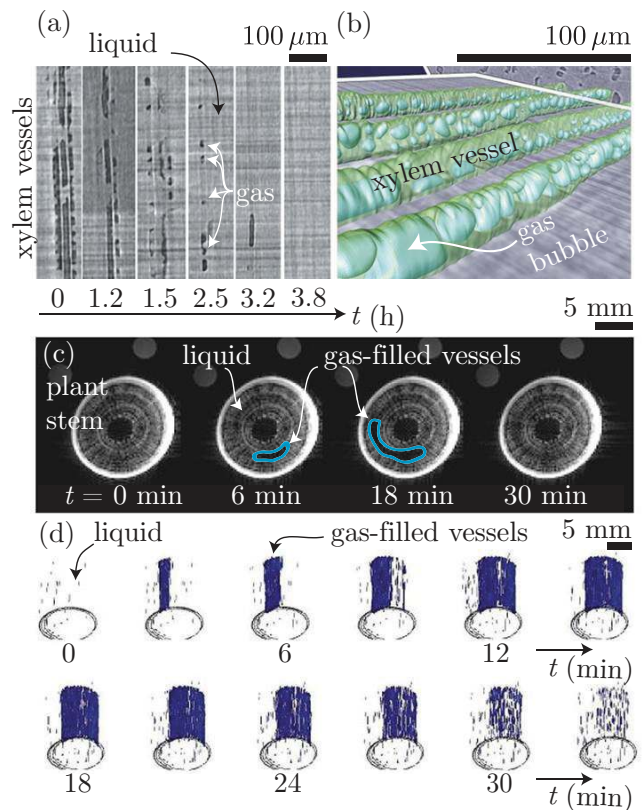

Figure 35 Evidence for restoration of transport function in xylem conduits by removal of gas bubbles. (a) Refilling of embolized conduits in a grape vine stem visualized by a time-series of x-ray tomography images. Dark areas are gas-filled, and droplets of water are visible on the walls of the embolized conduits. Over time, gas bubbles disappear and conductivity is restored. Flow is from bottom to top. (b) 3D reconstruction of the droplets in the vessels seen in (a) (for details see (Brodersen *et al.*, 2010)). (c) Changes in water content in a maple tree stem visualized by a time series of magnetic resonance images. Flow is in the normal direction. (d) 3D reconstruction of gas pocket formation and subsequent removal as seen on (c) (for details see (Zwieniecki *et al.*, 2013)). Adapted from (Brodersen *et al.*, 2010; Zwieniecki *et al.*, 2013)

drawn into conduits via osmosis. Positive pressures result in gases being pushed into solution and thus the refilling of embolized xylem conduits. Root pressure occurs most commonly in herbaceous species, or in deciduous trees prior to spring leaf production (Ewers *et al.*, 1997). Long-lived woody plants often show no evidence of root pressure, yet their xylem conductivity is robust against variation in xylem potentials (Sperry *et al.*, 1994). This may mean that they have the ability to restore conduit transport function even while retaining actively transpiring leaves. Such a restoration process would require the generation of local potential gradients to drive water from surrounding living cells into empty conduits (Zwieniecki and Holbrook, 2009), perhaps in a manner similar to the generation of root pressure. Evidence of gradient for-
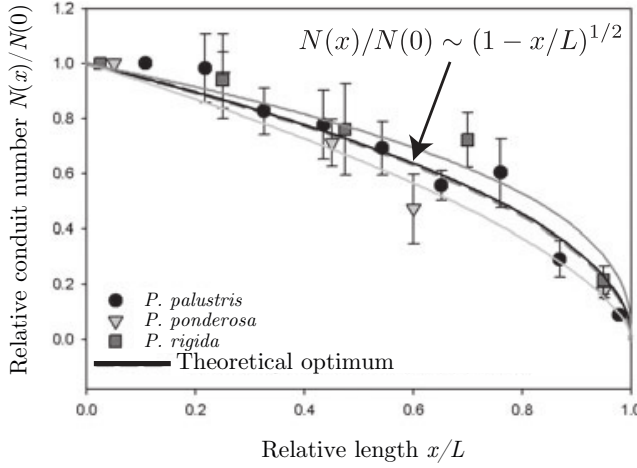
Figure 36 Pine needles are optimized for efficient water transport. Measured axial distribution of number of xylem conduits $N(x)$ plotted as a function of position x along the needle. The base of the needle is located at $x = 0$, while $x = L$ corresponds to the tip. Optimum theoretical distribution that minimizes the pressure drop across the needle is plotted as a reference line (Eq. (143)). Adapted from (Zwieniecki *et al.*, 2006).

mation activity, however, shows that adequate gradients may only exist in plants in which xylem tensions have been significantly relaxed by rain or fog events, as the highest recorded osmotic potential in non-functional conduits is in the range of 0.2 MPa (Secchi and Zwieniecki, 2012). Some evidence for embolism removal activity in non-transpiring woody plants that remain under low tension (less than 0.4 MPa) comes from recent observations in both x-ray tomography and MRI (Fig. 35); (Brodersen *et al.*, 2010; Zwieniecki *et al.*, 2013)).

B. Conduit Optimization

The potential for embolism formation and restoration of embolized conduits reflect a plant's biophysical potential for dealing with environmental extremes. However, xylem conduits are usually formed under conditions when any scarcity of water is within the range tolerated by particular species. In such situations, plants tend to build transport systems optimized for their environment (McCulloh *et al.*, 2003; Savage *et al.*, 2010; West *et al.*, 1999). Evidence is observed in the xylem of leaves, where tensions are expected to be the highest and water delivery to leaves is of crucial importance to allow for stomatal opening. Analysis of xylem structure in pine needles, characterized by a single vein composed of parallel conduits (tracheids), exhibit a high level of control over the construction of conduits. Zwieniecki *et al.* (2006) observed a characteristic conduit-tapering-trend in several different pine species (Fig. 36), and rationalized this by

considering the pressure drop required to drive a given rate of transpiration from the leaf surface. Assuming that the evaporation rate q from the needle is constant, we can calculate the pressure drop Δp for a given needle length l by integrating the pressure gradient

$$\frac{\partial p}{\partial x} = -\frac{\eta u(x)}{k(x)}, \qquad (140)$$

along the needle, cf. Eq. (5). Here, u is the flow speed, $k = a^2/8$ is the conductivity, a is the conduit radius, and η is the viscosity of the xylem sap. Volume conservation dictates that q, the rate of evaporation per unit length along the needle, is related to the flow speed u and conductive area A by

$$\frac{\partial}{\partial x}\big[A(x)u(x)\big] = -q. \qquad (141)$$

giving a linear variation of $A(x)u(x)$. Since the flow speed vanishes at the needle tip ($u(l) = 0$) we find for the pressure drop Δp

$$\Delta p = \eta q \int_0^l \frac{l - x}{k(x)A(x)} \, \mathrm{d}x. \qquad (142)$$

Experiments reveal that the conduit radius a is independent of the position x along the needle. This has two important consequences. First, the conductivity $k(x) = a^2/8 = \text{const}$ is independent of position. Likewise, the conductive area $A(x) = \pi a^2 N(x)$ is proportional to the number of channels $N(x)$ at position x. Minimizing the pressure differential (Eq. (140)) while keeping the total conduit volume $V = \pi a^2 \int_0^l N(x) \, \mathrm{d}x$ constant, leads to the optimum conduit distribution

$$N^*(x) = N(0) \left(1 - \frac{x}{l}\right)^{1/2}, \qquad (143)$$

where $N(0)$ is the number of conduits at the needle base $x = 0$. The predicted conduit distribution (Eq. (143)) is in good agreement with experimental data (Fig. 36). The quantitative advantage of arranging tracheas according to Eq. (143) can be gauged by computing the pressure drop Δp_{unif} assuming a uniform distribution of tubes with both conduit volume V and number $N(x) = \text{const}$. This yields $\Delta p^*/\Delta p_{\text{unif}} = 8/9$, suggesting that optimally redistributing tracheas along the length of the needle might lead to a reduction in pressure drop by about 10% Zwieniecki *et al.* (2006). Similar conduit arrangements have been observed in needle phloem (Ronellenfitsch *et al.*, 2015).

A similarly high level of precision exists in the distribution network of leaves that are characterized by reticulate, interconnected network of veins delivering water across flat surfaces. These reticulate vein networks have been considered from the perspective of the redundancy needed to tolerate a significant level of damage and still
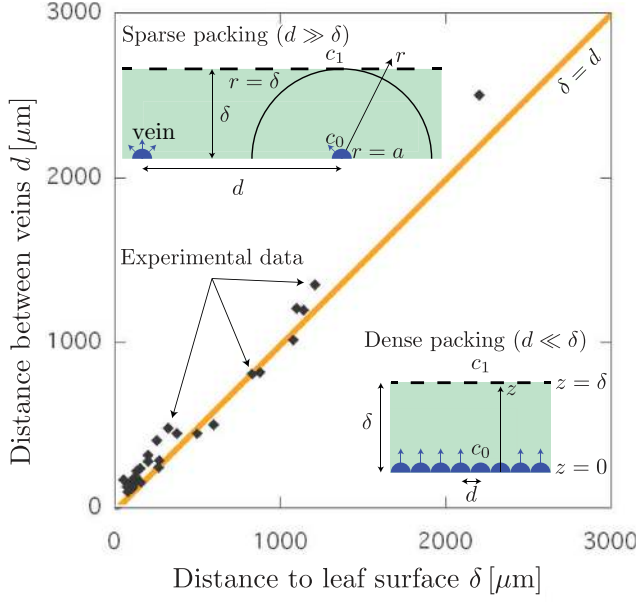
Figure 37 Measured distance between veins d versus distance to evaporative surface δ for different plant species. The solid line corresponds to the optimal case $d = \delta$. Adapted from (Noblin *et al.*, 2008).

allow for water distribution across the leaf blade (Katifori *et al.*, 2010). However, a recent study demonstrates that the density and placement of veins within leaves permits the hydration of the leaf surface such that even the most distal locations of the leaf blade are adequately and uniformly supplied with water, while no unnecessary (redundant) veins are built that would otherwise consume space that could be used for the chlorophyll bearing cells (Noblin *et al.*, 2008).

In the case of sparse vein packing, i.e. when the spacing between veins d is much greater than the leaf thickness δ, we assume that the total evaporation rate from the leaf Q is the sum of the contribution from each vein of radius a and length L (Fig. 37). This contribution can be found by solving the steady-state diffusion equation inside the leaf (Eq. (11)) with $\partial_t c = \boldsymbol{v} = \Upsilon = 0$). We approximate each vein as an isolated line source in an infinite half-plane. The solution to the Laplace equation in cylindrical coordinates with boundary conditions $c = c_0$ at the vein surface ($r = a$), and $c = c_1$ at the leaf surface ($r = \delta$) is

$$c(r) = c_0 + \frac{c_1 - c_0}{\log(\delta/a)} \log(r/a). \tag{144}$$

The evaporation rate for a single vein is $-\pi a L D \partial_r c|_{r=a} = L \pi D (c_0 - c_1)/\log(\delta/a)$. The number of veins N in a section of width W is $N = W/d$. The total evaporation rate from N veins is therefore

$$Q = \frac{\pi}{\log(\delta/a)} \frac{D(c_0 - c_1)}{d} LW \sim \frac{D(c_0 - c_1)}{d} LW. \tag{145}$$

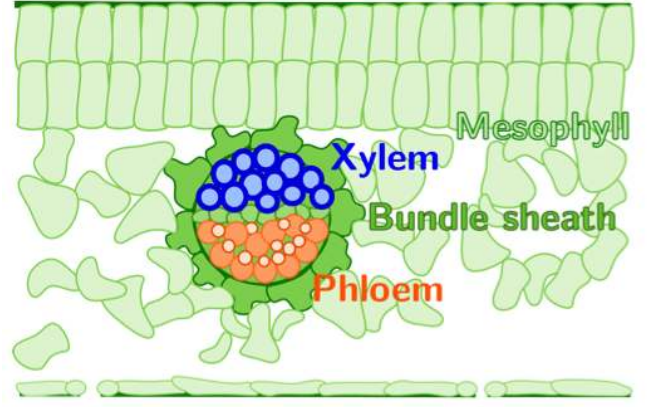Conversely, for high channel density ($d \ll \delta$) the iso-

Figure 38 Schematic representation of a cross-section of a leaf. The bundle sheath (dark green) forms a protective layer around the vasculature: xylem treachery elements (blue) and phloem sieve elements (small circles) with their neighbouring companion cells (orange cells). The water from the xylem passes out through the bundle sheath and presumably along the cell walls of the mesophyll (light green) and most of it evaporates through the stomata (the "holes" in the lower leaf surface). A small part enters the mesophyll where it takes part in the photosynthesis and the subsequent transport of sugars from the mesophyll back in through the bundle sheath, through the companion cells into the sieve elements. Courtesy of Hanna Rademaker.

concentration lines run mainly parallel to the leaf surface and the solution can be approximated by a linear profile: $c(z) = c_0 + (c_1 - c_0)z/\delta$. This gives for the evaporation rate

$$Q = \frac{D(c_0 - c_1)}{\delta} LW. \tag{146}$$

differing from Eq. (145) only by the replacement of d with δ. Equation (146) represents the largest possible evaporation rate for the system. We therefore observe that when the channel spacing approaches the leaf thickness ($d \simeq \delta$) the evaporation from N channels (Eq. (145)) approaches the saturation value (Eq. (146)) and no gain in evaporation rate can be achieved by adding more veins. This seemingly simple scaling law is observed in many plants (Fig. 37) which suggests that design features oriented toward optimal utilization of veins in providing water for evaporation are common among leaves (Noblin *et al.*, 2008). Recent work has demonstrated that only angiosperms maintain the anatomical optimum across all leaf thicknesses, while gymnosperms and ferns are limited by their inability to produce high vein densities (Zwieniecki and Boyce, 2014).

C. Water flow for the Polymer Trap Phloem Loading Mechanism

As we have seen, leaves maintain an extremely delicate balance between water and sugar translocation to

ensure the outflow and eventual evaporation of water from the xylem cells simultaneously with the inflow of water and sugar to the phloem cells (sieve cell-companion cell complex) nearby. As discussed in Section III and shown schematically in Fig. 38, the sugar which is generated in the chloroplasts of the mesophyll cells has to pass through the bundle sheath, a layer of tightly arranged cells around the vascular bundle, which protects the veins of both xylem and phloem from the air present in the space between the mesophyll cells and the stomata, before it is loaded into the sieve elements. Simultaneously, the water which leaves the xylem under tension, is, for the most part, evaporated from the walls of the mesophyll cells, but a small part goes into these cells and takes part in the photosynthesis. Another part goes (perhaps) directly into the nearby phloem, a few microns away, which is under positive pressure, through the aquaporins of the plasma membranes. The route taken by the water and the relation to the sugar transport is still not well-understood - even though it has been discussed since the time of Münch. Thus Fig 39 shows how Münch envisaged the coupled water/sugar transport in what is now called a passive loader (see Sec. III.B). As one can see, the single headed arrows (water) and the double headed ones (sugars) essentially have to move in opposite directions. Although the flow of water from xylem to palisade is small relative to transpiration, this seems rather counterproductive!

Recently, a study of active apoplasmic loading was carried out (Sze *et al.*, 2013, 2014), including six states for which one can relate the chemical reaction rates to the sugar and water transport through the phloem. In the case of passive loading and of active symplasmic loading – the so-called polymer trap described in Sec. III.B.2 – the sugar passes through plasmodesmata apparently without help of transport proteins, which should make the problem more straightforward to analyse. The polymer trap case is particularly interesting, since it relies on plasmodesmata that are extremely fine-tuned to allow the passage of the small sugars produced in the mesophyll (primarily the disaccharide sucrose), but not the heavier ones (the trisaccharide raffinose and the tetrasaccharide stachyose). As in active apoplasmic loading, it facilitates a build-up of a large sugar concentration in the sieve element-companion cell complex which is much larger than that in the mesophyll, allowing the plant to have a highly concentrated phloem without an equally high concentration in the leaves, which would make the latter very attractive for unwanted foragers. The feasibility of this loading strategy has recently been analysed by (Dölger *et al.*, 2014) based on the best available data from the melon *Cucumis melo* (Haritatos *et al.*, 1996; Schmitz *et al.*, 1987; Volk *et al.*, 1996). See also the recent review by (Schulz, 2014). The geometry of the problem is sketched in Fig. 40, where we show the bundle sheath cell to the left, a companion cell in the middle, and a sieve
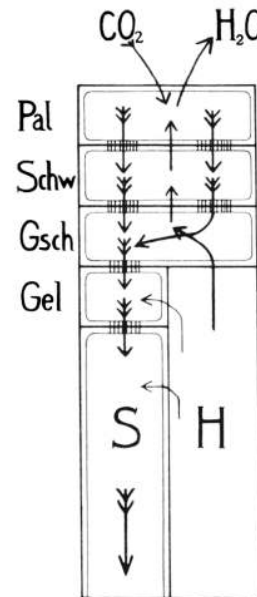

Fig. 22. Saftströmungen im assimilierenden Blatt, Ergänzung zum Schema Fig. 10 u. 12. Pal Palisadenparenchym, Schw Schwammparenchym, Gsch Gefäßbündelscheide, Gel Geleitzelle, S Siebröhre, H Holzbahn (Hydrom). Ungefiederte Pfeile: Wasser; einfach gefiederter Pfeil: CO_2; doppelt gefiederte Pfeile: Lösung der Assimilate. Entsprechend der Abnahme der Strömungswiderstände strömt im Gefäßbündel Wasser aus dem Hydrom ins Leptom.

Figure 39 Reproduction of Münch's Figure 22, which corresponds to the passive loading mode in woody angiosperms (Fig. 12c). Assimilates (sugars) in a photosynthetically active leaf (double-feathered arrows) flow from palisade parenchyma (Pal) through plasmodesmata via spongy parenchyma (Schw), bundle sheath (Gsch), companion cell (Gel) finally into to a sieve tube (S). Water (simple arrows) moves the opposite way from the xylem (H) across cell walls into the bundle sheath and continues up to the palisade parenchyma where it evaporates. A smaller part (shown by thin arrows) enters the phloem directly. From (Münch 1930) p. 153.

element to the right. The sugar comes into the bundle sheath in the form of sucrose from the mesophyll (not shown) and after passage to the companion cell through the plamodesmata marked "in", part of the sucrose is transformed to heavier sugars, raffinose and stachyose, and the mixture passes on through the larger "out" plasmodesmata into the sieve element. The hydrodynamic radius of raffinose is only around 25% larger than that of sucrose (Liesche and Schulz, 2013), so either the filtering properties of the "in" plamodesmata are extremely well tuned or the water is creating such large bulk flow that the sugars cannot move back through them. The latter does not seem possible, at least with the data available for *Cucumis melo*: The total sugar concentration in the companion cell c_2 is much larger (more than a factor of two) than that of the bundle sheath c_1, mostly due to the heavy sugars, and this strongly limits the water intake. If no additional water passes directly through the membrane of the companion cell, water conservation dictates that the same water flux must pass the "in" and the "out" plasmodesmata. Sugar must be conserved as well, and since no sugar passes the membrane the sugar that passes the "in" and the "out" plasmodesmata must be identical. The sugar concentrations (c_2 and c_3) in
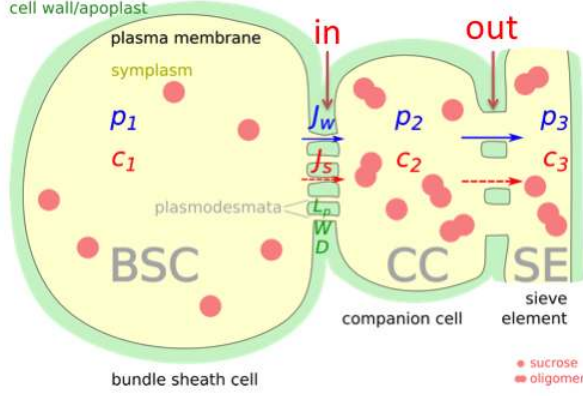
Figure 40 The polymer trap model with diffusion and bulk flow. The bundle sheath cell (BSC) is connected to the companion cell (CC) by narrow plasmodesmata, which prevent the oligomers from diffusing back into the bundle sheath, through the cell interface called "in". Similarly, the companion cell is connected to the sieve element (SE) through wider plasmodesmata through the "out" interface. The water flow rates J_w through the cell interfaces are marked with blue (full) arrows, the sugar flow rates J_s as red (dashed) arrows. These flows depend on the pressures p as well as on sucrose and oligomer concentrations c_i inside and outside the cells on the loading pathway. The semipermeable cell interfaces are characterized by a permeability L_p, a bulk hindrance factor W, and an effective diffusion coefficient D depending on the structure, density and size of the plamsmodesmata connecting them. Adapted from Dölger et al. (2014).

the companion cell are, however, much larger than the one (c_1) in the bundle sheath (roughly double), and the pores are larger in the "out" plasmodesmata, so obviously advective sugar transport cannot account for the sugar transport alone, and diffusion has to play a large role, at least through the "in" interface.

To understand the filtering properties of the "in" membrane, one has to estimate the transport of water and of sugar through its narrow plasmodesmata. Despite detailed electron microscopy (Fisher and Gifford, 1986; Volk et al., 1996) the unblocked space available for flow in these "channels" is not known with certainty, but it has been suggested by Waigmann et al. (1997) to model them as circular slits (i.e., annular regions) with half-width of around 1 nm, radius $r_{PD} \approx 25$ nm and length $d \approx 0.1\mu m$. In the limit of low Péclet number $\text{Pe} = uL/D$ for a channel of length L, flow velocity u and diffusion coefficient D, see Section II.B, the flow is diffusion-dominated and the variation of the solute concentration through the plasmodesmata is approximately linear. In this case the appropriate framework for describing the coupled sugar-water transport is the Kedem-Katchalsky equations given in Eqs. (21a) and (21b). Expressing flux densities of water J_w and sugar J_s in terms of the two driving forces, pressure difference (Δp) and concentration

difference (Δc) across the membrane one finds

$$J_w = L_p\big[\Delta\Psi + W\Delta\Pi\big], \qquad (147a)$$

$$J_s = W\, J_w c_i + \frac{1}{d}D\Delta c. \qquad (147b)$$

where L_p is the permeability, D is the diffusion coefficient, and W is the advective hindrance factor. W expresses how leaky the membrane is, i.e., how easily the solute can pass it. $W = 0$ (or $\sigma = 1$) allows no solute and the osmotic strength is the full osmotic pressure $\Pi = RT\,c$. In the opposite limit $W = 1$ the sugar travels freely through the membrane and is advected with the speed of the water flow.

In Dölger et al. (2014), these equations were written down for for the coupled fluxes of water and sugar through each of the interfaces shown in Fig. 40: bundle sheath/companion cell (marked "in") and companion cell/sieve element (marked "out"). They took the concentration c_i as the one on the "upwind" side, which is being advected through the membrane of width d. Across the "in"-membrane, these are the sucrose molecules, and in addition there will be an osmotic term $RTc^o = \Pi^o$ with $W = 0$ on the RHS of Eq. (147a), from the oligosacchrides (raffinose and stachyose) that cannot get back through the narrow plasmodesmata. Note that the boundary conditions and thus the flows are different from the classic osmotic flows in a closed system. Here one assumes a steady state with the flow of both water and sugar going to the right. This implies, of course that both water and sugar is provided to the bundle sheath from the mesophyll outside (to the left in Fig. 40), although the mesophyll/ bundle sheath interface is not explicitly taken into account.

I addition to these transport equations, sugar and water must be conserved, and, as mentioned above, if no additional water is taken up, the fluxes J_w through each of the interfaces must be inverse proportional to their areas. For the sugar, one has to be a bit more careful, since sugar transport measured in molar concentration × volumetric flow rate is not conserved, since molecular weights of the oligosacchrides are larger than that of sucrose.

In Dölger et al. (2014), the parameters for the Kedem-Katchalsky equations are computed for both of the membranes, "in" and "out". The transport coefficients for a membrane with narrow pores of density n_{PD}, where $d \gg h$, can be found in analogy with those estimated earlier in e.g. Section IV.C.1. Thus the membrane permeability is

$$L_p \approx n_{PD}\frac{4\pi r_{PD}h^3}{3\eta_{cyt}d} \qquad (148)$$

where η_{cyt} is the viscosity of the cytosol. Similarly, the diffusion coefficient can be found from

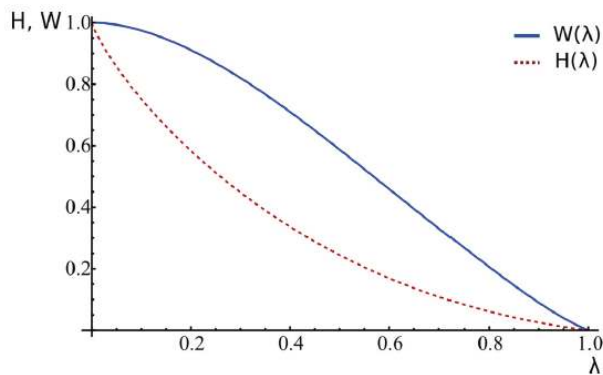$$D \approx 4\pi\, r_{PD}\, h\, n_{PD}\, H\, D_{cyt} \qquad (149)$$

Figure 41 (Color online) Diffusive and convective hindrance factors H (red, dashed) and W (blue, solid) in circular slit pores as function of the relative solute size λ. Both approximations given by Dechadilok and Deen (2006) decrease smoothly from 1 to 0 for an increasing solute size, where a hindrance factor of zero corresponds to total blockage of the respective molecule. Above $\lambda = 0.8$ the curves should be regarded as extrapolations. Adapted from Dölger *et al.* (2014).

where D_{cyt} is the diffusion coefficient of the molecule in question in the cytosol and $H = H(\lambda)$ is a hindrance factor for diffusion of a spherical particle in a narrow channel as function of the "aspect ratio" $\lambda = r_{solute}/h$, the ratio between the molecular radius and the channel half-width. The advective and diffusive hindrance factors $W(\lambda)$ and $H(\lambda)$ are given as series expansions in Dechadilok and Deen (2006) and shown in Fig. 41. To be able to block out raffinose, the channel half-width must be very close to the radius of the raffinose molecule, i.e., $h \leq 5.2$ Å and to estimate the passage of sucrose molecules of radius around 4.2 Å we have to use these functions for λ as large as 0.8 which is at the limit of their validity (Dechadilok and Deen, 2006), even more so since these molecules are not spherical, and since, for such small particles – only about three times larger than the water molecules themselves – hydrodynamics is questionable. If, despite all these caveats, we do use these values, we find that even with such small pores, one can, just by pure diffusion, get enough sucrose through the membrane to account for the observed transport rates. But, most likely, a substantial amount of water will follow with the sugar into the companion cell and on to the sieve element. If not, the companion cell would have to build up a counter-pressure, which will then also make it difficult to take up water into the sieve element-companion cell complex directly from the xylem through the plasma membrane. Lowering the pressure in the companion cell and the sieve cell will thus have two advantages: it will allow an enhanced sugar transport, aided by the "bulk" water flow, and it will transmit water directly into the phloem with the sugar with no need for additional water uptake across the higher-resistance membranes. In this way, the simplistic view of the Münch mechanism, where water is os-

motically transported into the phloem from the nearby xylem – as expressed by the bent arrows in Fig. 39 from (H) to (Gel) and (S) – is modified, at least for this kind of loading.

In the concrete example of *Cucumis melo*, we find that the water and sugar (sucrose) flows through the plasmodesmata in the "in" interface (i.e., from the bundle sheath to the companion cells, are related as $J_w^{in} \approx 0.3 c_1 J_s^{in}$ – as compared to $J_w^{in} \approx c_1 J_s^{in}$ for purely advective transport. So there the sugar transport is dominated by diffusions, but with a non-negligible water flow. For the "out" interface, this would very likely be the other way around, such that sugar translocation into the sieve elements would be carried predominantly by bulk water flow through the plasmodesmata. In fact it is conjectured in Dölger *et al.* (2014) that the sugar and water fluxes across this interface is matched to the sugar concentration in the phloem (i.e., the sieve element) such that $J_w^{out} = c_3 J_s^{out}$, which would imply that many elements like the one shown in Fig. 40, could emerge into the same phloem tube without diluting or up-concentrating the sap. Due to the (small) difference between the concentrations c_2 and c_3, there would still be some diffusive contribution to J_w^{out}, but, as mentioned above, there would be no need for *direct* water transport between the xylem and the phloem.

As noted above, our calculations were based on low Péclet numbers for the flows through the membranes. A characteristic value of water flux is $J_w = 2 \times 10^{-16} \text{m}^3 \, s^{-1}$ through the BSC-IC interface area $A \approx 10^{-9} \text{m}^2$, i.e., a velocity $u \approx 2 \times 10^{-5}$ m/s, which should be modified with the hindrance factor $W_{in} \approx 0.33$. With the length $d \approx 10^{-7}$m of the channel and an effective diffusion coefficient for sucrose $D \approx 4.7 \times 10^{-14} \text{m}^2 \, s^{-1}$ from (149), the Péclet number for the sucrose flow through the bundle sheath cell-companion cell interface (the "in" interface) is

$$\text{Pe} = \frac{dWu}{D} \approx 0.14. \qquad (150)$$

which validates the approach taken.

It remains to be seen, whether the lack of direct water transport from xylem to phloem is a more general phenomenon, valid also for other types of loading. In passive loaders, which include most trees, this might very likely be so, since the water motion might aid the sugar translocation and e.g., reduce the necessary concentration gradients. For active apoplasmic loaders, the situation is less clear since the transport does not take place throughout plasmodesmata, but directly through the membrane via aquaporins and sugar transporting proteins as described in Sec. III.B.1.

D. Final Remarks

In this section we have described the water transport in plants, primarily the one taking place in the

xylem, closely linked the the xylem physiology described in Sec. III.C. The description has been somewhat less detailed and mathematical than that of the sugar transport covered in the two prior sections. This is a deliberate choice since, as mentioned in the introduction, most recent reviews have concentrated on precisely the xylem, where the production of negative pressures and the flow in metastable states has created a lot of attention.

In the first part of the section, we assessed the experimental situation for the water transport through the xylem. We discuss the experimental methodology and the available data for flow rates, pressures and the occurrences of cavitation, which is the main problem for systems running at negative pressures. We then turn to the leaves and describe how important geometrical aspects of the venation structure can be understood by optimisation - either minimising pressure drops or maximising evaporation. The methods used there are close to the ones used in Sec. IV.C. Remaining within the leaves, we end by giving an introduction to recent progress in the understanding of the coupled water and sugar transport in the pre-phloem, responsible for loading sugars into the phloem. All of the areas covered here are actively pursued in current research and we shall describe some important open questions in the next section.

VII. CONCLUSIONS AND OPEN QUESTIONS

In this paper we have reviewed the state of our physical understanding of the basic processes that govern translocation of sap in plants. In the first part of the review, we introduced the basic tools and background needed for the second part: the physics of fluid translocation at low Reynolds numbers and the biology of the vascular system of plants. In the description of the vascular system, we have stressed the structural properties of the vasculature (sieve elements, vessels and tracheids) as well as their connections (plasma membranes, plasmodesmata, anastomoses and pit pores), and the special role played by the leaves in allowing transpiration as well as sugar loading and accommodating huge pressure gradients. We also point out that important details are missing in our understanding of the vascular system as a network.

In the second part, we have reviewed the current quantitative understanding of the processes that take place in the vascular conduits – Section IV–V on the flows in the phloem and Section VI on those in the xylem. We started in Section IV by reviewing the current experimental knowledge about phloem flow: velocities, pressures and sugar concentrations. We showed that they are at least in rough accordance with the Münch mechanism, and we presented evidence that gymnosperms and angiosperms, even though they seem to utilize the same basic principles, have significantly different sap velocities. We gave examples of biomimetic devices that run by osmotic pumping and elucidate basic features of the Münch mechanism. So far these devices are very simple, but we believe that a development of devices with more complex architecture and couplings is a very fruitful challenge. We concluded Section IV by a simple hydraulic description of sugar flows in terms of lumped resistors. In this way were are able to predict phloem speeds, sizes of the sieve tubes, leaf sizes and sugar concentrations in reasonable accordance with the available field data.

In Section V we then presented the more detailed hydrodynamical description of phloem translocation a la Münch, i.e., osmotically driven flows in long tubes, from which precise velocity and concentration profiles can be computed throughout even a large tree. These models confirmed the simple predictions made by the resistor theory, but also predicted strong velocity gradients as can be understood from their proximity to variants of the Burger's equation. Of course, these more detailed models also require more detailed assumptions e.g., in terms of loading mechanisms, but they do give a general framework which should be useful as better and more detailed measurements of the flows become available. Here important challenges are e.g., to include the interaction with the xylem in a way simple enough to make clear predictions. This will require a better understanding of the processes taking place in the leaves, where the xylem and phloem conduits are separated only by a few microns.

Finally, Section VI reviewed our understanding of the water transport though the xylem. The main challenge for the cohesion-tension theory is to explain how plants, in particular trees, transporting water at negative pressures, can avoid cavitation or embolisms that stop the flow and dry out the plants. Here we stressed the progress in the understanding of e.g., pit pores and the refilling of embolized vessels which have added substantial credibility to this theory. Of similarly importance is the vein architecture, and we gave examples of how important aspects of this architecture can be understood on the basis of optimisation. Finally, we combined water and sugar flow and gave a quantitative description of the water flow in the pre-phloem of active symplasmic loaders.

Our understanding of sap flow in plants has progressed immensely over the last century, as have many other branches of biology. As we have emphasized, many predictions made from theories describing the two processes responsible for water and sugar flow in plants have been confirmed. The field has developed in large part due to advances in experimental techniques. We have seen recent adaptions of x-ray computed tomography (Brodersen et al., 2010), nuclear magnetic resonance velocimetry (Windt et al., 2006), and confocal laser microscopy (Froelich et al., 2011; Knoblauch and van Bel, 1998; Liesche and Schulz, 2012; Schulz, 1992) to biophysical plant research that hold the promise for further progress. Simultaneously, the development and application of biophysical models and of synthetic, biomimetic systems,

which have elucidated many of the mechanism that drive and regulate sugar and water transport in plants, have originated through collaborations between researchers in biology, physics, chemistry, engineering, informatics, and many other fields. We believe that such interdisciplinary alliances hold the key to further progress in this field. We hope soon to see biomimetic plants models that can simulate coupled flows in the soil-plant-atmosphere continuum, transport between cells in the pre-vascular pathway, and mixing within individual cells as well as improvements of techniques to visualize and quantify vascular flows.

Many questions remain to be answered. The unifying mechanism of phloem transport is the Münch mechanism, an osmotically generated pressure flow originating in the leaves and established by sugar accumulation in the phloem vein ends. This is undoubtedly an important driving force for phloem sap, but a conclusive test of the Münch-pressure-flow hypothesis for long distance translocation requires measurement of differences in pressure and concentration between sink and source tissues in the parallel phloem and xylem conduits throughout a tree. Also, basic aspects of the transport network architecture, which forms the basis for modelling approaches, remain unexplored. For example, it is not clear whether the sieve tubes that start in the leaf minor veins continue as separate pathways up to the petiole, or whether the transport architecture is reorganized at specific junctions. In needles, almost one-dimensional leaves, the situation is somewhat simpler, and here one might be able to arrive at more complete picture (Ronellenfitsch et al., 2015).

Another open question concerns the influence of sieve element content on flow. The membrane material abundant in the sieve elements of gymnosperms (i.e., the endoplasmic reticulum covering the sieve areas and passing the sieve pores (Schulz, 1992) shown in Fig. 11d) should lead to increased resistance, but their effect cannot be seen in transport speed measurements. They have also been discussed in relation wound response and of pressure regulation and their content of aquaporins and sugar transporters should be investigated. Similarly, it remains uncertain how the highly abundant protein complexes in angiosperm sieve elements influence flow.

A full description of the Münch mechanism requires a more complete understanding of water flow in the leaves. Understanding the sugar transport involved in phloem loading which powers the Münch-pump requires a detailed quantification of inter-cellular transport of sugar *and* water all the way from the mesophyll to the phloem sieve elements. After leaving the xylem, water molecules can move apoplasmically or symplastically towards the stomata and the mesophyll. Which path it takes is important for the sugar concentration and pressure driving the phloem, and will be different for the different loading types described in Sec. III.B. At present it seems particularly challenging to understand the passive phloem loading, since intra-cellular water movement from vein to mesophyll would tend to cancel the shallow concentration gradient that is supposed to drive diffusion of sugars from mesophyll to the phloem.

For the xylem, the cohesion-tension theory seems to be solid, in the sense that the leaves do provide the tension needed for the flow, but the detailed understanding of the origins of this tension and water transport in a metastable state remains an important challenge. For the water transport, the mechanism of cavitation due to xylem tension is of major importance. Currently this is thought to result primarily from meniscal failure at pit membranes ("air-seeding"), but perhaps heterogeneous nucleation might play an important role (Lintunen et al., 2013)? Further, there might be structural and chemical properties of pit membranes preventing gas penetration (Herbette and Cochard, 2010; Jansen et al., 2009) and it is important to elucidate and quantify the basic underlying tradeoffs between safety (from cavitation) and efficiency (for water transport). Such tradeoffs could exist at the level of individual pits, whole conduits and entire networks and are thought to underlie the diversity in xylem structure and function across plant species and lineages (Lens et al., 2011, 2013; Tyree and Zimmermann, 2002).

It is still unknown whether cavitation/embolization is a reversible phenomenon. Can embolized conduits be returned to a functional state or must they be replaced (Zwieniecki and Holbrook, 2009)? If they can be "repaired," what is the mechanism, how rapidly can this occur (time-scale), and with what physiological constraints (e.g., xylem tensions)? Further, we may ask how plants control the development of xylem tensions so as to avoid cavitation. Here stomata are clearly the key players, although buffering of xylem tensions by water drawn from nearby tissues may also play an important role (Holbrook et al., 1995; Meinzer et al., 2009). The central question is what information, both physical and biochemical, allows stomata to respond to current supply and demand so as to prevent xylem tensions from reaching dangerous levels (Tyree and Sperry, 1989)?

In our view it remains an open question whether the tensions in the leaves are actually, as written in the textbooks, capillary in origin. We did, however, provide some new evidence (shown in Fig. 17) that changes in capillarity can strongly influence the ability of the minor veins in a leaf to transport water. In any case, it is believed that the cell walls of the mesophyll play a major role in these processes and thus that the key to the resolution of these questions lies in the detailed understanding of the structure of plant cell walls. The swelling of cell walls is also the basis for plant growth, and in this context the specific roles and detailed dynamics of two of the most important polysaccharides, pectin and hemicellulose, have been under intense scrutiny (see e.g., (Cosgrove, 2014; Peaucelle et al., 2011)). The implications for water transport are

not clear at present, but the interplay between growth and water flow seems an important issue for future studies.

So, from the point of view of a physicist, plants remain full of mysteries.

ACKNOWLEDGMENTS

LIST OF SYMBOLS

Symbol	SI unit	Description
a	m	conduit radius, pore radius
a^*	m	optimal conduit radius
A	m^2	area
c	M	concentration
d	m	vein spacing; pore length
D	$m^2\,s^{-1}$	diffusion coefficient
$\bar{D}$	1	dimensionless diffusivity
e	Pa	partial pressure of water vapor in air
e_0	Pa	saturated vapor pressure in air
E	$J\,m^{-2}s^{-1}$	Energy flux
E	Pa	Youngs modulus
g	$m\,s^{-2}$	acceleration of gravity
J	$M\,m\,s^{-1}$	current density/flux
k	m^2	Darcy constant
l	m	length
l_2, h	m	stem length
ℓ_p	m	distance between pores (in a sieve plate)
L	m	characteristic width of the conduit, vein length
L_p	$mPa^{-1}s^{-1}$	membrane permeability
l_p	m^3s^{-1}	permeability for single aquaporin
m_i	kg	mass of liquid molecule i
Mü	1	Münch number
N	1	number of conduits
p	Pa	pressure
Pé	1	Péclet number
Q	m^3s^{-1}	volumetric flow rate
q	m^2s^{-1}	volumetric flow rate per unit length
q	$m\,s^{-1}$	volumetric flux per surface area
r	m	radial coordinate
R	$Pa\,s\,m^{-3}$	hydraulic resistance, gas constant
Re	1	Reynolds number
Sc	1	Schmidt number
t_{diff}	s	diffusion time
t_{adv}	s	advection time
T	K	temperature
u	$m\,s^{-1}$	axial flow speed
u^*	$m\,s^{-1}$	axial flow speed at optimal conditions according to hydraulic resistor theory
U	$m\,s^{-1}$	characteristic flow speed
$\mathbf{v}_i$	$m\,s^{-1}$	velocity of a liquid molecule i
$\mathbf{v}(\mathbf{r}, t)$	$m\,s^{-1}$	velocity field in liquid, at position $\mathbf{r}$ at time t, i.e., momentum per mass in the volume
$\bar{v}$	$m\,s^{-1}$	flow speed averaged over the cross section
v_x, v_y, v_z	$m\,s^{-1}$	velocity along the cartesian coordinates
V	m	characteristic length scale
ΔV	m^3	Volume of liquid particle region
V_w	m^3	molar volume of water
W	m	leaf section width
W	1	advective hindrance factor
x, y, z	m	cartesian coordinates
γ	1	flow amplification factor
γ	$J\,m^{-2}$	surface tension
δ	1	leaf thickness
η	Pa s	viscosity
ν	$m^2\,s^{-1}$	kinematic viscosity
ρ	$kg\,m^{-3}$	density
ρ_{cw}	$kg\,m^{-3}$	density of the cell wall material
τ	1	non-dimensional time
μ	J	chemical potential
μ_0	J	reference chemical potential of water
σ	1	reflection coefficient
σ	Pa	compressive strength
$\Omega(\mathbf{r})$	–	Liquid particle region at $\mathbf{r}$
ϕ	1	covering fraction of pores
Π	Pa	osmotic pressure
Ψ	Pa	water potential

REFERENCES

Alberts, Bruce, Dennis Bray, Karen Hopkin, Alexander D Johnson, Julian Lewis, Martin Raff, Keith Roberts, and Peter Walter (2014), *Essential Cell Biology*, New York (Garland Science).

Aldis, Geoffrey K (1988a), "The osmotic permeability of a tubule wall," Bulletin of Mathematical Biology **50**, 547–558.

Aldis, Geoffrey K (1988b), "The unstirred layer during osmotic flow into a tubule," Bulletin of Mathematical Biology **50**, 531–545.

Ali, Zubaidah Mohammed, and Lorna J Gibson (2013), "The structure and mechanics of nanofibrillar cellulose foams," Soft Matter **9**, 1580.

Aloni, R, and W. P. Jacobs (1977), "Time course of sieve tube and vessel regeneration and their relation to phloem anastomoses in mature internodes of Coleus," American Journal of Botany **64** (6), 615–621.

Anstead, James A, Steven D Hartson, and Gary A Thompson (2013), "The broccoli (*Brassica oleracea*) phloem tissue proteome," BMC genomics **14** (1), 764.

Ayre, Brian G (2011), "Membrane-transport systems for sucrose in relation to whole-plant carbon partitioning," Molecular Plant **4** (3), 377–394.

Azouzi, Mouna El Mekki, Claire Ramboz, Jean-François Lenain, and Frédéric Caupin (2013), "A coherent picture of water at extreme negative pressure," Nature Physics **9** (1), 38–41.

Ball, Marilyn C (1988), "Ecophysiology of mangroves," Trees **2** (3), 129–142.

Baluška, František, Fatima Cvrčková, John Kendrick-Jones, and Dieter Volkmann (2001), "Sink plasmodesmata as gateways for phloem unloading. Myosin VIII and calreticulin as molecular determinants of sink strength?" Plant Physiology **126** (1), 39–46.

Barratt, DH Paul, Katharina Kölling, Alexander Graf, Marilyn Pike, Grant Calder, Kim Findlay, Samuel C Zeeman, and Alison M Smith (2011), "Callose synthase GSL7 is necessary for normal phloem transport and inflorescence growth in Arabidopsis," Plant Physiology **155** (1), 328–341.

Batashev, D R, M. V. Pakhomova, A. V. Razumovskaya, O. V. Voitsekhovskaja, and Y. V. Gamalei (2013), "Cytol-

ogy of the minor-vein phloem in 320 species from the sub-class asteridae suggests a high diversity of phloem-loading modes," Frontiers in Plant Science **4**, 312.

Bauch, J, W. Liese, and R. Schultze (1972), "The morphological variability of the bordered pit membranes in gymnosperms," Wood Science and Technology **6** (3), 165–184.

Behnke, H D, and eds. Sjolund, R. D. (1990), *Sieve Elements - Comparative Structure, Induciton and Development* (Springer Berlin Heidelberg).

van Bel, Aart JE (1996), "Interaction between sieve element and companion cell and the consequences for photoassimilate distribution. two structural hardware frames with associated physiological software packages in dicotyledons?" Journal of Experimental Botany **47** (Special Issue), 1129–1140.

van Bel, AartJ E, Ankie Ammerlaan, and AnthonieA van Dijk (1993), "A three-step screening procedure to identify the mode of phloem loading in intact leaves," Planta **192** (1), 31–39.

Berthier, Jean, and Pascal Silberzan (2010), *Microfluidics for Biotechnology*, 2nd ed. (Artech House, Norwood MA).

Birchard, Geoffrey F (1997), "Optimal hematocrit: theory, regulation and implications," American Zoologist **37** (1), 65–72.

Bird, R B, R. C. Amstrong, and O. Hassager (1987), *Dynamics of polymeric liquids*, 2nd ed., Vol. 1 (John Wiley and Sons, New York).

Bohn, S, B. Andreotti, S. Douady, J. Munzinger, and Y. Couder (2002), "Constitutive property of the local organization of leaf venation networks," Physical Review E **65**, 061914.

Boyer, J S (1985), "Water transport," Annual Review of Plant Physiology **36**, 473–516.

Boyer, John S, and Edward B. Knipling (1965), "Isopiestic technique for measuring leaf water potentials with a thermocouple psychrometer," Proceedings of the National Academy of Sciences of the United States of America , 1044–1051.

Boyer, JS (1995), *Measuring the water status of plants and soils* (Academic Press).

Brenner, Michael P (2014), "Fluid mechanical responses to nutrient depletion in fungi and biofilms," Physics of Fluids **26** (10), 101306.

Brodersen, Craig R, and Andrew J McElrone (2013), "Maintenance of xylem network transport capacity: a review of embolism repair in vascular plants," Frontiers in Plant Science **4**, 108.

Brodersen, Craig R, Andrew J McElrone, Brendan Choat, Mark A Matthews, and Kenneth A Shackel (2010), "The dynamics of embolism repair in xylem: in vivo visualizations using high-resolution computed tomography," Plant Physiology **154** (3), 1088–1095.

Brodersen, Craig Robert, Andrew Joseph McElrone, Brendan Choat, Eric Franklin Lee, Kenneth Andrew Shackel, and Mark Allen Matthews (2013), "In vivo visualizations of drought-induced embolism spread in *Vitis vinifera*," Plant Physiology **161** (4), 1820–1829.

Brown, Harvey R (2013), "The theory of the rise of sap in trees: Some historical and conceptual remarks," Physics in Perspective **15** (3), 320–358.

Bruus, H (2011), "Acoustofluidics 1: Governing equations in microfluidics," Lab Chip **11**, 3742 – 3751.

Bruus, Henrik (2008), *Theoretical Microfluidics* (Oxford University Press, Oxford).

Byott, GS (1976), "Leaf air space systems in C_3 and C_4 species," New Phytologist **76** (2), 295–299.

Canny, M J (1993), "Transfusion tissue of pine needles as a site of retrieval of solutes from the transpiration stream," New Phytologist **123** (2), 227–232.

Canny, Martin Joseph Patrick (1973), *Phloem translocation* (Cambridge University Press, Cambridge).

Capron, M, Ph. Tordjeman, F. Charru, E. Badel, and H. Cochard (2014), "Gas flow in plant microfluidic networks controlled by capillary valves," Phys. Rev. E **89**, 033019.

Carlquist, Sherwin (2001), *Comparative Wood Anatomy: Systematic, Ecological, and Evolutionary Aspects of Dicotyledon Wood* (Springer, Berlin, Heidelberg).

Carlquist, Sherwin (2012), "How wood evolves: A new synthesis," Botany **90**, 901–940.

Čermák, J, J Kučera, and N Nadezhdina (2004), "Sap flow measurements with some thermodynamic methods, flow integration within trees and scaling up from sample trees to entire forest stands," Trees **18** (5), 529–546.

Charnov, Eric L (1976), "Optimal foraging, the marginal value theorem," Theoretical Population Biology **9** (2), 129 – 136.

Choat, Brendan, Tyler W Brodie, Alexander R Cobb, Maciej A Zwieniecki, and N Michele Holbrook (2006), "Direct measurements of intervessel pit membrane hydraulic resistance in two angiosperm tree species," American Journal of Botany **93** (7), 993–1000.

Choat, Brendan, Alexander R Cobb, and Steven Jansen (2008), "Structure and function of bordered pits: new discoveries and impacts on whole-plant hydraulic function," New Phytologist **177** (3), 608–626.

Choat, Brendan, Steven Jansen, Maciej A Zwieniecki, Erik Smets, and N Michele Holbrook (2004), "Changes in pit membrane porosity due to deflection and stretching: the role of vestured pits," Journal of Experimental Botany **55** (402), 1569–1575.

Christman, Mairgareth A, and John S Sperry (2010), "Single-vessel flow measurements indicate scalariform perforation plates confer higher flow resistance than previously estimated," Plant, Cell & Environment **33** (3), 431–443.

Christy, A L, and D. B. Fisher (1978), "Kinetics of ^{14}C-photosynthate translocation in morning glory vines," Plant Physiology **61** (2), 283–90.

Christy, A Lawrence, and Jack M Ferrier (1973), "A mathematical treatment of Münch's pressure-flow hypothesis of phloem translocation," Plant Physiology **52** (6), 531–538.

Cochard, H, FW Ewers, and MT Tyree (1994), "Water relations of a tropical vine-like bamboo (*Rhipidocladum racemiflorum*): root pressures, vulnerability to cavitation and seasonal changes in embolism," Journal of Experimental Botany **45** (8), 1085–1089.

Cochard, Hervé, Eric Badel, Stéphane Herbette, Sylvain Delzon, Brendan Choat, and Steven Jansen (2013), "Methods for measuring plant vulnerability to cavitation: a critical review," Journal of Experimental Botany **64** (15), 4779–4791.

Core, H A, Wilfred A. Coté, and Day A. C. (1979), *Wood structure and identification* (Syracuse University Press).

Cosgrove, D (2014), "Re-constructing our models of cellulose and primarycell wall assembly," Current Opinion in Plant Biology **22**, 122–131.

Couder, Y, L Pauchard, C Allain, M Adda-Bedia, and S Douady (2002), "The leaf venation as formed in a tenso-

rial field," European Physical Journal B **28** (2), 135–138.

la Cour Petersen, M, J. Hejgaard, G. A. Thompson, and A. Schulz (2005), "Cucurbit phloem serpins are graft-transmissible and appear to be resistant to turnover in the sieve element-companion cell complex," Journal of Experimental Botany **56** (422), 3111–3120.

Couturier, Etienne, Nicole Brunel, Stephane Douady, and Naomi Nakayama (2012), "Abaxial growth and steric constraints guide leaf folding and shape in *Acer pseudoplatanus*," American Journal of Botany **99** (8), 1289–1299.

Couturier, Etienne, Sylvain Courrech du Pont, and Stephane Douady (2009), "A global regulation inducing the shape of growing folded leaves," PLoS ONE **4** (11), 10.1371/journal.pone.0007968.

Crafts, Alden Springer, and Carl E Crisp (1971), *Phloem Transport in Plants* (W. H. Freeman & Co, San Francisco, USA).

Dagan, Zeev, Sheldon Weinbaum, and Robert Pfeffer (1982), "Infinite-series solution for the creeping motion through an orifice of finite length." Journal of Fluid Mechanics **115**, 505–523.

Dainty, J (1963), "The polar permeability of plant cell membranes to water," Protoplasma **57** (1), 220–228.

Dannoura, Masako, Pascale Maillard, Chantal Fresneau, Caroline Plain, Daniel Berveiller, Dominique Gerant, Christophe Chipeaux, Alexandre Bosc, Jérôme Ngao, Claire Damesin, *et al.* (2011), "In situ assessment of the velocity of carbon transfer by tracing ^{13}c in trunk co$_2$ efflux after pulse labelling: variations among tree species and seasons," New Phytologist **190** (1), 181–192.

Dasgupta, Kasturi, Aswad S Khadilkar, Ronan Sulpice, Bikram Pant, Wolf-Rüdiger Scheible, Joachim Fisahn, Mark Stitt, and Brian G Ayre (2014), "Expression of sucrose transporter cDNAs specifically in companion cells enhances phloem loading and long-distance transport of sucrose but leads to an inhibition of growth and the perception of a phosphate limitation," Plant Physiology **165** (2), 715–731.

Daudet, FA, A Lacointe, JP Gaudillere, and P Cruiziat (2002), "Generalized Münch coupling between sugar and water fluxes for modelling carbon allocation as affected by water status," Journal of Theoretical Biology **214** (3), 481–498.

Davidson, A, F. Keller, and R. Turgeon (2011), "Phloem loading, plant growth form, and climate," Protoplasma **248** (1), 153–163.

De Schepper, Veerle, Tom De Swaef, Ingvar Bauweraerts, and Kathy Steppe (2013), "Phloem transport: a review of mechanisms and controls," Journal of Experimental Botany **64** (16), 4839–4850.

Debenedetti, G (1996), *Metastable Liquids: Concepts and Principles* (Princeton University Press, Princeton, NJ).

Dechadilok, Panadda, and William M. Deen (2006), "Hindrance factors for diffusion and convection in pores," Industrial And Engineering Chemistry Research **45** (21), 6953–6959.

Delzon, Sylvain, Cyril Douthe, Anna Sala, and Herve Cochard (2010), "Mechanism of water-stress induced cavitation in conifers: bordered pit structure and function support the hypothesis of seal capillary-seeding," Plant, Cell & Environment **33** (12), 2101–2111.

Dixon, Henry H, and Nigel G Ball (1922), "Transport of organic substances in plants." Nature **109**, 236–237.

Dixon, Henry H, and John Joly (1895), "On the ascent of

sap," Philosophical Transactions of the Royal Society of London. B , 563–576.

Doering-Saad, C, HJ Newbury, CE Couldridge, JS Bale, and J Pritchard (2006), "A phloem-enriched cDNA library from Ricinus: insights into phloem function," Journal of Experimental Botany **57** (12), 3183–3193.

Dölger, Julia, Hanna Rademaker, Johannes Liesche, Alexander Schulz, and Tomas Bohr (2014), "Diffusion and bulk flow in phloem loading: A theoretical analysis of the polymer trap mechanism for sugar transport in plants," Physical Review E **90** (4), 042704.

Dumais, Jacques, and Yoel Forterre (2012), "Vegetable dynamicks: The role of water in plant movements," Annual Review of Fluid Mechanics **44** (1), 453–478.

Durand, M (2006), "Architecture of optimal transport networks," Physical Review E **73**, 10.1103/PhysRevE.73.016116.

Easterling, KE, Harrysson R, Gibson LJ, and Ashby MF (1982), "On the mechanics of balsa and other woods," Proceedings of the Royal Society London A **383**, 31–41.

Ehlers, K, M. Knoblauch, and A. J. E. van Bel (2000), "Ultrastructural features of well-preserved and injured sieve elements: minute clamps keep the phloem transport conduits free for mass flow," Protoplasma **214** (1-2), 80–92.

Epron, Daniel, Michael Bahn, Delphine Derrien, Fernando Alfredo Lattanzi, Jukka Pumpanen, Arthur Gessler, Peter Högberg, Pascale Maillard, Masako Dannoura, Dominique Gérant, *et al.* (2012), "Pulse-labelling trees to study carbon allocation dynamics: a review of methods, current knowledge and future prospects," Tree Physiology **32** (6), 776–798.

Esau, K (1969), *The Phloem* (Gebr. Borntraeger, Stuttgart).

Eschrich, W (1975), "Sealing systems in phloem," in *Transport in Plants I* (Springer) pp. 39–56.

Eschrich, Walter, Ray F. Evert, and John H. Young (1972), "Solution flow in tubular semipermeable membranes," Planta **107** (4), 279–300.

Evert, Ray F (2006), "Esau's plant anatomy," in *Esau's Plant Anatomy* (John Wiley & Sons, Inc.) pp. 1–601.

Ewers, Frank W, Herve Cochard, and Melvin T Tyree (1997), "A survey of root pressures in vines of a tropical lowland forest," Oecologia **110** (2), 191–196.

Fellows, Robert J, and Donald R Geiger (1974), "Structural and physiological changes in sugar beet leaves during sink to source conversion," Plant Physiology **54** (6), 877–885.

Ferrier, JM, MT Tyree, and AL Christy (1975), "Theoretical time-dependent behavior of a Münch presure-flow system: the effect of sinusoidal time variation in sucrose loading and water potential," Canadian Journal of Botany.

Fisher, Donald B, and Cora E Cash-Clark (2000), "Sieve tube unloading and post-phloem transport of fluorescent tracers and proteins injected into sieve tubes via severed aphid stylets," Plant Physiology **123** (1), 125–138.

Fisher, Donald B, and John M Frame (1984), "A guide to the use of the exuding-stylet technique in phloem physiology," Planta **161** (5), 385–393.

Fisher, Donald B, and Roger M Gifford (1986), "Accumulation and conversion of sugars by developing wheat grains vi. gradients along the transport pathway from the peduncle to the endosperm cavity during grain filling," Plant Physiology **82** (4), 1024–1030.

Ford, Chelcy R, Mary Anne McGuire, Robert J Mitchell, and Robert O Teskey (2004), "Assessing variation in the radial profile of sap flux density in pinus species and its effect on

daily water use," Tree Physiology **24** (3), 241–249.

Franks, Peter J, and David J. Beerling (2009), "Maximum leaf conductance driven by CO2 effects on stomatal size and density over geologic time," Proceedings of the National Academy of Sciences **106** (25), 10343–10347.

Frisch, H L (1976), "Osmotically driven flows in narrow channels," Transactions of the Society of Rheology **20** (1), 23–27.

Fritz, E, and W. Eschrich (1970), "C-14-microautoradiography of water-soluble substances in phloem," Planta **92** (3), 267–281.

Froelich, Daniel R, Daniel L Mullendore, Kåre H Jensen, Tim J Ross-Elliott, James A Anstead, Gary A Thompson, Hélène C Pélissier, and Michael Knoblauch (2011), "Phloem ultrastructure and pressure flow: sieve-element-occlusion-related agglomerations do not affect translocation," The Plant Cell **23** (12), 4428–4445.

Fu, Q S, L. L. Cheng, Y. D. Guo, and R. Turgeon (2011), "Phloem loading strategies and water relations in trees and herbaceous plants," Plant Physiology **157** (3), 1518–1527.

Furch, Alexandra C U, Jens B. Hafke, Alexander Schulz, and Aart J. E. van Bel (2007), "Ca^{2+}-mediated remote control of reversible sieve tube occlusion in vicia faba," Journal of Experimental Botany **58** (11), 2827–2838.

Furch, Alexandra CU, Aart JE van Bel, and Torsten Will (2015), "Aphid salivary proteases are capable of degrading sieve-tube proteins," Journal of Experimental Botany **66** (2), 533–539.

Gahrtz, Manfred, Jürgen Stolz, and Norbert Sauer (1994), "A phloem-specific sucrose-H^+ symporter from *Plantago major* L. supports the model of apoplastic phloem loading," The Plant Journal **6** (5), 697–706.

Gamalei, Y (1989), "Structure and function of leaf minor veins in trees and herbs a taxonomic review," Trees-Structure and Function **3** (2), 96–110.

Gaupels, F, and A. Ghirardo (2013), "The extrafascicular phloem is made for fighting," Frontiers in Plant Science **4**, 187.

Geiger, D R (1975), "Phloem loading and associated processes," in *Phloem Transport*, edited by M. H. Zimmermann and J. A. Milburn (Springer-Verlag, New York) pp. 395–431.

Geiger, D R, Giaquint.Rt, S. A. Sovonick, and R. J. Fellows (1973), "Solute distribution in sugar-beet leaves in relation to phloem loading and translocation," Plant Physiology **52** (6), 585–589.

Giaquinta, R (1980), "Mechanism and control of phloem loading of sucrose," Berichte Der Deutschen Botanischen Gesellschaft **93** (1), 187–201.

Gibson, Lorna J (2012), "The hierarchical structure and mechanics of plant materials," Journal of The Royal Society Interface 10.1098/rsif.2012.0341.

Goeschl, J D, C. E. Magnuson, D. W. DeMichele, and P. J. H. Sharpe (1976), "Concentration-dependent unloading as a necessary assumption for a closed form mathematical model of osmotically driven pressure flow in phloem." Plant Physiology **58**, 556–562.

Gottwald, J R, P. J. Krysan, J. C. Young, R. F. Evert, and M. R. Sussman (2000), "Genetic evidence for the in planta role of phloem-specific plasma membrane sucrose transporters," Proceedings of the National Academy of Sciences of the United States of America **97** (25), 13979–13984.

Gould, N, M. R. Thorpe, J. Pritchard, J. T. Christeller, L.E. Williams, G. Roeb, U. Schurr, and P. E. H. Minchin (2012),

"*AtSUC2* has a role for sucrose retrieval along the phloem pathway: Evidence from carbon-11 tracer studies," Plant Science **188**, 97–101.

Gould, Nick, Peter E. H. Minchin, and Michael R. Thorpe (2004), "Direct measurements of sieve element hydrostatic pressure reveal strong regulation after pathway blockage," Functional Plant Biology **31** (10), 987–993.

Gould, Nick, Michael R. Thorpe, Olga Koroleva, and Peter E.H. Minchin (2005), "Phloem hydrostatic pressure relates to solute loading rate: a direct test of the Münch hypothesis," Functional Plant Biology **32** (11), 1019–1026.

Granier, A (1987), "Evaluation of transpiration in a douglas-fir stand by means of sap flow measurements," Tree Physiology **3** (4), 309–320.

Granier, A, P Biron, N Bréda, J-Y Pontailler, and B Saugier (1996), "Transpiration of trees and forest stands: short and long-term monitoring using sapflow methods," Global Change Biology **2** (3), 265–274.

Gurbatov, S N, A. N. Malakhov, and A. I. Saichev (1991), *Nonlinear Random Waves and Turbulence in Nondispersive Media: Waves, Rays, Particles* (Manchester University Press).

Haaning, Louise Sejling, Kaare Hartvig Jensen, Claus Hlix-Nielsen, Kirstine Berg-Srensen, and Tomas Bohr (2013), "Efficiency of osmotic pipe flows," Physical Review E **87** (5), 10.1103/PhysRevE.87.053019.

Hall, A J, and P. E. H. Minchin (2013), "A closed-form solution for steady-state coupled phloem/xylem flow using the Lambert-W function: Coupled phloem/xylem flow," Plant, Cell & Environment **36** (12), 2150–2162.

Hall, Shelagh M, and DA Baker (1972), "The chemical composition of Ricinus phloem exudate," Planta **106** (2), 131–140.

Hammel, HT (1968), "Measurement of turgor pressure and its gradient in the phloem of oak," Plant Physiology **43** (7), 1042–1048.

Hansen, Jesper S, Jeppe C. Dyre, Peter Daivis, Billy D. Todd, and Henrik Bruus (2015), "Continuum nanofluidics," Langmuir **31**, 13275–13289.

Haritatos, E, B. G. Ayre, and R. Turgeon (2000), "Identification of phloem involved in assimilate loading in leaves by the activity of the galactinol synthase promoter," Plant Physiology **123** (3), 929–937.

Haritatos, Edith, Felix Keller, and Robert Turgeon (1996), "Raffinose oligosaccharide concentrations measured in individual cell and tissue types in *Cucumis melo* L leaves: implications for phloem loading," Planta **198** (4), 614–622.

Hartig, Th (1860), "Beitrage zur physiologischen forstbotanik," Forst und Jagdzeitung **36**, 257–263.

Hartt, Constance E, Hugo P Kortschak, *et al.* (1963), "Tracing sugar in the cane plant." in *Proceedings of the International Society of Sugarcane Technologists; 11th Congress, Mauritius, 1962*, pp. 323–34.

Haynes, W M, Ed. (2012), *CRC Handbook of Chemistry and Physics*, 93rd ed. (CRC Press, Boca Raton, FL).

van Helden, Maarten, W Freddy Tjallingh, and Teris A van Beek (1994), "Phloem sap collection from lettuce (*Lactuca sativa* L.): chemical comparison among collection methods," Journal of chemical ecology **20** (12), 3191–3206.

Hendrix, John E (1968), "Labeling pattern of translocated stachyose in squash," Plant Physiology **43** (10), 1631–1636.

Henton, SM, AJ Greaves, GJ Piller, and PEH Minchin (2002), "Revisiting the Münch pressure–flow hypothesis for long-distance transport of carbohydrates: modelling the

dynamics of solute transport inside a semipermeable tube," Journal of Experimental Botany **53** (373), 1411–1419.

Hepler, Peter K (2005), "Calcium: a central regulator of plant growth and development," The Plant Cell **17** (8), 2142–2155.

Herbert, Eric, and Frédéric Caupin (2005), "The limit of metastability of water under tension: theories and experiments," Journal of Physics: Condensed Matter **17** (45), S3597.

Herbette, S, and H Cochard (2010), "Calcium is a major determinant of xylem vulnerability to cavitation," Plant Physiology **153**, 1932–1939.

Hillel, Daniel (1998), *Environmental Soil Physics* (Academic Press, San Diego, CA).

Ho, LC, RI Grange, and AF Shaw (1989), "Source/sink regulation," Transport of photoassimilates , 306–343.

Hocking, PJ (1980), "The composition of phloem exudate and xylem sap from tree tobacco (*Nicotiana glauca* Graham)," Annals of Botany **45** (6), 633–643.

Hogg, Edward H, T Andrew Black, Gerry den Hartog, Harold H Neumann, Reiner Zimmermann, Patrick A Hurdle, Peter D Blanken, Zoran Nesic, Paul C Yang, Ralf M Staebler, *et al.* (1997), "A comparison of sap flow and eddy fluxes of water vapor from a boreal deciduous forest," Journal of Geophysical Research: Atmospheres (1984–2012) **102** (D24), 28929–28937.

Holbrook, N Michele, Michael J. Burns, and Christopher B. Field (1995), "Negative xylem pressures in plants: A test of the balancing pressure technique," Science **270** (5239), 1193–1194.

Holbrook, N Michele, and Maciej A Zwieniecki (2008), "Transporting water to the tops of trees," Physics Today **61** (1), 76.

Holbrook, N Michelle, and Maciej A. Zwieniecki, Eds. (2005), *Vascular Transport in Plants*, 1st ed. (Academic Press, Boston, MA).

Holthaus, U, and K. Schmitz (1991), "Distribution and Immunolocalization of Stachyose Synthase in *Cucumis melo* L." Planta **185** (4), 479–486.

Holtta, T, T. Vesala, S. Sevanto, M. Peramaki, and E. Nikinmaa (2006), "Modeling xylem and phloem water flows in trees according to cohesion theory and Münch hypothesis," Trees **20** (1), 67–78.

Hong, Wei, Xuanhe Zhao, and Zhigang Suo (2010), "Large deformation and electrochemistry of polyelectrolyte gels," Journal of the Mechanics and Physics of Solids **58** (4), 558–577.

Hong, Wei, Xuanhe Zhao, Jinxiong Zhou, and Zhigang Suo (2008), "A theory of coupled diffusion and large deformation in polymeric gels," Journal of the Mechanics and Physics of Solids **56** (5), 1779–1793.

Horwitz, Leonard (1958), "Some simplified mathematical treatments of translocation in plants." Plant Physiology **33** (2), 81.

Jackson, GE, and J Grace (1996), "Field measurements of xylem cavitation: are acoustic emissions useful?" Journal of Experimental Botany **47** (11), 1643–1650.

Jansen, Steven, Pieter Baas, Peter Gasson, Frederic Lens, and Erik Smets (2004), "Variation in xylem structure from tropics to tundra: evidence from vestured pits," Proceedings of the National Academy of Sciences of the United States of America **101** (23), 8833–8837.

Jansen, Steven, Brendan Choat, and Annelies Pletsers (2009), "Morphological variation of intervessel pit membranes and implications to xylem function in angiosperms," American Journal of Botany **96** (2), 409–419.

Jansen, Steven, Bernhard Schuldt, and Brendan Choat (2015), "Current controversies and challenges in applying plant hydraulic techniques," New Phytologist **205** (3), 961–964.

Jarvis, Paul Gordon, and KG McNaughton (1986), "Stomatal control of transpiration: scaling up from leaf to region," Advances in ecological research **15**, 1–49.

Jensen, K H, T. Bohr, and H. Bruus (2010), "Self-consistent unstirred layers in osmotically driven flows," Journal of Fluid Mechanics **662**, 197–208.

Jensen, K H, W. Kim, N. M. Holbrook, and J. W. M. Bush (2013a), "Optimal concentrations in transport systems," Journal of The Royal Society Interface **10** (83), 20130138–20130138.

Jensen, K H, J. Lee, T. Bohr, and H. Bruus (2009a), "Osmotically driven flows in microchannels separated by a semipermeable membrane," Lab on a Chip **9** (14), 2093.

Jensen, K H, J. Lee, T. Bohr, H. Bruus, N. M. Holbrook, and M. A. Zwieniecki (2011), "Optimality of the Münch mechanism for translocation of sugars in plants," Journal of The Royal Society Interface **8** (61), 1155–1165.

Jensen, K H, E. Rio, R. Hansen, C. Clanet, and T. Bohr (2009b), "Osmotically driven pipe flows and their relation to sugar transport in plants," Journal of Fluid Mechanics **636**, 371.

Jensen, K H, A. X. C. N. Valente, and H. A. Stone (2014), "Flow rate through microfilters: Influence of the pore size distribution, hydrodynamic interactions, wall slip, and inertia," Physics of Fluids **26** (5), 052004.

Jensen, Kaare H, Kirstine Berg-Sørensen, Søren M.M. Friis, and Tomas Bohr (2012a), "Analytic solutions and universal properties of sugar loading models in münch phloem flow," Journal of Theoretical Biology **304**, 286–296.

Jensen, Kaare H, Johannes Liesche, Tomas Bohr, and Alexander Schulz (2012b), "Universality of phloem transport in seed plants," Plant, Cell and Environment **35**, 1065–1076.

Jensen, Kaare H, Jessica A. Savage, and N. Michele Holbrook (2013b), "Optimal concentration for sugar transport in plants," Journal of The Royal Society Interface **10** (83), 10.1098/rsif.2013.0055.

Jensen, Kaare H, and Maciej A. Zwieniecki (2013), "Physical limits to leaf size in tall trees," Physical Review Letters **110** (1), 10.1103/PhysRevLett.110.018104.

Jensen, Kaare Hartvig, Daniel Leroy Mullendore, Noel Michele Holbrook, Tomas Bohr, Michael Knoblauch, and Henrik Bruus (2012c), "Modeling the Hydrodynamics of Phloem Sieve Plates," Frontiers in Plant Science **3**, 10.3389/fpls.2012.00151.

Karam, G N (2005), "Biomechanical model of the xylem vessels in vascular plants," Annals of Botany **95** (7), 1179–1186.

Kargol, M, and A Kargol (2003), "Mechanistic equations for membrane substance transport and their identity with Kedem-Katchalsky equations," Biophysical Chemistry **103** (2), 117–127.

Katifori, Eleni, and Marcelo O. Magnasco (2012), "Quantifying Loopy Network Architectures," PLoS ONE **7** (6), 10.1371/journal.pone.0037994.

Katifori, Eleni, Gergely J. Szollosi, and Marcelo O. Magnasco (2010), "Damage and Fluctuations Induce Loops in Optimal Transport Networks," Physical Review Letters **104** (4),

10.1103/PhysRevLett.104.048704.

Kedem, O, and A. Katchalsky (1958), "Thermodynamic analysis of the permeability of biological membranes to non-electrolytes," BBA - Biochimica Et Biophysica Acta **27**, 229–246.

Kempers, Ronald, Ankie Ammerlaan, and Aart J. E. van Bel (1998), "Symplasmic constriction and ultrastructural features of the sieve element/companion cell complex in the transport phloem of apoplasmically and symplasmically phloem-loading species," Plant Physiology **116** (1), 271–278.

Kennedy, JS, and TE Mittler (1953), "A method of obtaining phloem sap via the mouth-parts of aphids," Nature **171**, 528.

Khan, Junaid A, Qi Wang, Richard D Sjölund, Alexander Schulz, and Gary A Thompson (2007), "An early nodulin-like protein accumulates in the sieve element plasma membrane of arabidopsis," Plant Physiology **143** (4), 1576–1589.

Kikuta, SB, and H Richter (2003), "Ultrasound acoustic emissions from freezing xylem," Plant, Cell & Environment **26** (3), 383–388.

Kim, Wonjung, and John W. M. Bush (2012), "Natural drinking strategies," Journal of Fluid Mechanics **705**, 7–25.

Kim, Wonjung, Tristan Gilet, and John WM Bush (2011), "Optimal concentrations in nectar feeding," Proceedings of the National Academy of Sciences **108** (40), 16618–16621.

King, R W, and J. A. D. Zeevaart (1974), "Enhancement of phloem exudation from cut petioles by chelating agents," Plant Physiology **53** (1), 96–103.

Kirby, Brian (2010), *Micro- and Nanoscale Fluid Mechanics: Transport in Microfluidic Devices* (Cambridge University Press, New York).

Knoblauch, Jan, Daniel L Mullendore, Kaare H Jensen, and Michael Knoblauch (2014), "Pico gauges for minimally invasive intracellular hydrostatic pressure measurements," Plant Physiology **166** (3), 1271–1279.

Knoblauch, M, and W. S. Peters (2004), "Forisomes, a novel type of ca^{2+}-dependent contractile protein motor," Cell Motility and the Cytoskeleton **58** (3), 137–142.

Knoblauch, M, M. Stubenrauch, A. J. E. Van Bel, and W. S. Peters (2012), "Forisome performance in artificial sieve tubes," Plant Cell and Environment **35** (8), 1419–1427.

Knoblauch, Michael, and Aart J. E. van Bel (1998), "Sieve tubes in action," The Plant Cell **10** (1), 35–50.

Knoblauch, Michael, and Winfried S. Peters (2010), "Münch, morphology, microfluidics - our structural problem with the phloem," Plant, Cell & Environment **33**, 1439–1452.

Knoblauch, Michael, Winfried S Peters, Katrin Ehlers, and Aart JE van Bel (2001), "Reversible calcium-regulated stopcocks in legume sieve tubes," The Plant Cell **13** (5), 1221–1230.

Köckenberger, W, JM Pope, Y Xia, KR Jeffrey, E Komor, and PT Callaghan (1997), "A non-invasive measurement of phloem and xylem water flow in castor bean seedlings by nuclear magnetic resonance microimaging," Planta **201** (1), 53–63.

Kohonen, Mika M (2006), "Engineered wettability in tree capillaries," Langmuir **22**, 3148–3153.

Komor, E (1977), "Sucrose Uptake by Cotyledons of *Ricinus communis* L - Characteristics, Mechanism, and Regulation," Planta **137** (2), 119–131.

Kramer, Paul J, and John S. Boyer (1995), *Water Relations of Plants and Soils* (Academic Press, San Diego).

Kühn, C, VR Franceschi, A Schulz, R Lemoine, and WB Frommer (1997), "Macromolecular trafficking indicated by localization and turnover of sucrose transporters in enucleate sieve elements," Science **275** (5304), 1298–1300.

Kühn, C, WP Quick, A Schulz, JW Riesmeier, U Sonnewald, and WB Frommer (1996), "Companion cell-specific inhibition of the potato sucrose transporter SUT1," Plant, Cell & Environment **19** (10), 1115–1123.

Kühn, Christina, and Christopher PL Grof (2010), "Sucrose transporters of higher plants," Current opinion in plant biology **13** (3), 287–297.

Kursanov, AL (1956), "Analysis of the movement of substances in plants by means of radioactive tracers," in *Proc. Intern. Conf. on the Peaceful Uses of Atomic Energy*, Vol. 12, p. 165.

LaBarbera, M (1990), "Principles of design of fluid transport systems in zoology," Science **249** (4972), 992–1000.

Lacointe, Andre, and Peter E. H. Minchin (2008), "Modelling phloem and xylem transport within a complex architecture," Functional Plant Biology **35** (9-10), 772–780.

Lalonde, S, M. Tegeder, M. Throne-Holst, W. B. Frommer, and J. W. Patrick (2003), "Phloem loading and unloading of sugars and amino acids," Plant Cell and Environment **26** (1), 37–56.

Lambers, Hans, F Stuart Chapin III, and Thijs L Pons (2008), *Plant Physiological Ecology* (Springer).

Lang, A (1978), "A model of mass flow in the phloem," Australian Journal of Plant Physiology **5** (4), 535–546.

Lang, Alexander (1973), "A working model of a sieve tube," Journal of Experimental Botany **24** (82), 896–904.

Lang, Alexander, and Peter Minchin (1986), "Phylogenetic distribution and mechanism of translocation inhibition by chilling," Journal of Experimental Botany , 389–398.

Lee, DR (1981), "Synchronous pressure-potential changes in the phloem of *Fraxinus americana* L." Planta **151** (4), 304–308.

Lee, Jinkee, N Michele Holbrook, and Maciej A Zwieniecki (2012), "Ion induced changes in the structure of bordered pit membranes," Frontiers in Plant Science **3**, 55.

Lens, F, J. S. Sperry, M. A. Christman, B. Choate, D. Rabaey, and S. Jansen (2011), "Testing hypotheses that link wood anatomy to cavitation ressitance and hydraulic conductivity in the genus acer," New Phytologist **190**, 709–723.

Lens, Frederic, Aude Tixier, Hervé Cochard, John S Sperry, Steven Jansen, and Stephane Herbette (2013), "Embolism resistance as a key mechanism to understand adaptive plant strategies," Current Opinion in Plant Biology **16** (3), 287–292, physiology and metabolism.

LeVeque, Randall J (1992), *Numerical Methods for Conservation Laws* (Birkhäuser).

Liesche, J, and A. Schulz (2013), "Modeling the parameters for plasmodesmal sugar filtering in active symplasmic phloem loaders," Frontiers in Plant Science **4**, 207.

Liesche, Johannes, Helle Juel Martens, and Alexander Schulz (2011), "Symplasmic transport and phloem loading in gymnosperm leaves," Protoplasma **248** (1), 181–190.

Liesche, Johannes, and Alexander Schulz (2012), "In vivo quantification of cell coupling in plants with different phloem-loading strategies," Plant Physiology **159** (1), 355–365.

Liesche, Johannes, Carel Windt, Tomas Bohr, Alexander

Schulz, and Kaare Hartvig Jensen (2015), "Slower phloem transport in gymnosperm trees can be attributed to higher sieve element resistance," Tree Physiology **(in press)**.

Lintunen, A, T. Hölttä, and M. Kulmala (2013), "Anatomical regulation of ice nucleation and cavitation helps trees to survive freezing and drought stress," Scientific Reports **3**, 2031.

Liu, Changming, Xiying Zhang, and Yongqiang Zhang (2002), "Determination of daily evaporation and evapotranspiration of winter wheat and maize by large-scale weighing lysimeter and micro-lysimeter," Agricultural and Forest Meteorology **111** (2), 109–120.

Liu, David D, Wesley M Chao, and Robert Turgeon (2012), "Transport of sucrose, not hexose, in the phloem," Journal of Experimental Botany **63** (11), 4315–4320.

Loepfe, Lasse, Jordi Martinez-Vilalta, Josep Pinol, and Maurizio Mencuccini (2007), "The relevance of xylem network structure for plant hydraulic efficiency and safety," Journal of Theoretical Biology **247** (4), 788–803.

Lotka, Alfred J (1922), "Contribution to the energetics of evolution," Proceedings of the National Academy of Sciences of the United States of America **8** (6), 147.

Lucas, W J, A. Groover, R. Lichtenberger, K. Furuta, S. R. Yadav, Y. Helariutta, X. Q. He, H. Fukuda, J. Kang, S. M. Brady, J. W. Patrick, J. Sperry, A. Yoshida, A. F. Lopez-Millan, M. A. Grusak, and P. Kachroo (2013), "The plant vascular system: Evolution, development and functions," Journal of Integrative Plant Biology **55** (4), 294–388.

Lundblad, Mattias, Fredrik Lagergren, and Anders Lindroth (2001), "Evaluation of heat balance and heat dissipation methods for sapflow measurements in pine and spruce," Annals of Forest Science **58** (6), 625–638.

MacRobbie, Enid A C (1971), "Phloem translocation. Facts and mechanisms: A comparative survey," Biological Reviews **46** (4), 429–481.

Maier, Chris A, and Barton D Clinton (2006), "Relationship between stem co_2 efflux, stem sap velocity and xylem co_2 concentration in young loblolly pine trees," Plant, Cell & Environment **29** (8), 1471–1483.

Maurel, Christophe, Lionel Verdoucq, Doan-Trung Luu, and Véronique Santoni (2008), "Plant aquaporins: membrane channels with multiple integrated functions," Annu. Rev. Plant Biol. **59**, 595–624.

McCaskill, Ashlee, and Robert Turgeon (2007), "Phloem loading in *Verbascum phoeniceum* L. depends on the synthesis of raffinose-family oligosaccharides," Proceedings of the National Academy of Sciences **104** (49), 19619–19624.

McCulloh, Katherine A, John S Sperry, and Frederick R Adler (2003), "Water transport in plants obeys Murray's law," Nature **421** (6926), 939–942.

McDermitt, DK (1990), "Sources of error in the estimation of stomatal conductance and transpiration from porometer data," HortScience **25** (12), 1538–1548.

Meinzer, F C, D. M. Johnson, B. Lachenbruch, and D. R. Woodruff (2009), "Xylem hydraulic safety margins in woody plants," Funct Ecol. **23** (5), 922–930.

Mencuccini, Maurizio, and Teemu Hölttä (2010), "The significance of phloem transport for the speed with which canopy photosynthesis and belowground respiration are linked," New Phytologist **185** (1), 189–203.

Minchin, P E H, M. R. Thorpe, and J. F Farrar (1993), "A simple mechanistic model of phloem transport which explains sink priority," Journal of Experimental Botany **44** (5), 947–955.

Minchin, P E H, and J. H. Troughton (1980), "Quantitative interpretation of phloem translocation data," Annual Review of Plant Physiology and Plant Molecular Biology **31**, 191–215.

Moorby, J, M Ebert, and NTS Evans (1963), "The translocation of 11c-labelled photosynthate in the soybean," Journal of Experimental Botany **14** (2), 210–220.

Morris, James R, Daniel L. Hartl, Andrew H. Knoll, Robert A. Lue, Andrew Berry, Andrew Biewener, Brian Farrell, N. Michele Holbrook, Naomi Pierce, and Alain Viel (2013), *Biology: How Life Works*, first edition edition ed. (W. H. Freeman, New York, NY).

Mortimer, DC (1965), "Translocation of the products of photosynthesis in sugar beet petioles," Canadian Journal of Botany **43** (2), 269–280.

Mullendore, Daniel L, Carel W Windt, Henk Van As, and Michael Knoblauch (2010), "Sieve tube geometry in relation to phloem flow," The Plant Cell **22** (3), 579–593.

Münch, Ernst (1927), "Versuche über den Saftkreislauf," Berichte der Deutschen Botanischen Gesellschaft **45** (6), 340–356.

Münch, Ernst (1930), *Die Stoffbewegungen in der Pflanze* (Gustav Fischer, Jena).

Murray, John F, Philip Gold, and B. Lamar Johnson Jr (1963), "The circulatory effects of hematocrit variations in normovolemic and hypervolemic dogs," Journal of Clinical Investigation **42** (7), 1150.

Nielsen, Claus Helix (2010), "Major intrinsic proteins in biomimetic membranes," in *MIPs and Their Role in the Exchange of Metalloids* (Springer) pp. 127–142.

Niklas, K J (1994), *Plant allometry: the Scaling of Plant Form and Process* (University of Chicago Press).

Nobel, Park S (2009), *Physicochemical and Environmental Plant Physiology* (Academic Press, Boston).

Noblin, X, L. Mahadevan, I. A. Coomaraswamy, D. A. Weitz, N. M. Holbrook, and M. A. Zwieniecki (2008), "Optimal vein density in artificial and real leaves," Proceedings of the National Academy of Sciences **105** (27), 9140–9144.

Onoda, Yusuke, Mark Westoby, Peter B Adler, Amy MF Choong, Fiona J Clissold, Johannes HC Cornelissen, Sandra Díaz, Nathaniel J Dominy, Alison Elgart, Lucas Enrico, *et al.* (2011), "Global patterns of leaf mechanical properties," Ecology letters **14** (3), 301–312.

Oparka, KJ, CM Duckett, DAM Prior, and DB Fisher (1994), "Real-time imaging of phloem unloading in the root tip of Arabidopsis," The Plant Journal **6** (5), 759–766.

Passioura, J B (1976), "Translocation and the diffusion equation," in *Transport and Transfer Processes in Plants*, edited by I. F. Wardlaw and J. B. Passioura (Academic Press, New York) pp. 357–361.

Patrick, JW (1997), "Phloem unloading: sieve element unloading and post-sieve element transport," Annual Review of Plant Biology **48** (1), 191–222.

Payyavula, Raja S, Kate HC Tay, Chung-Jui Tsai, and Scott A Harding (2011), "The sucrose transporter family in Populus: the importance of a tonoplast PtaSUT4 to biomass and carbon partitioning," The Plant Journal **65** (5), 757–770.

Peaucelle, A, S A Braybrook, L Le Guillou, E Bron, C Kuhlemeier, , and H Hoöfte (2011), "Pectin-induced changes in cell wall mechanics underlie organ initiation in Arabidopsis," Current Biology **21**, 1720–1726.

Pedley, TJ (1980a), "The interaction between stirring and osmosis. Part 1," Journal of Fluid Mechanics **101** (Dec),

843–861.

Pedley, TJ (1980b), "The interaction between stirring and osmosis. Part 2," Journal of Fluid Mechanics **107** (Dec), 281–296.

Pedley, TJ (1983), "Calculation of unstirred layer thickness in membrane transport experiments: a survey," Quarterly Review of Biophysics **16** (2), 115–150.

Pedley, TJ, and J Fischbarg (1978), "The development of osmotic flow through an unstirred layer," J. Theor. Biol. **70**, 427–447.

Peng, Duo, Xi Gu, Liang-Jiao Xue, James H Leebens-Mack, and Chung-Jui Tsai (2014), "Bayesian phylogeny of sucrose transporters: ancient origins, differential expansion and convergent evolution in monocots and dicots," Frontiers in Plant Science **5**, 615.

Petit, Giai, and Alan Crivellaro (2014), "Comparative axial widening of phloem and xylem conduits in small woody plants," Trees – Structure and Function **28** (3), 915–921.

Peuke, AD, M Rokitta, U Zimmermann, L Schreiber, and A Haase (2001), "Simultaneous measurement of water flow velocity and solute transport in xylem and phloem of adult plants of *Ricinus communis* over a daily time course by nuclear magnetic resonance spectrometry," Plant, Cell & Environment **24** (5), 491–503.

Phillips, Ronald J, and Stephanie R Dungan (1993), "Asymptotic analysis of flow in sieve tubes with semi-permeable walls," Journal of theoretical biology **162** (4), 465–485.

Pickard, William F (1981), "The ascent of sap in plants," Progress in Biophysics and Molecular Biology **37** (0), 181 – 229.

Pickard, William F (1982), "Why is the substomatal chamber as large as it is?" Plant Physiology **69** (4), 971–974.

Pickard, William F, and Barbara Abraham-Shrauner (2009), "A simplest steady-state Münch-like model of phloem translocation, with source and pathway and sink," Functional Plant Biology **36** (7), 629.

Pittermann, Jarmila, John S Sperry, Uwe G Hacke, James K Wheeler, and Elzard H Sikkema (2005), "Torus-margo pits help conifers compete with angiosperms," Science **310** (5756), 1924–1924.

Pockman, William T, John S Sperry, and James W O'Leary (1995), "Sustained and significant negative water pressure in xylem," Nature **378** (6558), 715–716.

Ponomarenko, A, O. Vincent, A. Pietriga, H. Cochard, E. Badel, and P. Marmottant (2014), "Ultrasonic emissions reveal individual cavitation bubbles in water-stressed wood," Journal of The Royal Society Interface **11** (99), 20140480–20140480.

Prado, Karine, and Christophe Maurel (2013), "Regulation of leaf hydraulics: from molecular to whole plant levels," Frontiers in Plant Science **4**, 10.3389/fpls.2013.00255.

Price, Charles A, and Joshua S. Weitz (2014), "Costs and benefits of reticulate leaf venation," BMC Plant Biology **14**, 10.1186/s12870-014-0234-2.

Pritchard, Jeremy (1996), "Aphid stylectomy reveals an osmotic step between sieve tube and cortical cells in barley roots," Journal of Experimental Botany **47** (10), 1519–1524.

Rand, R H (1983), "Fluid mechanics of green plants," Annual Review of Fluid Mechanics **15** (1), 29–45.

Raven, P, R. Evert, and S. Eichhorn (2005), *Biology of Plants*, 7th ed. (W. H. Freeman and Company Publishers, New York, NY).

Reidel, Edwin J, Emilie A Rennie, Véronique Amiard, Lail-

iang Cheng, and Robert Turgeon (2009), "Phloem loading strategies in three plant species that transport sugar alcohols," Plant Physiology **149** (3), 1601–1608.

Rennie, E A, and R. Turgeon (2009), "A comprehensive picture of phloem loading strategies," PNAS **106** (33), 14162–14167.

Riesmeier, Jorg W, Lothar Willmitzer, and Wolf B Frommer (1994), "Evidence for an essential role of the sucrose transporter in phloem loading and assimilate partitioning." The EMBO Journal **13** (1), 1.

Roberts, Alison G (2005), "Plasmodesmal structure and development," in *Plasmodesmata* (Blackwell Publishing Ltd) pp. 1–32.

Rockwell, Fulton E, James K Wheeler, and N Michele Holbrook (2014a), "Cavitation and its discontents: opportunities for resolving current controversies," Plant Physiology **164** (4), 1649–1660.

Rockwell, Fulton Ewing, N Michele Holbrook, and Abraham Duncan Stroock (2014b), "The competition between liquid and vapor transport in transpiring leaves," Plant Physiology **164** (4), 1741–1758.

Ronellenfitsch, Henrik, Johannes Liesche, Kaare H. Jensen, N. Michele Holbrook, Alexander Schulz, and Eleni Katifori (2015), "Scaling of phloem structure and optimality of photoassimilate transport in conifer needles," Proceedings of the Royal Society of London B: Biological Sciences **282** (1801).

Roscoe, R (1949), "The flow of viscous fluids round plane obstacles," Philosophical Magazine **40** (302), 338–351.

Roth-Nebelsick, A, D Uhl, V Mosbrugger, and H Kerp (2001), "Evolution and function of leaf venation architecture: A review," Annals of Botany **87** (5), 553–566.

Sack, Lawren, Elisabeth M Dietrich, Christopher M Streeter, David Sánchez-Gómez, and N Michele Holbrook (2008), "Leaf palmate venation and vascular redundancy confer tolerance of hydraulic disruption," PNAS **105** (5), 1567–1572.

Sack, Lawren, and Christine Scoffoni (2013), "Leaf venation: structure, function, development, evolution, ecology and applications in the past, present and future," New Phytologist **198** (4), 983–1000.

Sampson, Ralph Allen (1891), "On Stokes's current function," Philosophical Transactions of the Royal Society of London. A **182**, 449–518.

Santiago, Michael, Vinay Pagay, and Abraham D. Stroock (2013), "Impact of electroviscosity on the hydraulic conductance of the bordered pit membrane: A theoretical investigation," Plant Physiology **163** (2), 999–1011.

Savage, Jessica A, Maciej A Zwieniecki, and N Michele Holbrook (2013), "Phloem transport velocity varies over time and among vascular bundles during early cucumber seedling development," Plant Physiology **163** (3), 1409–1418.

Savage, V M, L. P. Bentley, B. J. Enquist, J. S. Sperry, D. D. Smith, P. B. Reich, and E. I. von Allmen (2010), "Hydraulic trade-offs and space filling enable better predictions of vascular structure and function in plants," Proceedings of the National Academy of Sciences **107** (52), 22722–22727.

Schmitz, K, B. Cuypers, and M. Moll (1987), "Pathway of Assimilate Transfer between Mesophyll-Cells and Minor Veins in Leaves of *Cucumis melo* L," Planta **171** (1), 19–29.

Scholander, Per F, Edda D Bradstreet, EA Hemmingsen, and HT Hammel (1965), "Sap pressure in vascular plants neg-

ative hydrostatic pressure can be measured in plants," Science **148** (3668), 339–346.

Scholander, PF (1968), "How mangroves desalinate seawater," Physiologia Plantarum **21** (1), 251–261.

Schuepp, P H (1993), "Tansley review No. 59. Leaf boundary layers," New Phytologist , 477–507.

Schultz, Stanley G (1980), *Basic principles of membrane transport* (Cambridge University Press).

Schulz, A (1986), "Wound phloem in transition to bundle phloem in primary roots of *Pisum sativum* L. 2. The plasmatic contact between wound-sieve tubes and regular phloem," Protoplasma **130** (1), 27–40.

Schulz, A (1992), "Living sieve cells of conifers as visualized by confocal, laser-scanning fluorescence microscopy," Protoplasma **166** (3-4), 153–164.

Schulz, A (1995), "Plasmodesmal widening accompanies the short-term increase in symplasmic phloem unloading in pea root tips under osmotic stress," Protoplasma **188** (1-2), 22–37.

Schulz, A (2014), "Diffusion or bulk flow: how plasmodesmata facilitate pre-phloem transport of assimilates," Journal of Plant Research **(in press)**.

Schulz, A, and H.-D. Behnke (1987), "Feinbau und differenzierung des phloems von buchen, fichten und tannen aus waldschadengebieten," Projekt Europisches Forschungszentrum fr Manahmen zur Luftreinhaltung (PEF) im Kernforschungszentrum Karlsruhe **16**, 1–95.

Schulz, A, C. Khn, J. W. Riesmeier, and W. R. Frommer (1998), "Ultrastructural effects in potato leaves due to antisense-inhibition of the sucrose transporter indicate an apoplasmic mode of phloem loading," Planta **206** (4), 533–543.

Schulz, Alexander (1990), "Conifers," in *Sieve Elements*, edited by H. D. Behnke and R. D. Sjolund, Chap. 4 (Springer Berlin Heidelberg) pp. 63–88.

Schulz, Alexander (1999), "Physiological control of plasmodesmal gating," in *Plasmodesmata: Structure, function, role in cell communication*, edited by Aart J.E. van Bel and W.J.P. van Kesteren (Springer, Heidelberg) pp. 173–204.

Schumacher, Anneliese (1948), "Beitrag zur kenntnis des stofftransportes in dem siebröhrensystem höherer pflanzen," Planta **35** (5), 642–700.

Schumacher, W (1950), "Zur bewegung des fluoreszeins in den siebrhren," Planta **37** (5), 626–634.

Schurr, Ulrich (1998), "Xylem sap sampling: new approaches to an old topic," Trends in Plant Science **3** (8), 293–298.

Schymanski, Stanislaus J, Dani Or, and Maciej Zwieniecki (2013), "Stomatal control and leaf thermal and hydraulic capacitances under rapid environmental fluctuations," PLoS ONE **8** (1), e54231.

Secchi, Francesca, and Maciej A Zwieniecki (2012), "Analysis of xylem sap from functional (nonembolized) and nonfunctional (embolized) vessels of *Populus nigra*: chemistry of refilling," Plant Physiology **160** (2), 955–964.

Sevanto, Sanna, N Michele Holbrook, and Marilyn C Ball (2012), "Freeze/thaw-induced embolism: probability of critical bubble formation depends on speed of ice formation," Frontiers in Plant Science **3**.

Siebrecht, Sylke, Klaus Herdel, Uli Schurr, and Rudolf Tischner (2003), "Nutrient translocation in the xylem of poplar-diurnal variations and spatial distribution along the shoot axis," Planta **217** (5), 783–793.

Simonin, K A, E. Burns, B. Choat, M. M. Barbour, T. E. Dawson, and P. J. Franks (2014), "Increasing leaf hydraulic conductance with transpiration rate minimizes the water potential drawdown from stem to leaf," Journal of Experimental Botany 10.1093/jxb/eru481.

Sovonick-Dunford, Susan, D Roger Lee, and Martin H Zimmermann (1981), "Direct and indirect measurements of phloem turgor pressure in white ash," Plant Physiology **68** (1), 121–126.

Sperry, John S, Uwe G Hacke, and Jarmila Pittermann (2006), "Size and function in conifer tracheids and angiosperm vessels," American Journal of Botany **93** (10), 1490–1500.

Sperry, John S, Kirk L Nichols, June EM Sullivan, and Sonda E Eastlack (1994), "Xylem embolism in ring-porous, diffuse-porous, and coniferous trees of northern Utah and interior Alaska," Ecology , 1736–1752.

Stadler, R, J. Brandner, A. Schulz, M. Gahrtz, and N. Sauer (1995), "Phloem loading by the PMSUC2 sucrose carrier from *Plantago major* occurs into companion cells," Plant Cell **7** (10), 1545–1554.

Stadler, R, K. M. Wright, C. Lauterbach, G. Amon, M. Gahrtz, A. Feuerstein, K. J. Oparka, and N. Sauer (2005), "Expression of GFP-fusions in Arabidopsis companion cells reveals non-specific protein trafficking into sieve elements and identifies a novel post-phloem domain in roots," Plant Journal **41** (2), 319–331.

Stark, H, and S. Schuster (2012), "Comparison of various approaches to calculating the optimal hematocrit in vertebrates," Journal of Applied Physiology **113** (3), 355–367.

Stephenson, N L, A. J. Das, R. Condit, S. E. Russo, P. J. Baker, N. G. Beckman, D. A. Coomes, E. R. Lines, W. K. Morris, N. Ruger, E. Alvarez, C. Blundo, S. Bunyavejchewin, G. Chuyong, S. J. Davies, a. Duque, C. N. Ewango, O. Flores, J. F. Franklin, H. R. Grau, Z. Hao, M. E. Harmon, S. P. Hubbell, D. Kenfack, Y. Lin, J.-R. Makana, A. Malizia, L. R. Malizia, R. J. Pabst, N. Pongpattananurak, S.-H. Su, I-F. Sun, S. Tan, D. Thomas, P. J. van Mantgem, X. Wang, S. K. Wiser, and M. A. Zavala (2014), "Rate of tree carbon accumulation increases continuously with tree size," Nature **507** (7490), 90–93.

Stone, HA, A.D. Stroock, and A. Ajdari (2004), "Engineering flows in small devices," Annual Review of Fluid Mechanics **36** (1), 381–411.

Stroock, Abraham D, Vinay V. Pagay, Maciej A. Zwieniecki, and N. Michele Holbrook (2014), "The physicochemical hydrodynamics of vascular plants," Annual Review of Fluid Mechanics **46** (1), 615–642.

Swanson, Robert H (1994), "Significant historical developments in thermal methods for measuring sap flow in trees," Agricultural and Forest Meteorology **72** (1), 113–132.

Sze, Tsun-Kay Jackie, Prashanta Dutta, and Jin Liu (2013), "Study of protein facilitated water and nutrient transport in plant phloem," Journal of Nanotechnology in Engineering and Medicine **4** (2).

Sze, Tsun-Kay Jackie, Jin Liu, and Prashanta Dutta (2014), "Numerical modeling of flow through phloem considering active loading," Journal of Fluids Engineering-Transactions of the ASME **136** (2), 10.1115/1.4025869.

Tabeling, Patrick (2005), *Introduction to Microfluidics* (Oxford University Press, Oxford).

Taiz, Lincoln, and Eduardo Zeiger (2010), *Plant Physiology*, fifth edition ed. (Sinauer Associates, Inc., Sunderland, MA).

Tekoglu, C, L. J. Gibson, T. Pardoen, and P. R. Onck (2011), "Size effects in foams: Experiments and modeling,"

Progress in Materials Science **56**, 109–138.

Thompson, M V, and N. M. Holbrook (2003a), "Scaling phloem transport: water potential equilibrium and osmoregulatory flow," Plant, Cell and Environment **26** (9), 1561–1577.

Thompson, Matthew V, and N. Michele Holbrook (2003b), "Application of a single-solute non-steady-state phloem model to the study of long-distance assimilate transport," Journal of Theoretical Biology **220** (4), 419–455.

Thompson, RG, DS Fensom, RR Anderson, R Drouin, and W Leiper (1979), "Translocation of ^{11}C from leaves of *Helianthus*, *Heracleum*, *Nymphoides*, *Ipomoea*, *Tropaeolum*, *Zea*, *Fraxinus*, *Ulmus*, *Picea*, and *Pinus*: comparative shapes and some fine structure profiles," Canadian Journal of Botany **57** (8), 845–863.

Thoning, Kirk W, Pieter P. Tans, and Walter D. Komhyr (1989), "Atmospheric carbon dioxide at Mauna Loa Observatory: 2. analysis of the NOAA GMCC data, 1974–1985," Journal of Geophysical Research: Atmospheres **94** (D6), 8549–8565.

Tomlinson, Philip Barry (1994), *The Botany of Mangroves* (Cambridge University Press).

Tomos, A Deri, and Roger A Leigh (1999), "The pressure probe: a versatile tool in plant cell physiology," Annual Review of Plant Biology **50** (1), 447–472.

Turgeon, R (2010), "The role of phloem loading reconsidered," Plant Physiology **152** (4), 1817–1823.

Turgeon, R, and E. Gowan (1990), "Phloem loading in *Coleus blumei* in the absence of carrier-mediated uptake of export sugar from the apoplast," Plant Physiology **94** (3), 1244–9.

Turgeon, R, and P. K. Hepler (1989), "Symplastic continuity between mesophyll and companion cells in minor veins of mature *Cucurbita pepo* L. leaves," Planta **179** (1), 24–31.

Turgeon, R, and R. Medville (1998), "The absence of phloem loading in willow leaves," Proc Natl Acad Sci U S A **95** (20), 12055–60.

Turgeon, R, R. Medville, and K. C. Nixon (2001), "The evolution of minor vein phloem and phloem loading," American Journal of Botany **88** (8), 1331–1339.

Turgeon, R, J. A. Webb, and R. F. Evert (1975), "Ultrastructure of Minor Veins in *Cucurbita pepo* Leaves," Protoplasma **83** (3), 217–232.

Turgeon, R, and L. E. Wimmers (1988), "Different Patterns of Vein Loading of Exogenous [^{14}C]Sucrose in Leaves of *Pisum sativum* and *Coleus blumei*," Plant Physiology **87** (1), 179–182.

Turgeon, Robert, and Shmuel Wolf (2009), "Phloem transport: cellular pathways and molecular trafficking," Annual Review of Plant Biology **60**, 207–221.

Tyree, Melvin T, A Lawrence Christy, and Jack M Ferrier (1974), "A simpler iterative steady state solution of münch pressure-flow systems applied to long and short translocation paths," Plant Physiology **54** (4), 589–600.

Tyree, Melvin T, and Michael A Dixon (1983), "Cavitation Events in *Thuja occidentalis* L.: Utrasonic Acoustic Emissions from the Sapwood Can Be Measured," Plant Physiology **72** (4), 1094–1099.

Tyree, Melvin T, and John S Sperry (1989), "Vulnerability of xylem to cavitation and embolism," Annual Review of Plant Biology **40** (1), 19–36.

Tyree, Melvin T, and Martin Huldrych Zimmermann (2002), *Xylem Structure and the Ascent of Sap* (Springer, New York).

Verboven, Pieter, Els Herremans, Lukas Helfen, Quang T.

Ho, Metadel Abera, Tilo Baumbach, Martine Wevers, and Bart M. Nicolai (2015), "Synchrotron X-ray computed laminography of the three-dimensional anatomy of tomato leaves," Plant Journal **81** (1), 169–182.

Vogel, Steven (2004), "Living in a physical world," J. Biosci **29** (4), 391–397.

Vogel, Steven (2012), *The Life of a Leaf* (University of Chicago Press, Chicago).

Vogel, Steven (2013), *Comparative Biomechanics: Life's Physical World*, second edition ed. (Princeton University Press, Princeton).

Volk, GM, R. Turgeon, and DU Beebe (1996), "Secondary plasmodesmata formation in the minor-vein phloem of *Cucumis melo* L and *Cucurbita pepo* L," Planta **199** (3), 425–432.

Waigmann, E, A. Turner, J. Peart, K. Roberts, and P. Zambryski (1997), "Ultrastructural analysis of leaf trichome plasmodesmata reveals major differences from mesophyll plasmodesmata," Planta (Heidelberg) **203** (1), 75–84.

Wang, Jinwen, Derrick S. Dlamini, Ajay K. Mishra, Mary Theresa M. Pendergast, Mavis C. Y. Wong, Bhekie B. Mamba, Viatcheslav Freger, Arne R. D. Verliefde, and Eric M. V. Hoek (2014), "A critical review of transport through osmotic membranes," Journal of Membrane Science **454**, 516–537.

Wardlaw, IF, DJ Carr, and MJ Anderson (1965), "The relative supply of carbohydrate and nitrogen to wheat grains, and an assessment of the shading and defoliation techniques used for these determinations," Crop and Pasture Science **16** (6), 893–901.

Wegner, Lars H, and Ulrich Zimmermann (2002), "On-line measurements of K$^+$ activity in the tensile water of the xylem conduit of higher plants," The Plant Journal **32** (3), 409–417.

Wegst, Ulrike G K (2011), "Bending efficiency through property gradients in bamboo, palm, and wood-based composites," Journal of the Mechanical Behaviour of Biomedical Materials **4**, 744–755.

Wei, C, E Steudle, MT Tyree, and PM Lintilhac (2001), "The essentials of direct xylem pressure measurement," Plant, Cell & Environment **24** (5), 549–555.

Weir, G J (1981), "Analysis of Müunch theory," Mathematical Biosciences **56** (1), 141–152.

Weissberg, Harold L (1962), "End correction for slow viscous flow through long tubes," Physics of Fluids **5** (9), 1033.

West, Geoffrey B, James H. Brown, and Brian J. Enquist (1999), "A general model for the structure and allometry of plant vascular systems," Nature **400** (6745), 664–667.

Wheeler, Tobias D, and Abraham D. Stroock (2008), "The transpiration of water at negative pressures in a synthetic tree," Nature **455** (7210), 208–212.

Whitham, G B (1974), *Linear and Nonlinear Waves* (John Wiley & Sons).

Will, Torsten, W Fred Tjallingii, Alexandra Thönnessen, and Aart JE van Bel (2007), "Molecular sabotage of plant defense by aphid saliva," Proceedings of the National Academy of Sciences **104** (25), 10536–10541.

Windt, Carel W, Frank J Vergeldt, P Adrie De Jager, and Henk Van As (2006), "MRI of long-distance water transport: a comparison of the phloem and xylem flow characteristics and dynamics in poplar, castor bean, tomato and tobacco," Plant, Cell & Environment **29** (9), 1715–1729.

Wong, Keith HK, Juliana M. Chan, Roger D. Kamm, and Joe Tien (2012), "Microfluidic models of vascular functions,"

Annual Review of Biomedical Engineering **14** (1), 205–230.

Wright, John P, and Donald B Fisher (1980), "Direct measurement of sieve tube turgor pressure using severed aphid stylets," Plant Physiology **65** (6), 1133–1135.

Wright, K M, A. G. Roberts, H. J. Martens, N. Sauer, and K. J. Oparka (2003), "Structural and functional vein maturation in developing tobacco leaves in relation to atsuc2 promoter activity," Plant Physiology **131** (4), 1555–1565.

Xia, Y, and G. M. Whitesides (1998), "Soft lithography," Annual review of materials science **28** (1), 153–184.

Xie, Bo, Xiaomin Wang, Maosheng Zhu, Zhongming Zhang, and Zonglie Hong (2011), "CalS7 encodes a callose synthase responsible for callose deposition in the phloem," The Plant Journal **65** (1), 1–14.

Yang, Shi-Jian, Yong-Jiang Zhang, Mei Sun, Guillermo Goldstein, and Kun-Fang Cao (2012), "Recovery of diurnal depression of leaf hydraulic conductance in a subtropical woody bamboo species: embolism refilling by nocturnal root pressure," Tree physiology **32** (4), 414–422.

Young, John H, Ray F Evert, and Walter Eschrich (1973), "On the volume-flow mechanism of phloem transport," Planta **113** (4), 355–366.

Zhang, C, L. Han, T. L. Slewinski, J. Sun, J. Zhang, Z. Y. Wang, and R. Turgeon (2014), "Symplastic phloem loading in poplar," Plant Physiology **166** (1), 306–313.

Zheng, Q, DJ Durben, GH Wolf, and CA Angell (1991), "Liquids at large negative pressures: water at the homogeneous nucleation limit," Science **254** (5033), 829–832.

Ziegler, H (1975), "Nature of transported substances," in *Transport in Plants I* (Springer) pp. 59–100.

Ziegler, Hubert, and Georg Heinrich Vieweg (1961), "Der experimentelle nachweis einer massenströmung im phloem vonheracleum mantegazzianum somm. et lev," Planta **56** (4), 402–408.

Zimmermann, M H, and H. Ziegler (1975), "List of sugars and sugar alcohols in sieve-tube exudates," in *Encyclopedia of Plant Physiology, NS Vol 1. Transport in Plants 1: Phloem Transport*, edited by M. H. Zimmermann and J. A. Milburn (Springer, New York) pp. 480–503.

Zimmermann, MH, and P.B. Tomlinson (1965), "Anatomy of Palm *Rhapis excelsa*. 1. Mature Vegetative Axis," Journal of the Arnold Arboretum **46**, 160–181.

Zwieniecki, Maciej A, and Charles K. Boyce (2014), "Evolution of a unique anatomical precision in angiosperm leaf venation lifts constraints on vascular plant ecology," Proceedings of the Royal Society of London B: Biological Sciences **281** (1779), 10.1098/rspb.2013.2829.

Zwieniecki, Maciej A, and N. M. Holbrook (2000), "Bordered pit structure and vessel wall surface properties. implications for embolism repair," Plant Physiology **123**, 1015–1020.

Zwieniecki, Maciej A, and N Michele Holbrook (2009), "Confronting Maxwell's demon: biophysics of xylem embolism repair," Trends in plant science **14** (10), 530–534.

Zwieniecki, Maciej A, Peter J Melcher, and Eric T Ahrens (2013), "Analysis of spatial and temporal dynamics of xylem refilling in *Acer rubrum* L. using magnetic resonance imaging," Frontiers in Plant Science **4**, 265.

Zwieniecki, Maciej A, Peter J Melcher, and N Michele Holbrook (2001), "Hydraulic properties of individual xylem vessels of fraxinus americana," Journal of Experimental Botany **52** (355), 257–264.

Zwieniecki, Maciej A, Howard A. Stone, Andrea Leigh, C. Kevin Boyce, and N. Michele Holbrook (2006), "Hydraulic design of pine needles: one-dimensional optimization for single-vein leaves," Plant, Cell and Environment **29** (5), 803–809.